SAPIENZA
UNIVERSITÀ DI ROMA

Dottorato di ricerca:
Scienze della Terra

Curriculum:
Scienze Applicate alla Protezione dell'Ambiente e dei Beni Culturali

Dipartimento di Scienze della Terra

Coordinatore**:**
G. B. ANDREOZZI

Tutori:
Adriana MARAS
Davide BLEINER

Archaeometric investigations on red pigments: the provenance of cinnabar and the discrimination of synthetic and natural ochres

Indagini archeometriche su pigmenti rossi: la provenienza del cinabro e la discriminazione tra ocre naturali e di sintesi

Michela BOTTICELLI

XXVIII ciclo

Abstract:

Le indagini di provenienza possono fornire un contributo essenziale sia all'archeologo che al *conservation scientist*. La comprensione dei processi

produttivi in pittura, a partire dalla fase estrattiva in miniera, contribuisce contemporaneamente alla definizione della tecnica esecutiva ma anche delle rotte commerciali, col fine ultimo di apprezzare il valore artistico e storico di un'opera d'arte. Inoltre, le indagini di provenienza possono essere utili nella determinazione dei falsi.

Fino a questo momento, le metodologie diagnostiche più comuni nelle indagini di provenienza hanno previsto la determinazione di isotopi o elementi in tracce. Nel caso specifico del cinabro, che è oggetto di questo lavoro, gli isotopi dello zolfo sono più comunemente impiegati nello studio di questo pigmento, per quanto esistano anche studi preliminari basati sugli isotopi di piombo e mercurio circoscritti a campioni da cava e non specificatamente a scopo archeometrico. Tuttavia, queste tecniche non hanno, finora, restituito la possibilità di distinguere il cinabro proveniente da depositi differenti.

Nel caso in cui alcune miniere siano discriminabili, tale risultato viene nella maggior parte dei casi ottenuto a mezzo di tecniche dispendiose, economicamente e temporalmente. Inoltre, sebbene siano note dall'VIII secolo d.C. ricette per la produzione di un analogo pigmento sintetico, non esiste, ad oggi la possibilità di stabilire quando il naturale sia preferito al sintetico nella produzione artistica antica e il grado di diffusione di queste stesse ricette orientali nel mondo occidentale.

In quest'ottica, il primo obiettivo della presente ricerca è di definire una metodologia sperimentale alternativa per la determinazione della provenienza del cinabro e della sua discriminazione rispetto ai prodotti di sintesi. Peso maggiore è stato dato a tecniche facilmente reperibili, micro o non-distruttive e a basso costo, criteri preferibili

nel settore dei Beni Culturali, vale a dire nello studio di opere con carattere di unicità.
La seconda parte di questo lavoro è invece focalizzata sullo studio di ocre rosse, al fine di valutare una prassi investigativa che restituisca la possibilità di discriminare il pigmento naturale dal suo equivalente sintetico. L'uso di un prodotto sintetico, ottenuto dal riscaldamento di ocra gialla, è probabilmente noto fin dalla Preistoria. Differenti tecniche diagnostiche (microscopio elettronico a trasmissione, spettroscopia infrarossa e diffrazione a raggi-X) sono state impiegate fino ad oggi allo stesso scopo, per quanto un protocollo sistematico non sia stato ancora definito e permangano dubbi sulla discriminazione naturale/sintetico.

Il presente elaborato si compone, dunque, di due sezioni:

1. Indagini archeometriche sul cinabro;
2. Indagini archeometriche sull'ocra rossa.

La sezione 1 è stata prevista per valutare, per la prima volta, l'efficienza della diffrazione su polveri (XRPD) e della spettroscopia Raman negli studi di provenienza sul cinabro. Tale obiettivo è stato perseguito analizzando campioni di cinabro a provenienza nota concessi da diversi Musei di Mineralogia e Scienze Naturali italiani. L'analisi dei diffrattogrammi è stata seguita da affinamento Rietveld, al fine di individuare variazioni dei parametri strutturali eventualmente connesse ad una diversa provenienza. Gli stessi campioni sono stati analizzati anche attraverso spettroscopia μ-Raman, al fine di evidenziare variazioni composizionali legate ad una diversa provenienza. Allo stesso scopo, la spettrometria di massa a plasma accoppiato induttivamente (ICP-MS) è stata impiegata su un set ristretto di campioni, per determinare una prima lista di elementi in tracce che

possono fungere da *markers* per la provenienza del cinabro, non essendo presenti in letteratura studi precedenti al riguardo. Una volta stabiliti gli elementi di interesse, la loro concentrazione è stata misurata a più alta risoluzione mediante SF (*sector field*)-ICP-MS.

L'analisi diffrattometrica ha mostrato che i campioni provenienti dalla Cina possono essere discriminati sulla base del volume e dello *strain* residuo della cella cristallina, essendo questi parametri notevolmente superiori alla media per questa località. Questo dato è stato confermato dalla spettroscopia Raman. In particolare, il trattamento statistico dei dati spettroscopici ha messo in evidenza i parametri che contribuiscono a fornire informazioni archeometriche: una banda Raman addizionale nei campioni cinesi, attribuita al selenio come sostituente dello zolfo, ha confermato la loro discriminazione. La stessa tecnica analitica ha anche consentito inoltre di distinguere l'unico campione sintetico dai naturali.

L'analisi statistica delle concentrazioni degli elementi in traccia ottenute in ICP-MS ha evidenziato quali elementi possono essere considerati come *markers* di provenienza. Il rame sembra essere un buon discriminante per i campioni di Almadén, la principale risorsa estrattiva europea. Il selenio si conferma come un elemento fortemente caratterizzante per i campioni Cinesi. Di fatto, appare possibile caratterizzare l'impiego di cinabro proveniente da miniere cinesi, in modo rapido e non-distruttivo. Questa informazione potrebbe rivelarsi di grande interesse sia per il riconoscimento di falsi, quando l'approvvigionamento da risorse orientali può essere escluso su base storica, che nella definizione delle rotte commerciali dal Medio Oriente all'Europa. Non è da

sottovalutare anche la discriminazione del cinabro sintetico, che appare evidente dai dati spettroscopici.

La sezione 2 ha per oggetto l'ocra rossa, in campioni naturali e sintetici. Questi ultimi sono stati ottenuti in laboratorio a partire da campioni di ocra gialla riscaldati secondo due procedimenti differenti. Anche un campione di ocra gialla è stato sintetizzato in laboratorio, secondo una procedura comunemente descritta in letteratura per la produzione del cosiddetto "giallo di Marte". Il riscaldamento di questo campione con le stesse modalità delle ocre naturali ha permesso di ottenere due "rossi di Marte", anch'essi oggetto della presente indagine.
I campioni sono stati preventivamente caratterizzati in XRPD. La stessa tecnica è stata anche impiegata su un quantitativo minimo degli stessi campioni e seguita dall'affinamento Rietveld al fine di valutare variazioni strutturali indotte dalla sintesi che possano agire da *markers* nella discriminazione del prodotto di sintesi dal naturale. In particolare, la valutazione della dimensione dei cristalliti sembra essere promettente nella discriminazione sia dei gialli che dei rossi.
Anche la morfologia dei campioni è stata investigata mediante microscopio elettronico a scansione (SEM), al fine di mettere in luce differenze nella forma dei cristalli di sintesi. L'acquisizione delle immagini da elettroni secondari (SE) ha evidenziato che il giallo di Marte è chiaramente discriminabile per morfologia dai suoi equivalenti naturali. Infatti, nel prodotto di sintesi i cristalli di goethite si sviluppano in forma acicolare, chiaramente distinguibili al livello di ingrandimento raggiungibile con la strumentazione impiegata e in

contrasto con la forma arrotondata che caratterizza tutti i campioni di ocra gialla naturale analizzati.
Contemporaneamente, gli effetti composizionali indotti dalla sintesi sono stati valutati mediante spettroscopia infrarossa. Questa tecnica diagnostica si è rivelata sensibile nella differenziazione del giallo di Marte dalle ocre gialli naturali sulla base della valutazione delle bande attribuite ai gruppi ossidrilici. Al contempo, l'indagine in μ-FTIR è risultata essere la più efficace nella discriminazione dei rossi di sintesi. In particolare, la valutazione quantitativa delle bande caratteristiche degli ossidi e idrossidi di ferro ha consentito di individuare, in via preliminare, quali parametri possono incidere sulla discriminazione dalle ocre naturali, apportando un contributo significativo anche nella separazione dei prodotti ottenuti mediante procedure di sintesi differenti.

Alle donne e ai sostantivi forti
della mia famiglia:
a mia madre e alle mie nonne,
alla resistenza
al sorriso
e al calore familiare.

Acknowledgements

Here we are: time for gratitude.

I would first like to thank my thesis advisors, Prof. Adriana Maras, of the Department of Earth Sciences at "Sapienza" University, for the support of my PhD study and related research, for her patience, motivation and suggestions. Her guidance helped me in all the time of research and writing of this thesis. I would also like to thank my second advisor, Prof. Davide Bleiner, Head of the Laboratory for Advanced Analytical Technologies at the EMPA Institute of Dübendorf, Switzerland, for his supervision and hospitality at the EMPA institute.

My sincere thanks go also to the experts who were involved in the validation survey for this research project: Prof. David Hradil, of the Institute of Inorganic Chemistry at the Academy of Sciences of the Czech Republic and Dr. Marcel Guillong, of the ETH, Zurich, Switzerland. Without their competent participation and input, the revision could not have been successfully conducted.

Besides them, my gratitude goes then to all the professionals who gave me a concrete support in Italy and during the time I spent abroad.

In Italy: Prof. Paolo Ballirano for his insightful comments and encouragement, but also for the hard question incentivizing me to widen my research from

various perspectives; Prof. Gianni Andreozzi, for the OM images and for the precious time spent solving the administrative questions as PhD coordinator; Mr. Marco Albano, for the SEM investigations; all the Museums providing me the samples for my research project – the Museum of Mineralogy of "Sapienza" University, the Museum of Mineralogy of the University of Pavia, the Museum of Mineralogy of the University of Florence and the Museum of Natural History of Venice.

In Portugal: special thanks go to Prof. António Candeias, Prof. José Mirão and Prof. Cristina Diaz, who provided me the opportunity to join their team at the Hercules Laboratory of Évora. They welcomed me in the best way, giving me complete access to the laboratory and research facilities. Without their precious support it would not be possible to conduct this research. The hospitality and help of the rest of the staff must me mentioned as well, as it was fundamental to encourage the research and life in a foreign country: for this reason I am in debt to Milene Gil, who passionately introduced me to her research activities; to Massimo Beltrame, Ginevra Coradeschi and Valentina Valbi, my Italian *ambassadors* in Portugal, for introducing me in these wonderful people and country; to Cátia Prazeres, my *indigenous geologist*, for the precious time spent in serious and silly conversations; to Anne-France Maurer, my French *tenant* in Portugal, for her precious academic support and hospitality; to Lucija Šobrel and Iain White, the international couple, simply for sharing their philosophy of life. I cannot forget to mention all the rest of the

people giving me support into the Lab (in order of appearance): Catarina Pereira Miguel, Rui Bordalo, Luís Dias, Cátia Relvas, Margarida Padeira Nunes, Marina González, Tânia Rosado, Ricardo Oliveira and Pedro Barrulas.

In Switzerland: I would like to acknowledge all the staff of the Laboratory for Advanced Analytical Technologies at the EMPA Institute of Dübendorf, Switzerland. A special thanks goes to Dr. Adrian Wichser for introducing me to the ICP-MS analysis. Thanks to all my fellow colleagues, who shared with me an office but also life experiences: Francesco Barbato, Mabel Ruiz, Yunieski Arbelo Pena and Leili Masoudnia.

Last but not the least: I would like to thank my family.
All my gratitude goes to my mum, for heeding my complaints and gently but firmly encouraging me to go on. Thanks to my dad, for his silent but constant efforts that made me reach the end of these studies. And thanks also to my brother, for affection and laughs, they spiritually supported me throughout writing this thesis and my life in general.
Thanks to my love, Enrico, who was forced to join the crazy world of academics and apparently survived unharmed. He gave me solace and sweets in the bad moments, strength and savouries in the labour days. Thanks also to the support and distractions offered by his family: Nadia, Mario, Tamara and Ludovica became a second family here in Rome.

I would also like to express my gratitude to all the people who crossed the PhD corridor – the “Break Room” – sharing victories and defeats of this common pathway: Laura Medeghini, Federica Maisto, Federica Marano, Chiara Adami, Giordano Macelloni, Maddalena Falco, Carmine Allocca, Sara Gambella and Gaia Appolloni. Thanks to my historic academic friends, Giulia Ricci, Francesca Volpi and Marica Grano: the precious, condensed time we spend together has always been an essential strength during this PhD years. And finally thanks to the friends from unmindful time (again, in order of appearance): Cristina Marozzi, Elisa Giacomozzi, Ilenia Isidori, Elisa Bitti, Alessio Cocci, Daniela Piermarini, Laura Ciccalè, Chiara Rap, Domenico Sorrentino, Michela Clementi, Diego Campus, Gaetano Lanatà. I know I can count on them, even if they are far away and time becomes a worse enemy while getting older.

CONTENTS

INTRODUCTION

Archaeometric investigations can give a fundamental contribution both to the Archaeologist and to the Conservation Scientist. The comprehension of the productive processes in paintings starts from the mineral extraction. This contributes to the delineation of executive techniques, but also to the definition of trade routes. It also leads to appreciate the artistic and historical value of an artwork. More than that, archaeometric studies may be fundamental in the detection of forgeries. This research work carries on archaeometric studies on two red pigments: cinnabar and red ochre. In particular, it is focused on the provenance of cinnabar and on the discrimination of synthetic and natural ochres.

The first section of this thesis deals with cinnabar. Cinnabar is a precious pigment, its importance being partly due to its low availability. With high probability, when the mineral was used as a pigment in the Roman Age, the district of Almadén, Spain, was the most exploited region. However, it is still not established if further local ores were chosen for supply, because a scientific methodology has still to be assessed. Up to the present, isotope and trace element analysis have been commonly applied to provenance studies. For cinnabar, sulphur isotopes are the most common. Preliminary studies were also carried out by lead or mercury isotopes, although they were not conceived for archaeometric

purposes. In any case, there is still no possibility to distinguish cinnabar from different localities. Whenever some mines are discriminated, this result is reached with time-consuming and expensive techniques.

Thus, the first section provides insights on a new methodology to establish cinnabar provenance. Importance was given to low-cost, non-destructive techniques, as preferred in conservation science, that is in the study of unique artworks. Samples with known provenance (Almadén, Idria, Tuscany, Russia, China and minor European deposits) were collected from Italian Mineralogical and Earth Science Museums. X-ray powder diffraction (XRPD) with Rietveld refinement was used to highlight structural variations related to a different origin. Inductively coupled plasma-mass spectrometry (SF-ICP-MS) was tested in parallel on these mineral samples. In particular, a first screening at low resolution was necessary to establish the elements to be revealed in the cinnabar samples because reference works were not available. Once the elements of interest were assessed, high resolution SF (*sector field*)-ICP-MS was applied on a limited sample-set. μ-Raman analysis was also chosen to add structural information without sample waste. Data were finally elaborated by principal component analysis (PCA).

The second part of the present work deals with the study of red and yellow ochres. The aim is to define an investigative methodology to discriminate the natural product to the

synthetic one. The use of a synthesized red, due to the heating of the yellow ochre, is probably known from Prehistory. A large variety of diagnostic techniques (transmission electron microscopy, IR spectroscopy and X-ray diffraction) have been tested to reach the target. However, a standard protocol has to be defined because there are still doubts in the recognition of the synthetic ochre.
At the same time, a preliminary study was carried out on the synthetic yellow, commonly known as “Mars yellow”, produced in laboratory following ancient recipes.

The synthetic red samples were also laboratory-synthesized, through the heating of natural and commercial ochres. The heating was carried out following two different pathways: the first simulating a low technological level, as in the Prehistoric production; the latter reaching more extreme conditions. Two samples of Mars red were additionally obtained from the heating of the Mars yellow.
The mineralogical phases characterizing the samples were first determined by XRPD. The same technique, applied in transmission on a small amount of sample and coupled with Rietveld refinement, was used to assess structural variations induced by the synthesis.
The morphology of the samples was investigated through SEM analysis. In parallel, compositional effects were examined through IR spectroscopy.

SECTION 1: CINNABAR

"Il mercurio, per la loro opera,
sarebbe indispensabile,
perché è spirito fisso volatile,
ossia principio femminino,
e combinato con lo zolfo,
che è terra ardente mascolina,
permette di ottenere l'Uovo Filosofico,
che è appunto la Bestia con due Dossi,
perché in essa sono uniti e commisti
il maschio e la femmina."

(P.L. – Il sistema periodico)

Cinnabar – or *vermilion* – is a precious, red pigment, used on all kinds of supports from ancient times, after the extractions of the homonymous mineral from caves or after its synthesis.

The present section has the aim to test the efficiency of X-ray powder diffraction (XRPD) and Raman spectroscopy in defining the provenance of cinnabar. To do that, mineral samples coming from known localities and kindly given by Italian Mineralogical Museums were analysed. Cinnabar is not easily found in nature. This means that the research can focus

on a small number of deposits. Inductively coupled plasma mass spectrometry (ICP-MS) was used in parallel to obtain the elemental composition of the collected sample-set, up to trace elements. Data were then statistically analysed and compared to define clusters of provenance. The aim was also to identify which elements are characteristic of a single deposit.

1.1 THE MINERAL

Cinnabar is a mineral of the Sulphide class, with chemical formula HgS. It has been mostly known for 2000 years for the extraction of mercury. Its presence is usually related to hydrocarbons and hot springs and it is frequently in veins, filling volcanic rocks. It is commonly associated to native mercury and other sulphide from heavy metals, such as pyrite, stibnite and marcasite. Alternatively, it can constitute a gangue with opal, chalcedony, quartz, gypsum, dolomite and calcite (King, 2002). Less frequently it is found with fluorite and barite (Gettens *et al.*, 1972).

CHEMICAL AND STRUCTURAL PROPERTIES

Cinnabar is an essentially pure mercury sulphide, with mercury contents around 86.2%, slightly varying from sample to sample. King (2002) underlined the natural affinity of cinnabar for selenium, with concentration ranging from 10 ppm to 1.48%. The unit cell can also host nickel, iron, manganese, cadmium or zinc. The latter is related to sphalerite oxidation, from which cinnabar remains as a relict. It is known that cinnabar cannot react with single nitric, sulfuric or hydrochloric acid, even if concentrated or diluted, although being quite susceptible to *aqua regia* in modest heating, giving as a reaction product a mercury chloride, crystalline and opaque.

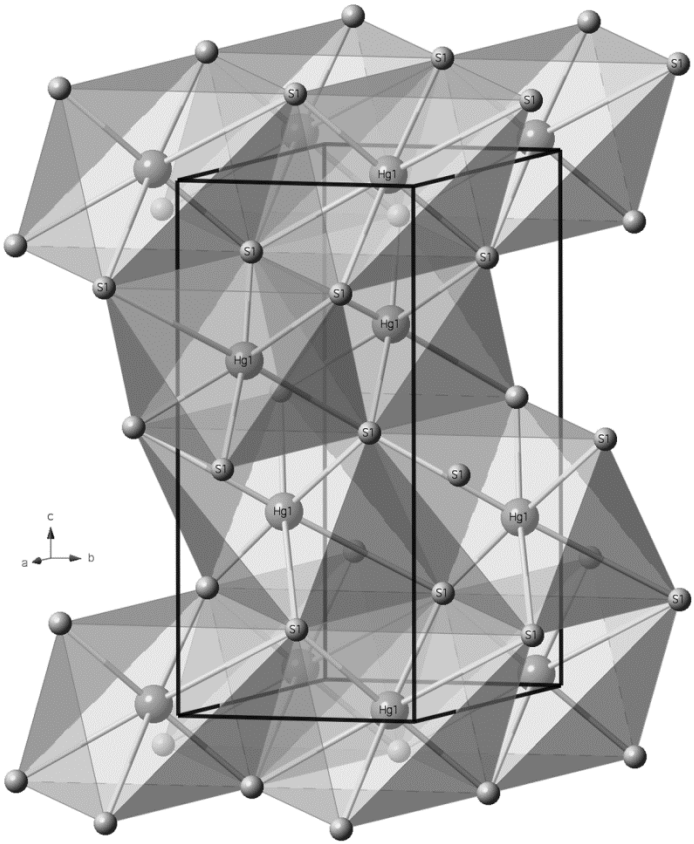

Figure 1 – Cinnabar structure after Ballirano *et al.* (2013).

Cinnabar structure consists of infinite spirals of *Hg-S-Hg* spirals rotating around the *c* axis (Figure 1). As recently revised by Ballirano *et al.* (2013), each Hg is four-fold coordinated to two sulphur atoms at ~2.4 Å and two at ~3.1 Å, plus two further contacts at ~3.25 Å. It belongs to the trigonal crystal system,

the spatial group being $P3_121$, with cell parameters: a = 4.1489(2) Å and c = 9.4947(5) Å (Ohmiya, 1974). Cinnabar is the α-form among three polymorphs. The β-form is cubic **metacinnabar**, into which cinnabar converts at an impurity-dependent temperature, varying from 373 K (HgS 99.97 wt.%) to 635 K (HgS 99.999 wt.%). It belongs to $F\bar{4}3m$ space group, with a = 5.8461(4) Å at room-T. The third, high-temperature, polymorph is the hexagonal **hypercinnabar**. Designated as γ-HgS, it was first described by Potter & Barnes (1978).

OPTICAL PROPERTIES

Cinnabar particles are easily recognizable for colour and characteristics, under reflected or transmitted light microscopy. In plane-polarized light the mineral shows red-orange colour and weak pleochroism (pale to dark orange-red). In particular, the hue tends to orange if the particles are finer (Eastaugh *et al*., 2008).

Cinnabar has perfect cleavage and particles can be conchoidally fractured. Crystals show a hexagonal habit, unless the sample is ground. Under strongly convergent light and at least 200x of magnification, cinnabar colour is bright red. In a binder with low refraction index, the edges of the grains appear to be black, being the relief extreme. On the contrary, under reflected light and high magnification, the red particles acquire a waxy brightness. Finally, the crystals show strong interference colours under crossed polars, due to the

high birefringence. However, they can assume a deep red colour and mask the interferences when body colour, relief and internal reflections combine.

Cinnabar can be recognized for the high refractive index (3.02) and for a polar rotation 15 times higher than quartz, with distinct right and left-handed crystals. High refractive index corresponds to high dispersive power, which substantially attributes an excellent hiding power to the pigment (Gettens, 1972).

1.2 THE PIGMENT: VERMILION AND CINNABAR

"*Sunt autem colores* austeri *aut* floridi.
Utrumque natura aut mixtura evenit.
Floridi sunt
- quos dominus pingenti praestat -
minium, armenium, cinnabaris,
chrysocolla, indicum, purpurissum;
ceteri austeri."

*(*Pliny the Elder, *Naturalis Historia*, *VII, Vol.XXXV)*

Knowledge about the ancient use of cinnabar as a pigment is mostly due to Pliny the Elder. The author includes it in the "***floridus***" pigments. This term is assigned, according to Ranuccio Bianchi Bandinelli (Bianchi Bandinelli, 1980), to all the transparent pigments, to distinguish them from the hefty ones. Indeed, cinnabar has an excellent hiding property, as discussed before. Thus, a classification related to purity or brightness seems more reliable, in Colombo's opinion (2003). However, the question gives an idea of how many doubts are still linked to this pigment, starting from the etymology.

ORIGIN OF THE WORD "CINNABAR"

The word *cinnabar* comes from the Greek ***kinnàbaris*** and was then translated into the Latin ***cinnàbaris***. According to Pianigiani (1993), it comes from ***kinabràο***, which means "to smell bad", testifying the connection with the badly smelling sulphur vapors. Alternatively, a Persian derivation is reported both in Gettens (1972) and Rapp (2009): *cinnàbaris* comes from ***zinjifrah***, literally "dragon's blood", attributed to the mineral for the similarity with a so-called red varnish. Altough this is the most common word, other terms are associated to it and in parallel to different pigments, increasing the confusion while translating ancient treatises.

The words ***vermiculum*** or ***vermilium*** must be cited first. These terms have been limited to a synthetic product since the 17th century (Harley, 2001), while in the past they could be used for both, natural and synthetic, especially in medieval treatises. The source is the word *vermis*, worm, which in turn suggests an organic pigment from the insect *Kermes Vermilio*. Moreover, Teophrastus (315 a.C.) includes two pigments in the same term ***cenobrium***: the mercury sulphide imported from Spain and a lead-based one. It seems probable that the latter is minium, a pigment cited by Pliny the Elder in the *Naturalis Historia* (trans. Rackham *et al.*, 1963), despite the superimposition of meanings. For this reason the word ***minium*** has been introduced to differentiate red lead from cinnabar.

HISTORICAL BACKGROUND

Over the last decades, archaeologists started to look for the evidence of a preliminary use of cinnabar in Europe, despite the first written record dates it back to Roman Age, as Pliny the Elder reports in his *Naturalis Historia* (trans. Rackham *et al.*, 1963). Cinnabar has been identified on Neolithic and Chalcolithic archaeological sites dated from the 5th to the 2nd millennium BC (Hunt-Ortiz *et al*., 2011). Domínguez-Bella and Morata-Céspedes (1995) proposed a decorative use and Martín-Gil *et al*. (1995) a ritual function, both on bones, while other authors refer of its application on pottery (Rogerio-Candelera *et al*., 2013 and Fernández-Martínez & Rucandio 2003). In the Eastern world, the first historically documented use of cinnabar as a red pigment is in the Shang (1523-1023 BC) and Chou (1027-256 BC) dynasties. It is not a coincidence that it happened in China, where cinnabar has always represented one of the most important materials, in paintings but also in rituals (burials and decoration of bones) and alchemic recipes for the philosopher stone. Probably, this is the reason why Chinese craftsmen were the first to introduce a synthetic process for the production of the pigment, around 300 AD (Ball, 2004).

In the Chinese ***dry recipe*** 17.5 pounds of sulphur are mixed with 37.5 pounds of mercury in an iron pot. They are heated to be homogenized. Then, 37.5 additional pounds of mercury are added and homogenized with water. Rough vermilion is

thus ground and heated in a furnace for 18 hours, together with pottery fragments, in the same iron sealed container. The content is cooled down to have cinnabar sublimation on the walls of the container and on the ceramic fraction. This deposit is removed, finely ground and mixed with water, alum and glue. The final product, after 24 hours, shows an upper part, with fine grains, and a lower, coarser one, to be ground again before washing and final drying (Hurst, 1982).

Before reaching the Western world, cinnabar is already known both in Minor Asia and India. For the first area, this information is confirmed by the finding of Hittite sculpture on the river Cehyan in Cilicia, for example, where cinnabar is used with red ochre in the 8th century BC (Colombo, 2003).

In India the use of cinnabar is mainly on paper, as testified by the 4th century AD manuscript *Raghuvamsa*. The executive technique on the same material is refined through years: in the book *Śimparatna*[1] it is suggested to prepare the pigment by grinding in water and exudate of *nīm* (gum arabic) for the tempera technique. Other recipes are in the *Jaina Citra Kalpadruma*: it is recommended to refine it in a mortar with sugary water or cider juice and gum, in small bar to dry and store. Even in Sanskrit language, a slight confusion exists between cinnabar and minium, the latter being cited but not revealed on mural paintings. Analogously, the superimposition

[1] It is a classical book on arts from Southern India, authorized by Srikumara in the 16th century AD.

of the words minium/cinnabar is common in the Chinese Arts History: Schafer *et al.* (1956) state that minium was considered a kind of cinnabar and for that reason it was alternatively called "lead cinnabar", "yellow cinnabar", "cinnabar powder" or "vermeil powder".

The use of cinnabar is rare in Egyptian art. It is not a coincidence that the pigment is not cited in Lucas & Harris' "*Ancient Egyptian Materials and Industries*" (2012). However, Le Fur (1990) states that some evidence can be found in the Lower Egyptian (663-525 B.C.), as confirmed by the diagnostic investigations carryed out by Quirke in 1993 and later (2011) by Bonizzoni *et al*. In particular, cinnabar has been identified by X-ray fluorescence and Fourier transform μ-Raman spectroscopy on funerary papyri and sarcophagy.

Maximum spread in the Western area occured in the 6th century in Greece, as Theophrastus states in his treatise "On stones" (Mottana & Napolitano, 1997). News about cinnabar supply and use in painting in the Roman world derives mostly from Vitruvius' *De Architectura* (rev. Piccolo, 2009) and Pliny's *Naturalis Historia* (trans. Rackham *et al*., 1963). Both authors report the existance of workshops in Rome for the preparation of the mineral as a pigment. Pliny also states that cinnabar was the most appreciated red pigment. It was chosen for the finest decorations and considered as a holy substance in rituals dedicated to Mars and in cosmesis (Rapp, 2009). Some prestigious examples can be easily found in Pompeii, in the

wall paintings of “Villa dei Misteri”, “Casa dei Vettii” and “Casa di Augusto” (Augusti 1967; Ling 1991).
For the same reason a monopoly in Rome was established to prepare the pigment and legally fix its price – 70 sesterces per pound - by law. Cinnabar was the most expensive among the red pigments (Table 1).

Table 1 - Comparison of the prices established for red pigments in Roman time according to Pliny (modified from Colombo, 2003).

	Mineral	**Price (per pound)**	**Homogenized price (dinars per pound)**
Cinnabar	Cinnabar	70 sesterce	17,50
Cerussa Usta	Minium	6 dinars	6,50
Sinopia	Hematite	2 dinars	2,00
Sandaraca	Realgar	5 as	0,31

This is the reason why painters used to mix cinnabar with other, less expensive, pigments such as *minium*, *rubrica* or *syricum*[2]. It seems that Romans did not know how to synthesize vermilion. What can be deduced from historical references is that Arabs spread the recipe in the Western world in the 8th century AD, introducing once again the terminology *cinabrum*. The description of the dry recipe can be found for the first time in an anonymous Latin manuscript

[2] Mixture of sinopia and sandix (synthetic red lead) used as a base for cinnabar. The name comes from the Island of Syros.

of the 9th century: the "*Compositiones ad tigenda"* [3]. It is cited again some years later, in the 10th century book "*Mappae Clavicula"* [4] and remarked in 1122 by Theophilus (trans. Hendrie, 1847). The possibility to synthesize it, instead of paying the import, together with a high hiding power and a quite good durability, make this pigment one of the most appreciated reds. That is why the recipe spreads easily, as Cennino Cennini writes in his "*Il libro dell'Arte*" (trans. Thompson, 1993). In the same book the author suggests to buy the pigment in a unique unmilled fragment, to be sure that it is never forged with cerusse or red ochre.

Cinnabar success extends to the following centuries, as it can be read in the 1523 document "*Leggi veneziane sulle industrie chimiche*" (Venetian laws on chemical factories), that fixes the opening of a new factory for the production of vermilion in Marghera, near Venice. In fact, Venice is the most active center in the 16th century manufacture and cinnabar is almost ubiquitous in Venetian Art during Renaissance, as stated by Lazzarini (1987).

However, Harley (2001) also reports the exclusion of the synthetic during all the 17th century, expecially in miniature

[3] Manuscript from the Capitulary Library of Lucca, No.490, published by Muratori, A.L., Antiquitate Italicae Medii Aevi, 1738-1743, volume II, Diss. 24, pp.365-392.

[4] Manuscript hold by the National Library of Paris, No. 6514, transcribed by Thomas Phillipps in 1847.

portraits, because of its opacity and coarseness, in favour of its application on maps and printed materials.

In the 17th century Amsterdam gains the name of the most productive center. The Dutch recipe differs from the Chinese one: 100 parts by weight of mercury are mixed with 20 of sulphur to obtain an amorphous mercury sulphide, black. This dark product corresponds, with high probability, to the so called “ethiopian mineral” that has to be ground and put in a ceramic alembic to have sublimation by heating at 853 K, with the subsequent transformation into red vermilion. Then, the product has to be treated with an alkali solution (to remove excess sulphur), washed with water and ground (Gray & Porter, 1830). Dutch cinnabar has been exported regularly in high amounts, untill a maximum of 32.000 pounds in 1760 for the United Kindom only (Harley, 2001). After that time, the production decreases due to Chinese and German competition.

Finally, a **wet recipe** must be cited, thanks to the German chemist Gottfried Schulz, who introduced it in 1687. The process is less laborious and expensive, compared to the dry one. Once the “Ethiopian mineral” is obtained, it can be just heated up to 318 K with ammonium or potassium sulphide for a few hours (Hurst, 1982). The final product is finer than the dry one, more homogeneous and with a red-orange colour.

CHROMATIC FEATURES

Cinnabar is a semiconductor and its colour is due to band gap mechanisms. It implies an energy gap between the valence and conduction energy in the electronic structure of the compound. This band gap has to be overcome to have light absorption and electronic excitement. The band gap in cinnabar corresponds to 2.0 eV. This means that all energies but red are absorbed and the specific range of the visible spectrum emitted causes the perception of a red colour (Choudhury, 2014).

The chromatic features of cinnabar can be evaluated through Munsell's colour system. Feller (Feller, 1967) states that the brightest hues correspond to a R range from 5 to 7.5, where R identifies the red component of a sample: 5R stands at the mid-point of the red segment, while 7.5R is a red tending more toward yellow-red. Alternatively, in the chromatic diagram CIE, the average values assigned to cinnabar range from (x = 0.55, y = 0.34) to (x = 0.54, y = 0.32), according to Gettens *et al*. (1972).

COMPATIBILITY AND DETERIORATION

Cinnabar is particularly inert, especially when used in mixture with other pigments, for example white lead, and in oil. Gettens & Sterner (1941) state that the usual deterioration products of white lead, *i.e.* lead sulphide, have never been found when it is used with cinnabar.

Different is the case of mural paintings: Vitruvius (rev. Piccolo, 2009) and Cennini (trans. Thompson, 1993) both state that cinnabar is not well-suited for the fresco technique. Alkali features of plasters are not compatible with its chemical composition. The pigment must be applied only when the plaster is well dry, in tempera, with a protein-based binder and protected by a final layer of wax and oil, the so-called "encaustic", according to Ling (1991). This incompatibility is also confirmed by Pliny the Elder in his Naturalis Historia (trans. Rackham *et al*., 1963). The author also refers about cinnabar photosensitivity, that is its tendency to darken when exposed to sunlight.

The problem of darkening was not studied up to the 17th century, when an inflamed debate started. De Massoul (1797) was against the use of cinnabar, especially in oil, while Bate (1654) and Williams (1787) encouraged it. However, the process itself, and its causes, started to be tackled at the beginning of the 20th century. Allen and Crenshaw (1912) proposed that the degradation is induced by heating and corresponds to a polymorphic transition from α-HgS, red, to black β-HgS, metacinnabar. They stated that the transition is reversible up to 598 K, while it becomes irreversible above 718 K. However, the presence of metacinnabar has never been revealed on deteriorated painted surfaces, as underlined by Daniels in 1987.

The hypothesis of a α→β transition persisted until 2000, with McCormack's study. For the first time, he pointed out the active involvement of chlorine (0.5-1 weight percent) or halogens, even if Davidson had already found a connection between cinnabar darkening and potassium iodide in 1980. Areas prone to this mechanism are photosensibles and show the presence of halogen species: terlinguaite (Hg_2OCl), calomel (Hg_2Cl_2), corderoite (α-$Hg_3S_2Cl_2$), eglestonite (Hg_4Cl_2O), kleinite [$Hg_2N(Cl,SO_4)\cdot nH_2O$] and analogous minerals Hg-S-Cl. Some years later Spring e Grout (2002) defined the activators of this process: chlorine of natural (sea or volcanic activity) or anthropic origin (air-conditioning, industrial processes or painting/conservation materials).

Different is the case of paintings exposed to high temperature, as after Pompeii eruption. Ballirano *et al.* (2013) found that the α-HgS → β-HgS phase transition in an oxidizing atmosphere occurs at a temperature exceeding 673 K. A characteristic temperature of 653 K has been estimated for a pyroclastic deposit of the 79 AD Pompeii eruption, from thermal remanent magnetization (Cioni, 2004). In principle, this means that the temperature of the deposit could not be the only blackening factor of red areas in mural paintings containing cinnabar, the transition temperature being higher than that of Pompeii eruption. This is true if the pigment has the same composition and provenance of the sample analysed by Ballirano *et al.* (2013) Thus, the eventual occurrence of a

partial or total α-HgS → β-HgS conversion, leading to the blackening of the pigment, should be attributed to impurities admixed to cinnabar, which may significantly modify the conversion route. This is in agreement with the recent work of Radepont *et al.* (2011, 2015). The authors confirmed the presence of the same minerals previously identified by McCormack (2000) and Keune & Boon (2005), studying degraded original works of art with colour altering from grey, white, pink to dark purple or even black. They concluded that the alteration factors are highly oxidative compounds (NaOCl shows faster processes and different product than NaCl), activated by exposure to U.V. radiation. The process leads first to the presence of the $Hg_3S_2Cl_2$ polymorphs corderoite (α-phase) and kenhusite (γ). The latter was for the first time identified by Radepont *et al.* (2011) as a mineral involved in cinnabar alteration. The final product is calomel. In the proposed model only corderoite is responsible for the black colour.

ROMAN SUPPLIES

From Teophrastus (Mottana & Napolitano, 1997) it is possible to know that in ancient Greece cinnabar was exploited from the mines in Iberia (Spain) and in the Colchide region (Black Sea). The author also states that a further locality existed near *Ephesus*. According to Healy (1993), this locality corresponds to *Iconium* (modern Konya, Turkey) and it

has been probably exploited from the VI century BC, to obtain the main couloring agent for greek statues and white-background *lekythoi*[5]. From Iconium came a kind of cinnabar defined by Teophrastus as "worked". The word is in opposition with "natural", which is instead attributed to the product coming from Iberia or Colchid, hard and comparable to a rock. The worked type looks like a brilliant purple sand. This sand is collected and finely ground in mortar. Then it is washed by decantation in copper basins. This is also the way to purify it from the gangue, thanks to a great difference in gravity between cinnabar and gangue minerals (8 and less than 3 respectively). For its high gravity, cinnabar deposits faster and separats from gangue and water. The method is attributed by the same author and later by Pliny to *Kallias*, a greek miner.

The same localities are probably known and used even in Roman times. In particular, the term Iberian has been wrongly attributed to Georgia in the past. However, Healy (1993) has more recently remarked the correspondance of Iberia to the mercury mines of "Sisapu" or "Sisopo", in the Roman province *Hispania Baetica.* This region has been recognized as the most famous mercury mine of Almadén, in Spain. The district reached its maximum spread in the Roman age, quoting Pliny,

[5] Type of Greek pottery devoted to oil storage, characterized by a long cylindrical body and a narrow neck with a loop-shaped handle [http://www.britannica.com/art/lekythos].

after a minor initial exploiting of the Cholchid region. The predominance of this site is probably associated with a higher purity of the extracted material, as it can be devised from the *Naturalis Historia* (trans. Rackham *et al*., 1963): "In the cinnabar mines of Almadén the sandy vein is pure, free from silver, and it can be melt as gold" (XXXIII, 121).

1.3 PROVENANCE: STATE OF THE ART

As King (2002) remarked, cinnabar is strictly related to volcanic activity and associated processes. Mercury deposits are along the so-called “mercury belts”, in the Mediterranean, Central Asia and Pacific Ocean (Figure 2).

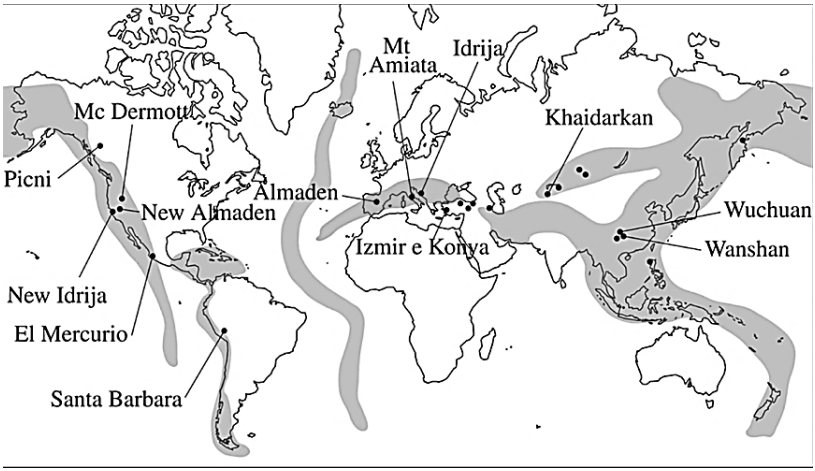

Figure 2 - Mercury belts in the world (modified from Pattelli *et al.*, 2014).

Even if cinnabar occurrence is widespread, just a few mines in the world have an economic impact. The most important is Almadén, in Spain. Its extractive activity is two times and half higher than in Idria, Slovenia, the second quarry for importance. The latter had, in turn, a four times greater exploitation than Monte Amiata, the third locality, in Italy. Other minor sites can be cited, like Moschellandsberg in Germany, Nikitowska in Russia or Avala in Serbia. China is also

a big source, cinnabar mining activity being documented within the Hunan-Guizhou mercury zone and the Gongguan-Huilong ore field (Zhang, 1996).

Provenance data on cinnabar can be found in geological studies: different attempts have been made to address the origin and the genetic processes of Hg bearing deposits, being mainly focused on Almadén. Sulphur and lead isotopes data are available (Jébrak *et al*., 2002; Saupé & Arnold, 1992) and have been compared in archaeometric researches to establish the provenance of cinnabar fragments from wall paintings (Spangenberg *et al.*, 2010) or Prehistoric artefacts (Hunt-Ortiz *et al.*, 2011). However, in the case of sulphur isotopes data, the calculated $\delta^{34}S$ range (+1.0 ‰ to +10.8‰) is wide enough, because it includes different mineralization styles within the same district. In parallel, values given in references (Spangenberg *et al.*, 2010) for other quarries, such as Génépy or Idria, fall in the same range. This leads to the conclusion that sulphur isotopes analysis has low efficiency in the attribution of provenance for cinnabar. However, in archaeometric investigations sulphur isotopes analysis predominates. The first work dates back to 2003, when Damiani and co-workers compared sulphur isotopes data from wall painting decorations (House of Diana, ancient *Cosa*, Grosseto, Italy) to those of the main European mercury deposits: Almadén, Idria, Monte Amiata, Génépy and Moschellandsberg (Damiani *et al.,* 2003). They obtained

results similarly achieved in the most recent work, published in 2010 (Spangenberg *et al*. 2010), on painted decorations from ancient *Aventicun*, Switzerland: it has been proved that some localities can be excluded from the list of supply, such as Moschellansberg (Germany), Monte Amiata (Italy) and Génépy (France). However, there is still no possibility to discriminate between Almadén and Idria, both important localities in cinnabar trades.

Considering lead isotopes, the first *a priori* problem arises from the difficulty to measure ^{204}Pb, caused by ^{204}Hg interference in mass spectrometers (Higueras *et al.,* 2005). For this reason Mazzocchin *et al*. (2008) excluded ^{204}Pb from their research. $^{206/207}$Pb, $^{208/207}$Pb, $^{208/206}$Pb and $^{207/206}$Pb ratios were measured both on mineralogical samples – Idria, Monte Amiata and Almadén - and wall painting fragments from the Villas of Verona, Vicenza, Pordenone, Trieste, Padua, Montegrotto and Pompeii (Italy). The comparison did not allow the discrimination among distant quarries*, i.e.* Almadén and Monte Amiata. Even when high-resolution techniques are used and ^{204}Pb can be measured, a second *a priori* problem has to be faced: when applied to archaeometric researches, isotopic analysis cannot refer to a statistically significant number of samples. For example, in Hunt-Ortiz (2011) lead isotopes values were used to exclude the small mineralization of Usagre and Las Alpujarras, in Spain, as a source in

Prehistoric art, despite the comparison was only among 4 mineral samples and 3 archaeological fragments.

Finally, recent studies (Hintelmann & Lu, 2003) also proved that relative variations in mercury isotope ratios exist among different cinnabar ores. However, samples are easily affected by contaminations from the environment and Hg mass fractionation, thus leading to under/overestimations in Hg isotopes concentrations.

Historical information helps excluding some quarries from Roman sources. That is the case with Idria: in Spangenberg *et al.* (2010) despite the overlapping of $\delta^{34}S$ values between Idria and Almadén, the former was *a posteriori* excluded because it was known to be mined only since 1493 (Rečnik, 2013). But what to do if no historical record is available? For example, the site of Avala has never been considered a resource, though archaeological findings prove that cinnabar from that area was used as a pigment in the Prehistoric site of Vinča, near Belgrade, Serbia (Chapman, 1981; Jovanović, 1984; Mioč *et al.*, 2004). Thus, the subject is still under debate: sulphur and lead isotopes give values still too close to distinguish geographically far mines. This target acquires further importance when taking into account the great complexity of the main mining locality, Almadén: 11 different districts coexist in an area of 10·20 km^2 (Rytuba, 2003).

1.4 GEOLOGIC SETTING

In order to evaluate compositional differences in the collected samples, the distinctive geological features of the mining localities and their history are hereby summarized.

The presence of cinnabar in geologic environments is often related to black shales. Their hydrothermal reworking originates three mechanisms of deposition (Hazen *et al*., 2012):

1. From submarine mafic volcanism near continental margins;
2. Hydrothermal alteration and replacement of serpentinite where the precursor fluids derive from a nearby marine sedimentary basin;
3. Hot-spring-type shallow deposits where Hg is concentrated by volcanically heated, often silicic, near-surface waters (young and active deposits).

European Hg-deposits are mostly represented by type 1 mineralization, while Chinese deposits belong to type 2.

ALMADÉN, SPAIN

Almadén is known all over the world for mercury extraction, its activity covering one third of the world total production. Historical references and archaeological findings both fix the beginning of the mining activity in the 8th century BC, controlled by the ancient town of *Sisapo* (Prieto *et al.*, 2012). Romei (1890) cites the Republican decree *Senatus*

consultus forbidding extractive activity in Italy to justify the maximum spread of Almadén during the Roman age (in Pliny's "*Naturalis Historia*", book III, trans. Rackham *et al*., 1963). The exploitation of Almadén mines continued under the Arabian control from the 8th to the 13th century AD and never stopped until 2000.

The Almadén district is located in the province of Castilla la Nueva, 300 km far from Madrid, Spain. The area belongs to the Central Iberian Zone, characterized by a Hercynian tectono-metamorphic event. This low grade metamorphism is responsible for the present structural shaping of the geological landscape.

Mercury ores are related to sedimentary and volcanic rocks in a large Paleozoic synclinorium over the Precambrian basement. Within the synclinal sequence, four kind of quartzite have been recognized (Higueras *et al.*, 2000): the Armorican (Lower Ordovician), the Canteras (Middle to Upper Ordovician), the Criadero (Upper Ordovician-Lower Silurian) and the Base one (Lower Devonian). The main mercury mineralization is hosted in the Criadero quartzite, intruded by basaltic sills and diatremes (locally called *Frailescas*) from the Silurian to Devonian sequence. The mineralization can be (Figure 3):

a) ***Stratabound***, larger deposits in the Criadero quartzite, soon after sedimentation, with a simple

mineralogy of cinnabar and minor pyrite hosted at the base of the Silurian;

b) ***Epigenetic***, fully discordant, with small veins in quarzitic rocks or massive replacements in mafic volcanoclastic rocks, both highly dispersed along the stratigraphic column up to the Devonian.

The deposits of *Almadén, El Entradicho* and *Vieja Conceptión* belong to type *a* mineralization. Type *b* has been recognized in *Las Cuevas*, *Nueva Conceptión* and *Nuevo Entredicho* (Jébrak *et al*., 2002).

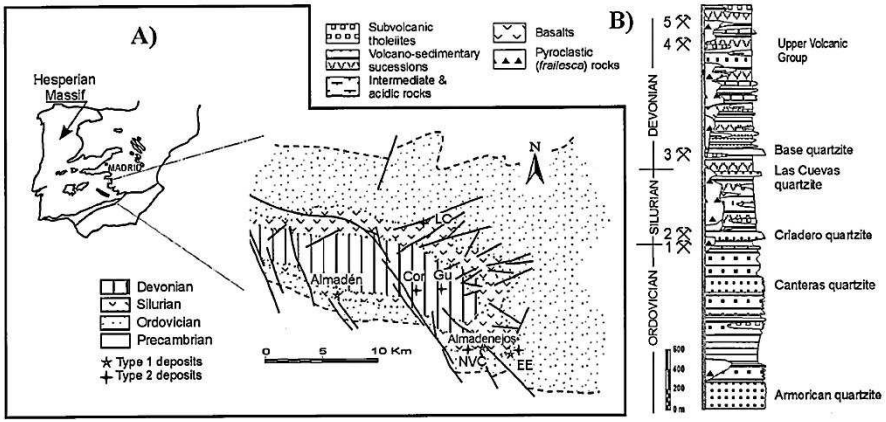

Figure 3 – **A**. Geological map of the Almadén syncline, reporting the main deposits: Cor = Corchuelo; Ee = El Entradicho; Gu = Guadalperal; Lc = Las Cuevas; Nvc = Neava and Vieja Conception. **B**. Stratigraphy of the Almadén syncline: number 1 refers to type *a* deposits (Almadén, El Entradicho, Vieja Conception) while number 2 (Las Cuevas), 3 (El Burcio), 4 (Corchuelo) and 5 (Guadalperal) belong to type b deposits (from Higueras *et al*., 2000).

The overall Silurian-to-Devonian sequence of magmatic rocks underwent regional metamorphism. Quartz is associated to chlorite, albite and carbonates (± ankerite, ± siderite, ± magnesite, ± calcite), while chlorite can also be associated to ± prehnite, ± pumpellyite, ± epidote and ± actinolite. An overprint of muscovite/illite-kaolinite-pyrophyllite assemblage is also present and directly related to type *b* depositions.

Higueras and co-workers (2005) suggested that the source of Hg may be both from the ancient upper continental crust and an enriched mantle-derived magmatic type. They also proposed the formation of Hg-organic complexes from the Silurian black shales to promote mercury transport in a hydrothermal paragenesis. This means that a thermally driven convection of seawater was favoured by the interaction with a long-lasting, submarine magmatic activity in the Silurian and Devonian, leading to recrystallizations. The mechanism explains why two Hg mineralizations, one younger and one older, can be found in the Almadén district. Moreover, the high variability of $\delta^{34}S$ remarked by Higueras *et al.* (2000) suggests that the mineralizing fluids contain sulphur of seawater and magmatic origin (in order of time).

IDRIA, SLOVENIA

The Idria deposit is the second largest mercury ore in the world. It is located 50 Km West of Ljubljana, Slovenia. Rečnik (2013) dates the mining back to the end of the 15th

century, when important superficial mineralization of mercury and cinnabar was exploited by Venetians. After a rapid consumption of this superficial resource, a deeper richer mineralization was reached by tunnels and shafts, the first of these being built in 1500 and named Antonio Shaft. The extraction activity was abruptly increased to more than 600 tons in the 18th century, to overcome the competition with England, at that time a big importer of mercury from China and India. Mines were finally closed in 1995. The Idria deposit partly occupies the Slovenian carbonate platform, which shows deep faults after the intra-continental rifting and later tectonics (Medium-Upper Anisic). These faults were the channels where mercury vapours from the ultramafic upper-mantle rocks condensed and accumulated. Mercury mineralization starts within black shales and lenses of sandstone and conglomerate from the Carboniferous; a younger mineralization is within dolostone from the Upper Permian and Lower Triassic; important, concordant orebodies are also in the micaceous dolostone, oolitic limestone, granular dolostone and Skonca beds (locally named seawater sedimentary and pyroclastic deposits) from the Ladinian, as shown in Figure 4.

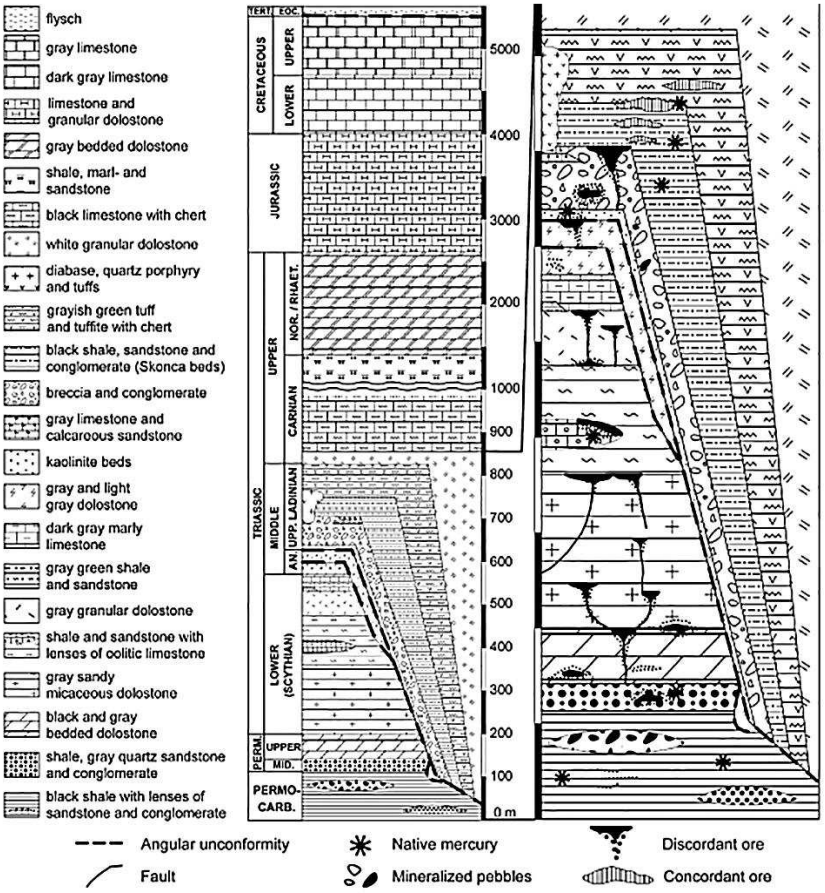

Figure 4 - Stratigraphy of the Idria deposit (in Lavrič & Spangenberg, 2003).

Tectonic transformations and hydrothermal activity in acidic, reducing conditions took place even contemporary to this early mineralization, giving rise to new fractures and channels for later mineralization. Thus, the deposit mainly

originated from two phases in the Ladinian (Lavrič & Spangenberg, 2003).

Phase I is ***sedimentary-exhalative*** and ***syngenetic***, with replacements and open-space fillings of small and rare cinnabar crystals. This led to post-mineralization deformation and remobilization of ore and gangue minerals and to discordant veinlets in fault zones from the Permocarboniferous to the Upper Ladinian. For example, metasomatic cinnabar from calcite is a product of this phase.

Phase II is ***epigenetic*** and contemporary to the deposition of the Skonca beds and volcanoclastic rocks. It is a consequence of the increased regional geothermal gradient and volcanic activity. It entails the ***metasomatic*** re-mineralization of ancient rocks, such as anidrite, gypsum and calcite.

In the Carboniferous mercury is native, with marcasite-pyrite concretions, sulphur being available only in small amounts. When the concentration of sulphur increases and the environment is highly reductive, mercury vapours from the Upper Mantle degassing react with it. Sulphur can originate from the Middle Triassic volcanic and hydrothermal activity (seawater sulphates). However, the major contributor is sedimentary Pyrite from Precarboniferous black shales and Upper Permian dolostones, gypsum and anidrite lenses. Lavrič & Spangenberg (2003) proposed that sulphur also comes from hydrocarbons, as a product of pyrolysis of residual organic fossils. They migrate along the fracture, mixing to

hydrothermal solutions and giving rise to pyrobitumen and colloform cinnabar, eventually with idrialine.

The Idria mercury ore is considered monomineralic. Cinnabar is the ubiquitous mineral, while native mercury is sporadic. Other primary minerals are marcasite, pyrite, dolomite, quartz, metacinnabar, calcite, fluorite, barite, celestine, kaolinite and palygorskite, as summarized in Table 2. Pyrite is mostly syngenetic, in the Carboniferous shales and Skonca beds. Together with marcasite, it comes from the reaction of S ions with Fe ions, the former being the result of sulphur-reducing bacteria. They can be found within fractures re-filled by mercury as a consequence of tectonic transformation. Metacinnabar deposition in hemispherical aggregates is promoted by the presence of Fe or Zn, that lower the temperature of the α-HgS→β-HgS transition (Dickson & Tunell, 1959). Sometimes metacinnabar appears over calcite crystals, in turn overlapping on cinnabar. Otherwise, calcite from local re-crystallization shows cinnabar inclusions and black globules of metacinnabar. Dolomite and quartz are also due to local re-crystallization into geodes when meteoric water percolates into the ancient dolostone. Into the same geodes kaolinite and palygorskite can also occur. The latter originates in vitreous tuffs of paludal ambient and is later involved in the percolating system.

Secondary minerals are sulphates, gypsum, limonite and vivianite, with the organic pyrobitumen and idrialine. Gypsum

is mostly a precursor of the mercury ore, interlayered in Permian dolostone. It is the product of an intense evaporitic lagoonal activity. Otherwise, it can be due to the oxidation of iron sulphides within the so-called *gossan*[6]: the produced sulphate ions react with calcite giving well-developed gypsum crystals (Table 2).

Table 2 - Mineral assemblage and paragenetic sequence of the Idria deposit. The thickness of bars is related to the abundance of the corresponding mineral (thick line = high, thin line = medium, dotted line = low). Sed = sedimentary, hyd = hydrothermal, VFC/VFD = void-filling calcite/dolomite (in Lavrič & Spangenberg, 2003).

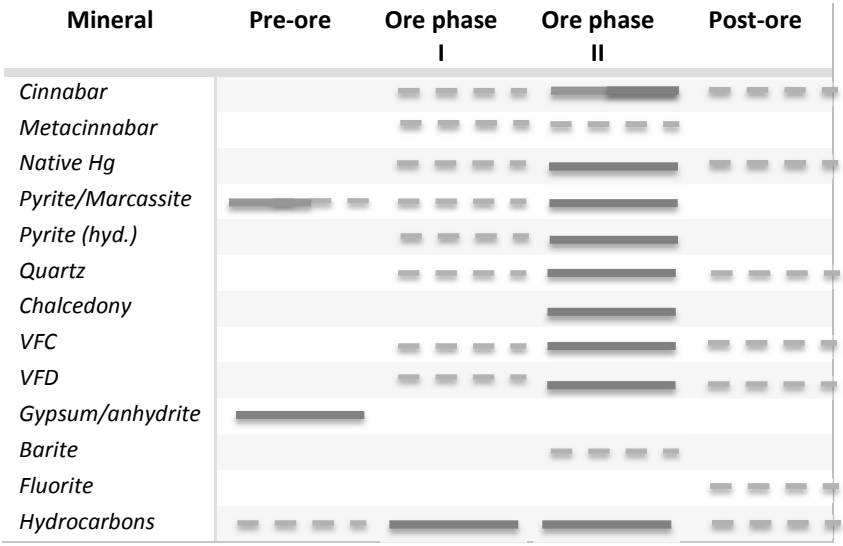

[6] An exposed, oxidized portion of a mineral vein, especially a rust-colored outcrop of iron ore (Random House Kernerman Webster's College Dictionary).

MONTE AMIATA, ITALY

The Monte Amiata deposit is located in Southern Tuscany, Italy, around an extinct volcan actually exploited for geothermal energy. The most ancient activity of this deposit is attributed to the Etruscan period, when cinnabar was mined both for cosmesis and painting. The use of cinnabar as a pigment in this area is attested by recent findings: Sodo *et al.* (2008) describe the mural paintings of an Etruscan tomb, "Orco II", in Tarquinia. Red areas are attributed to the double presence of red ochre and cinnabar, recognised by Raman spectroscopy. Evidence of the same activity are also documented by the finding of a Macedonian coin, dated 300 BC, in one cave within Cornacchino mine (Castell'Azzara in Fig. 6). Indeed, Mochi (1915) backdates the exploitation to the Stone or Bronze Age. In fact, the discovery of a quartzite pick[7], some mallets[8] and hoes made out of deer antlers (found in Sieel-Solforate and Cornacchino) suggest the existence of prehistoric cinnabar mines in the area of Monte Amiata.

Under Roman control, the mines were managed by the conquerors to extract mercury (*argentum vivum*) from

[7] Mochi (1915) refers that the pick was found in Cornacchino and belongs to the collection of the Museo Nazionale di Antropologia ed Etnologia of R. Istituto di Studi Superiori in Florence (inventory code 16289).

[8] In the Giglioli collection: *La Collezione Etnografica del Prof. E. H. Giglioli geograficamente classificat*a. Città di Castello, 1912, part II, pp. 8 and 15. Specimens N. 10384, 10370, found in Cornacchino and S. Fiora respectively.

cinnabar. The extraction continued until mining was forbidden by the already cited *Senatus Consultus* of the 4th century BC. Later on, no evidence of the mining activity is reported up to 1217. In this year the division of the Aldobrandi County occurred while the mines were kept in common. This can give an idea of the high profit given by the extraction of live-wire - as mercury was antiquely called (Romei, 1890). A great proof of this long-lasting supply are the miniated letters of historical statutes from local villages: they are frequently painted with cinnabar during the 15th century.

From 1437, when the mine went under the Sforza dinasty, to the 19th century, the activity was unstable with predominant closing periods. The exploitation of mercury restarted after the decrease of the Spanish mines, in 1846 and definitely ceased in the 20th century.

The Amiata belongs to the Tuscan Magmatic Province (TMP) and develops over the Siena-Radicofani basin of marine sediments, brought above sea level during a Middle Pliocene regional doming phase. The volcanic complex developed over it during the Pleistocene. The region underwent a general contraction during the Neogene and into the Quaternary, concurrently with Appenin orogeny (27-8 Ma). The stacking of the following tectono-stratigraphic units occurred (from the top, see Figure 5), as reported in Cataldi (1967), Batini *et al.* (2003), Morteani *et al.* (2011), Brogi *et al.* (2011) and Allocca (2013):

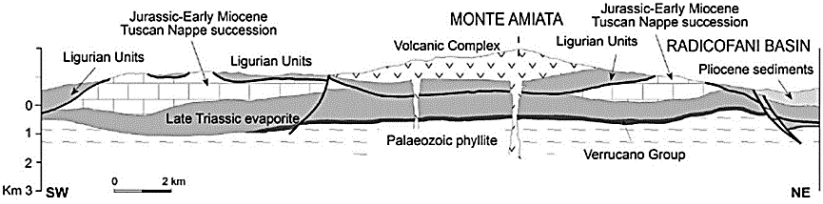

Figure 5 - Geological section of Monte Amiata area (modified from Brogi *et al.,* 2011).

a. ***Lavas*** belonging to the Magmatic Complex originated by the three eruptions of the volcano (*trachydacites* of the 305 to 241 ka eruption; *porphyritic rhyodacite* of the lava flow from 300 to 190 ka and *olivine-latite* from the lava flow dated 209 ka);
b. ***Continental and marine sediments*** (Miocene to Quaternary, including the clastic deposits from Neogene) filling post-appenninic graben structures;
c. ***Cretaceous turbidites*** from the Ligurian Unit, L, mainly made of *shales* and besides *marls*, *limestones* and *sandstones* (Jurassic oceanic basement-Cretaceous-Oligogenic products thrust eastward over the Tuscan domain during Late Oligocene-Early Miocene).
d. ***Evaporites and marine terrigenous sediments*** belonging to the Tuscan Nappe (TN), with *limestones*, *radiolarites*, *marls* and *dolomites* (from Late Triassic to Early Miocene, when it thrusted over the Tuscan and Umbrian-Marchean Domain);

e. ***Substratum of metamorphic products*** in the Tuscan Metamorphic Complex composed by the Verrucano Group (Triassic *phyllites* and *metacarbonates*, *quartzite* and *conglomerates*) and Carboniferous-Upper Permian graphitic *phyllite* and *metasandstone*.

Two main mineral ore can be found in this region: stibnite and cinnabar, the latter extraction being the third in world production. As pointed out by Morteani *et al.* (2011), stibnite and cinnabar can rarely occur in association in the mines of Monte Amiata. More often, pure stibnite is in veins with carbonates and quartz as gangue minerals. It is assumed that both mineralizations are related to Monte Amiata volcanism, but while the Hg content in geothermal fluids partitions into the vapour phase, Sb is retained in the liquid leading to their separated formation. Cinnabar occurrences can exist near stibnite, but separated from it. Known cinnabar mines are: Bagni di San Filippo, Abbadia S. Salvatore, Bagnore, Solforate, Senna, Cornacchino, Morone-Selvena, Cortevecchia, Catabbio, Reto Montebuono, Cerreto Piano and Capita (Figure 6). Here, cinnabar is the main ore mineral, with small amounts of stibnite, orpiment and realgar. Gangue minerals can be, in order: microcrystalline calcite, celestite, gypsum, native sulphur and hydrocarbons. The latter compounds testify the key-role of organic substances in the genesis of cinnabar.

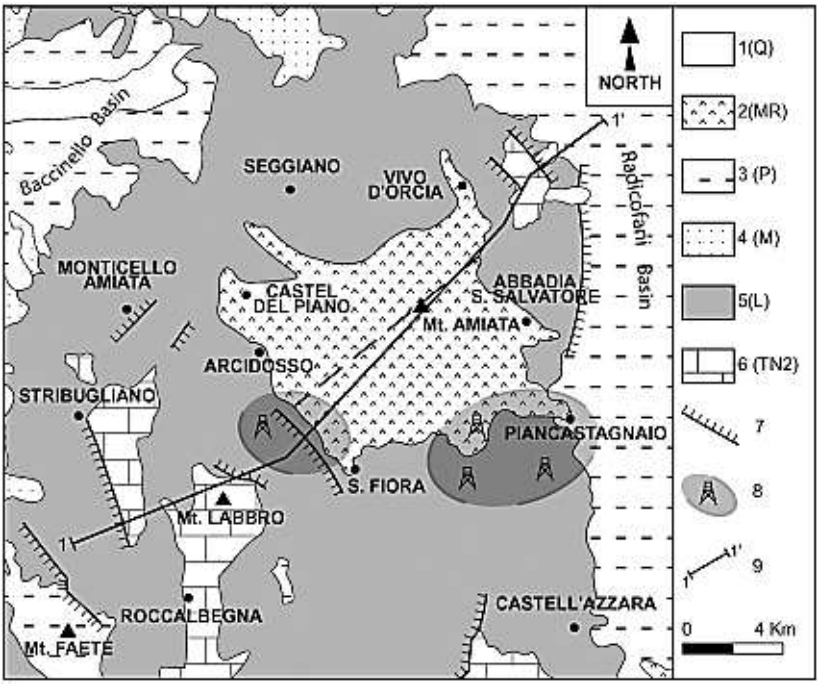

Figure 6 - Geological map of the Monte Amiata with the main mining localities (modified from Batini *et al.*, 2003). 1—Quaternary continental sediments; 2—Magmatic rocks; 3—Pliocene marine sediments; 4—Miocene continental, brackish and marine sediments; 5—Ligurian Units l.s. (Jurassic-Eocene); 6—Tuscan Nappe (Late Trias-Early Miocene); 7—normal faults; 8—Main geothermal fields; 9—Trace of the geological cross-section.

MOSCHELLANDSBERG, GERMANY

The Moschellandsberg Hg-deposit is located 80 km far from Frankfurt, Germany. Krupp (1989) suggested that it has been mined since medieval time. However, historical

information about the mining activity starts only in 1440. The deposit had its maximum spread from the 16th to 18th century and closed in 1942, the left mercury content being so low at that time.

The mercury deposit develops on a 2-km-wide caldera. The Hg-mineralization occurs on the southern part, where sandstone, conglomerates and mudstone are intruded in an andesitic rock older than the caldera. As it can be seen in Figure 7, the top of Moschellandsberg Mountain is covered by a breccia body which filled a late hydrothermal explosion crater (PYROCL. BR. in Figure 7). The mineralization follows faults and fractures. These structures are widened and filled with breccias as a result of hydraulic fracturing and later fluidization mechanisms. Then breccia undergoes hydrothermal alteration, showing cinnabar impregnations. Cinnabar can also occur in veins in andesite and silicified sandstone. Krupp (1989) proposed different hydrothermal alteration processes:

a. ***Silicification*** in the upper part of the deposit, with pore filling within sedimentary rock; the newly formed silica cement acts as a wall, stopping hydrothermal fluids and leading to hydrothermal eruptions;
b. ***Propylitic alteration*** concentrates on volcanic rocks and coincides with a carbonation of feldspars and ferromagnesian minerals to produce calcite, chlorite and pyrite.

c. ***Advanced argillitic alteration***, direct or as a further step of the propylitic alteration; it predominates on the upper part of the deposit, close to the major channelways of the hydrothermal fluids; it originates kaolinite, dicktite, illite, hematite and anatase.

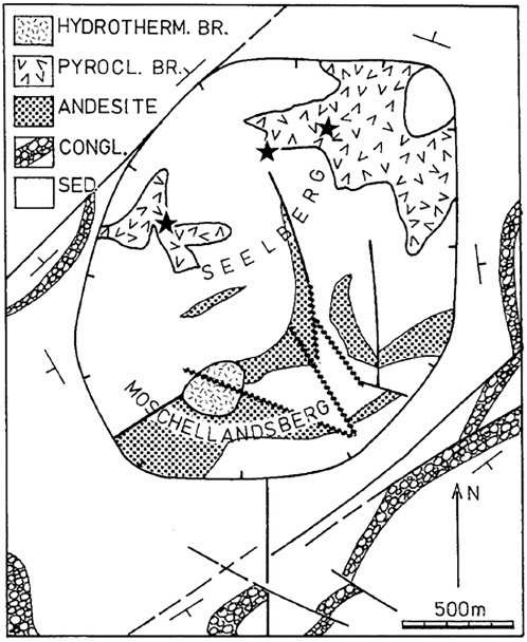

Figure 7 - Geological map of the Moschellandsberg volcanic complex, in Krupp (1989). *SED*. = Permo-Carboniferous fluviolacustrine sediments; *CONGL*. = conglomerates; *PYROCL. BR*. = pyroclastic breccia; *HYDROTHERM. BR.* = hydrothermal breccia filling the explosion crater. *Wavy lines* represent mineralized fractures. *Stars* are the argentiferous, base-metal, antimony and arsenic ores in the separated area of Seelberg.

Cinnabar occurrence develops on the upper 100 meters in vertical direction. Hydrothermal associated products are: major kaolinite, dickite, quartz and minor siderite, hematite and barite. The mineralization extends up to 175 m from the top of the deposit, gaining complexity. Siderite is more abundant and is accompanied by chalcopyrite, bornite, stibnite, native mercury, tetrahedrite, tennantite and other subordinate mineral phases, as summarized in Table 3.

Table 3 - Paragenetic sequence in the Moschellandsberg deposit, with relative abundance (thick line = high; thin line = medium; dotted line = low) and phase of occurrence, modified from Krupp (1989).

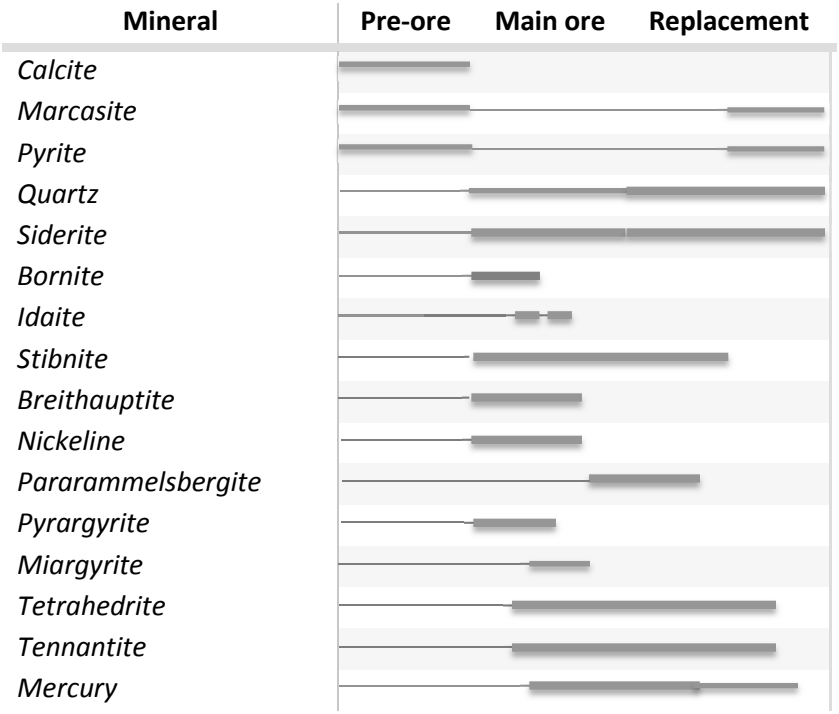

Mineral	Pre-ore	Main ore	Replacement
Metacinnabar			
Galena			
Sphalerite			
Dicktite			
Kaolinite			
Anatase			
Hematite			
Chalcopyrite			
Cinnabar			
Moschellansbergite			
Schachnerite			
Paraschachnerite			
Cubanite			
Chalcocite			
Digenite			
Livingstonite			
Pyrrhotite			
Greigite			
Smythite			
Gersdorffite			
Ulmannite			
Skutterudite-Chloanite			
Vaesite			
Barite			
Asphalt			

MINOR MERCURY DEPOSITS

Avala, Serbia

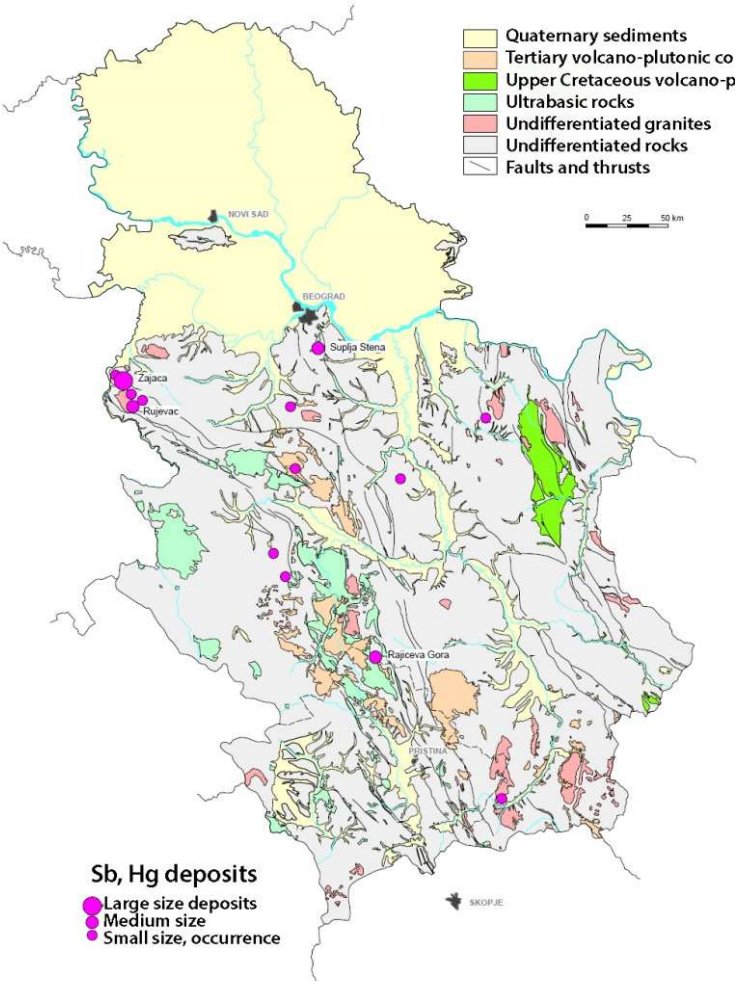

Figure 8 - Mercury and antimony deposits in Serbia. Suplja Stena is among the medium deposits (modified from Monthel *et al*., 2002).

The mercury mineralization in Serbia occurs near Mount Avala, 15 km South-East from Belgrade, within the Sumadija district, in the locality called Suplja Stena (Figure 8). Recent studies (Mioč *et al.,* 2004) proved the use of cinnabar in the Vinča prehistoric culture. This archaeological site is located 20 km North of Avala. Mioč *et al.* (2004) proposed that Avala itself corresponds to the site of supply. Evidence of cinnabar use is reported even for the Neolithic age, the main function being the decoration of pottery. Cinnabar has been identified by XRPD and spectroscopic analysis in all excavated layers, even in ceramic utensils. This suggests that the mineral was collected, separated from the other ore phases and used for special purpose after grinding. In the Roman period the interest in this mine decreased because the mines of Almadén and Idrija were conquered by the Romans.

The Sumadija district belongs to the Serbo-Macedonian Metallogenic Province. It hosts several types of mineralization that are attributed to Tertiary volcanic-plutonic complexes. Lead-zinc deposits are the most important (Rudnik mine), followed by the extraction of silver and lead (Kosmaj Babe mine). The deposit of Avala presents very rich mineralogical associations, with a predominance of pyrite, pyrrhotite, galena, sphalerite and chalcopyrite. They are irregularly shaped bodies, developed at the edges of Tertiary andesite and dacite dykes and stocks, which intruded Early Cretaceous flysch sediments. Mercury mineralization is included in the

minor metal concentrations. It is disseminated and stockworks, or it can occur in 10-cm-thick veins in the serpentinite, eventually intersected with numerous quartz and limonite veins. Chromium has been proposed by Gajić-Kvaščev *et al.* (2012) as a distinctive element for these occurrences within serpentinite along fracture zones. Other associated elements are: Ba, As, Ni, and Co. The deposit produced 230 t of Hg, but today it is abandoned. The Takovo and Trbusnica antimony mineralization can be also mentioned for the association with cinnabar in Triassic silicified sandstone, near subvolcanic dacite intrusions of the Neogene.

Nikitovska, Ukraine

The Nikitovska Hg-deposit is located in the Donets Basin, in the south-eastern portion of the Eastern European craton, within Ukraine and the Rostov area of Russia. Mining activity is documented up to the 1990s. No information is available about its beginning.

This basin belongs to the Pripyat-Dnieper-Donets (PDD) paleorift, undergoing inversion. The basin is fulfilled with 20-km-deep Late Palaeozoic sediments where mercury-antimony mineralization is associated to minor deposits of base metals. The Palaeozoic sequence (from 750 m to 5 km in depth, from the margins to the centre) starts with a Middle/Upper Devonian to Lower Carboniferous succession of syn-rift volcanic and intrusive rocks, carbonates and continental

clastic and volcanoclastic sediments, testifying an intense magmatic activity due to the rifting phase. The post-rift Carboniferous 14-km-succession consists mostly of shallow-marine and continental sediments interbedded with coal seams (Danišík *et al*., 2010). Permian sedimentary rocks up to 2.5 km thick are dominated by shallow-marine and coastal sand-shale with sparse interbeds of limestone, coal and thick layers of evaporite. The Mesozoic sequence shows both sedimentary and magmatic rocks (andesites, trachyandesites, lamprophyres, dolerites). Eocene to Upper Miocene rocks comprise sands, clays and marls (200 m up to 400 m). A large, main fold, parallel to the basin, is also present and is called the Main (or Gorlovka) Anticline (MA).

Here is where the ore deposits develop, as described by de Boorder and co-workers in 1996 (Figure 9). Cinnabar can occur in veins along faults or bedding planes (locally). Gangue minerals are quartz, carbonates and clays. Native mercury is also present in association with cinnabar, but also or in coal seams or bituminous shales. Since cinnabar corresponds to inverted folds and fractures, de Boorder *et al.* (1996) have speculated that the deposit is of Permian age.

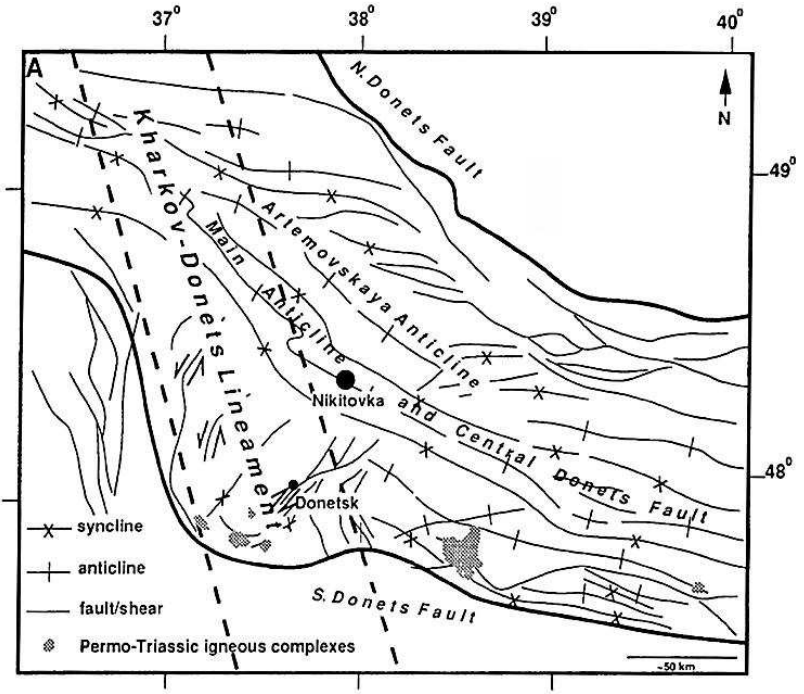

Figure 9 - Nikitovka mercury-antimony mining district (modified from de Boorder *et al.*, 1996).

Hořovice, Czech Republic

Occurrence of cinnabar in Czech Republic is documented for 40 sites, in competitive amounts with respect to Idria during their intermittent mining activity, from the 14th century to the 19th century. The sample of the present works, in particular, comes from the locality of Jedová hora (formally Giftberg) Hill, near Neřežín and 55 km SW of Prague, in central

Bohemia. The mine is also cited as Horschowitz, Horowitz or Horrowitz (Figure 10).

Some evidence of the mining activity is indirectly given from a tax agreement between the Holy Roman Emperor and the Czech King Charles IV: it fixed the payment of taxes to Rome with cinnabar from Western Bohemia. In the 16th century, the exploitation reached its highest peak, representing from 10 to 30% of Idria production. The competition was so tense that Idria prohibited the transport of cinnabar across the Alps to Venice from 1525 to 1527 (Velebil & Zachariáš, 2013). The mercury deposit at Horovice belongs to the Barrandian Basin, composed of unmetamorphosed Ordovician sedimentary and volcano-sedimentary sequences.

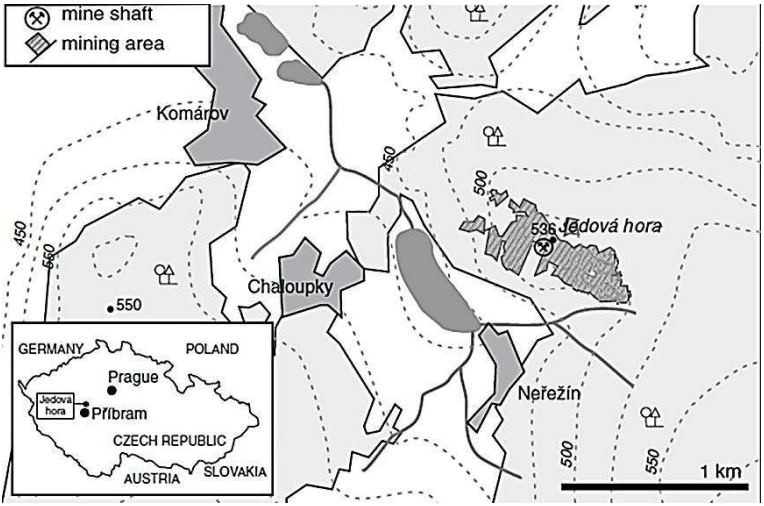

Figure 10 - Jedová hora mine, Horovice (modified from Hojdová *et al.*, 2009).

Carnia, Italy-Austria

This cinnabar deposit is located on the border between Italy and Austria, in the 100-km-long Paleocarnic Chain of Eastern Alps. Metallic mineralization extends from the Devonian to the Upper Carboniferous. Cinnabar exploitation focuses especially on Monte Avanza mine, the activity ranging from 778 to 1697 and then going on when Veneto region was annexed to Italy in 1858, discontinuously up to 1952 (Zucchini, 1998).

In the Devonian, a mixed siliciclastic-carbonate system originated from the variability of subsidence and mobility of the sea bottom. In parallel, pelagic goniatids and clymenids limestone are deposited from the Frasnian up to the Tournaisian. The whole sequence lifted up in the Lower Carboniferous and evolved to a paleorift with erosion, reworking and paleokarst due to *Horst* and *Graben* tectonics. Transgressive siliciclastic sediments grew as an independent stratigraphic unit over this unconformity, separated by palaeotectonic lineaments. The associated mineralization is commonly called “silicious crust type” (SCT) and is overlaid by different transgressive siliciclastic facies.

Pirri (1977) recognised the following minerals in the SCT: blende, galena, chalcopyrite, tetrahedrite, skutterudite, cinnabar, bournonite, jamesonite, boulangerite, enargite, bornite, arsenopyrite, fluorite and barite. Gangue minerals are Ca and Fe carbonates, quartz and bitumen. Alteration phases

are: covelline, digenite, cerussite, anglesite, smithsonite, hydrozincite, malachite and azurite.
Cinnabar can be found only in the Western area, on Monte Palombino and Monte Peralba-Avanza (Figure 11). Mineralization is of the stockwork type, monomineralic, within breccias. It is associated mainly with tetrahedrite, in turn related to blende and galena.

Pirri also suggested the presence of prismatic needles of boulangerite, although with some doubts. Pyrite – in fine dispersed crystals - and marcasite, when occurring, are related to Carboniferous sediments (Table 4).

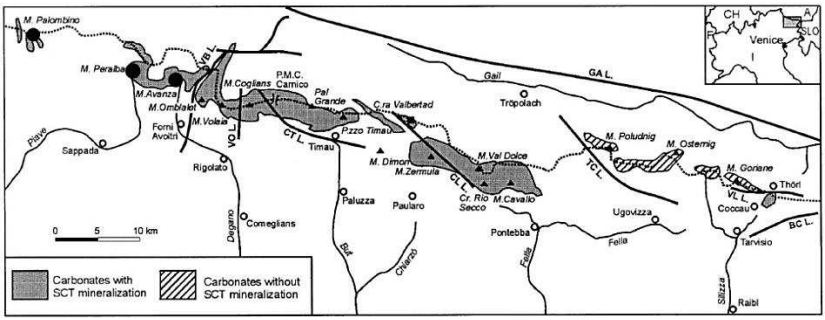

Figure 11 - Schematic map of the Carnic Alps, carbonates formations and siliceous crust-type mineralization (SCT) are evidenced. Full big circles represent cinnabar deposits (modified after Brigo *et al.*, 2001).

Table 4 - Paragenetic sequence of Eastern Carnia, with mineral abundance: thick line = high; thin line = medium; dotted line = low (modified from Pirri, 1977).

Mineral	M.Palombino	M.Peralba	M.Avanza
Blende			
Tetrahedrite			
Chalcopyrite			
Cinnabar			
Boulangerite			
Pyrite- Marcasite			
Barite			
Bitumen			
Quartz			

Lucca, Italy

In the Tuscan province of Lucca, in the North-Western area of the Apuane Alps, two deposits are known: the Levigiani and Ripa deposits. According to Dini *et al.* (2001), these mines were discontinuously exploited since the Middle Ages up to 1972. They are both located in the so called Apuan Metamorphic Complex (AMC), made of Paleozoic and Mesozoic sequences affected by the Appenninic tectono-metamorphism. A common Paleozoic basement is composed of phyllites, quartzites intercalated by metabasites, together with porphyroids and porphyric shists as a result of felsic volcanic rocks and meta-arkosic rocks metamorphism, respectively. Over this basement, two main units can be

distinguished: the Massa Triassic Unit (SW side) and the Apuane Unit (Triassic to Oligocene), as evidenced in Figure 12.

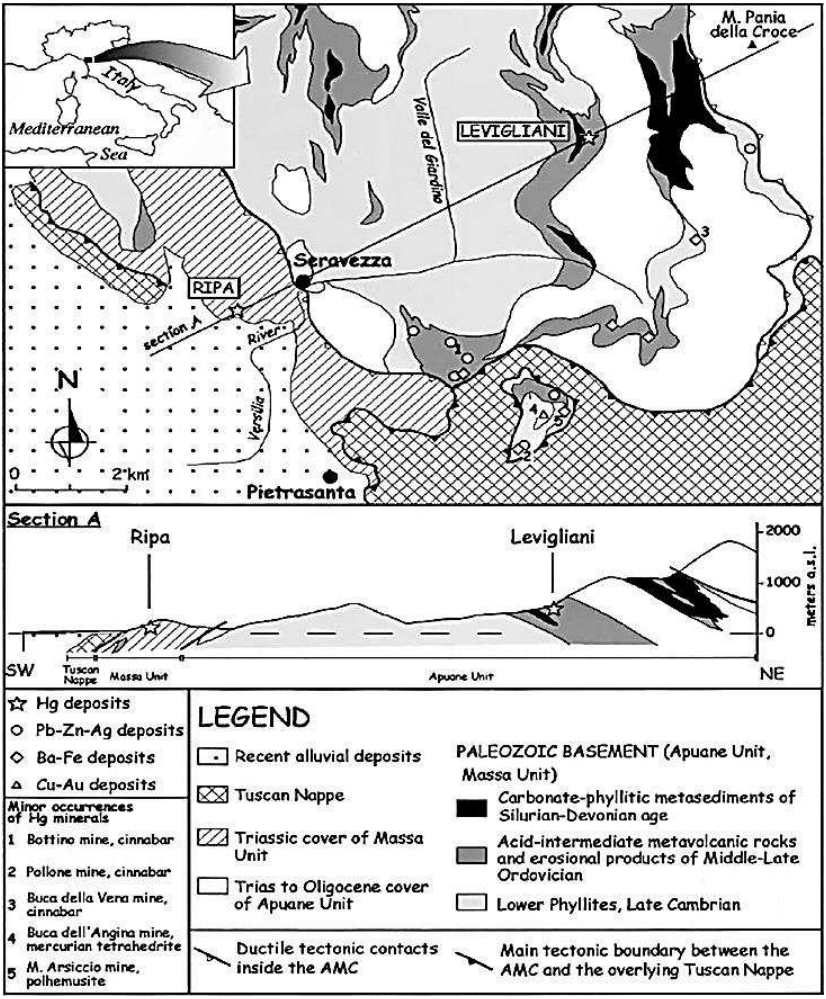

Figure 12 - Geological map of the Apuan Alps, stressing the position of hg and other ore deposits (modified from Dini *et al*., 2001).

Two main syn-metamorphic tectonic events are recorded for the AMC area. Kligfield (1986) identified as D_1 the syncollisional event with consequent SW-NE folding and foliation and with D_2 a second synextensional event giving rise to a dome. Minerals originated by D_1 are: quartz, albite, muscovite, pyrophyllite, chloritoid and chlorite. From D_2, blastesis of muscovite, chlorite and pyrophyllite were produced. Dini and co-workers suggest an increase in the metamorphic grade from the Apuane to the Massa Unit. This explains the different features of the Levigiani and Ripa deposits. In fact, the former is hosted in the Apuane Unit while the latter develops in the Massa Unit.

The ***Levigiani*** Hg deposit is located at the level of the Paleozoic Metasandstones, Quartzites and Phyllites (MQP), in association with syn-D_1 blastic carbonate-chloritic phyllites and calc-alcaline metabasites. Cinnabar association with metabasites could suggest the link with high geothermal gradients and magmatism, as revealed for other Hg-deposits (*i.e.* Almadén). Analogies with Almadén can be also found in the presence of a shallow submarine environment testified by the sedimentary reworking products (the carbonate-chloritic phyllites). Cinnabar occurs as disseminations and in veins. The disseminations lay on a schistosity plan resulted from D_1 deformation. Cinnabar and quartz are coherently oriented with the D_1 extension, often surrounding euhedral pyrite crystals. At the same time, veins occur along extensional

fractures due to D_2 deformation. This complex geological setting is accompanied by a composite mineral assemblage. Dini *et al.* (1995) recognised two types:

- **A.** cinnabar, metacinnabar and pyrite from the metamorphic thermal peak;
- **B.** cinnabar, sphalerite, pyrite, native mercury, chalcopyrite, galena and pyrrhotite; this type partially replaced type A mineralization in the retrograde stage of AMC metamorphism.

Gangue minerals are quartz, Mg-siderite, dolomite, ankerite, calcite, muscovite and albite, in both types of mineralization.

On the contrary, the ***Ripa*** Hg deposit hosted by the Massa Unit is less complex. Cinnabar develops in veins within phyllites and quartzites of the second cycle of deposition, associated with pyrite, or as disseminations replacing quartz, both exclusively during the first stage of D_2 deformation. Muscovite, pyrophyllite, kyanite, quartz and minor chlorite derive from the D_1 metamorphic event and they sometimes constitute gangue minerals in cinnabar deposition. The same event was responsible for the formation of veins where cinnabar deposition took place later. At the same time, pyrophyllite cross-cutting within cinnabar veins suggests that the main deposition occurred before the uplift (early D_2). As pointed out by Dini *et al.* (2001), Lucca cinnabar ores strongly differ from the ones of Monte Amiata, the former

being older, deep seated and apparently not related to magmatism.

Rosenau, Slovakia

Rosenau is the German word attributed to the mining town of Rožňava, in the region of Košice, Slovakia. The town was founded by Germans in the 13th century. Rybár *et al.* (2010) refers about the first historical notes on iron mining, dated back to 1243. The site was also mentioned as Rosnaubana in 1291, for the exploitation of silver. Copper and lead have been mined too. However, iron industry alone made Rožňava one of the most important and long-lasting industrial regions of the Hungarian Kingdom (Rybár *et al*., 2012), within the Association of Upper-Hungarian Mining Towns. The activity had its peak in the 16th century and continued up to 1992, when the oldest mine, Maria, was closed. No reference can be found about the historical exploitation of cinnabar in this region, even if its presence is documented (Urban *et al.*, 2006; Hurai *et al.*, 2008; Hurai *et al.*, 2010).

The box on the top of Figure 13 shows the Alpine-Carpathian orogenic belt to which Western Carpathians belong, as a result of the Late Jurassic-Tertiary subduction-collision between the North-European platform and drifting continental fragments from Apulia/Adria.

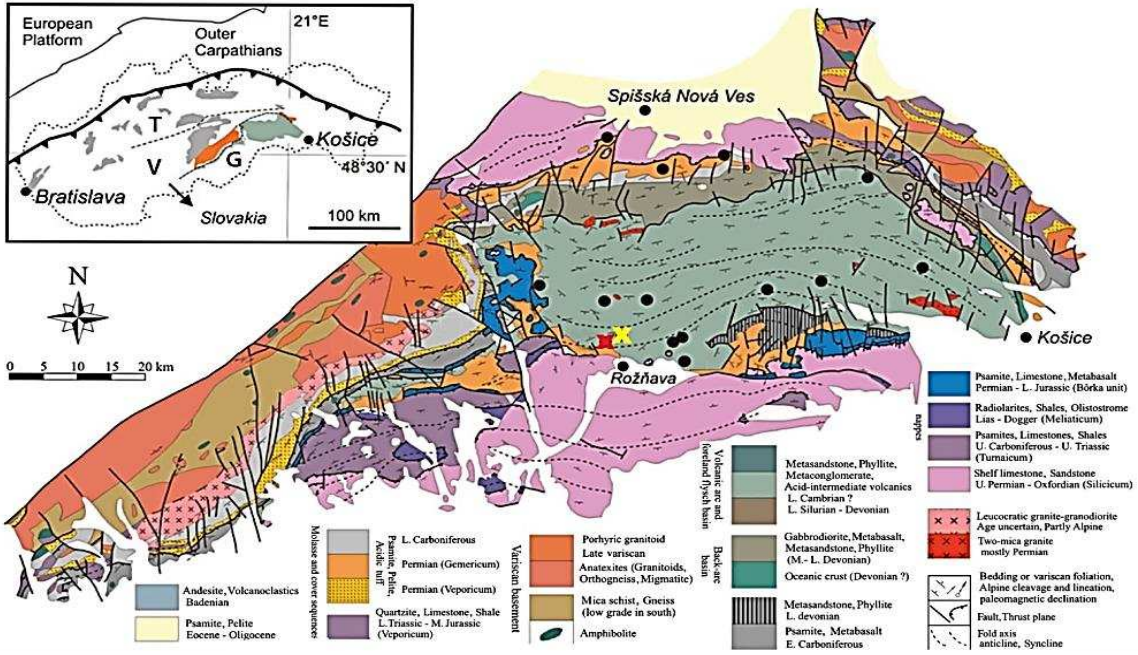

Figure 13 - Geological map of the Gemeric unit where the Rosenau deposit locates (modified from Hurai *et al.,* 2008). The yellow and red crosses indicate the Mária and Nadabula mines respectively, both belonging to the town of Rožňava. The three Slovakian tectonic units are evidenced (T = Tatric, V = Veporic and G = Gemeric). Full circles correspond to siderite, barite or quartz-stibnite veins.

The event gave rise to three tectonic units in Slovakia: the Tatric, thrusted under the Veporic, lying in turn over the Gemeric. The latter unit is where more than a thousand of hydrothermal veins concentrate parallel to regional metamorphic cleavage (Hurai *et al.,* 2008). The Gemeric unit is predominantly made of Palaeozoic low-grade volcano-sedimentary rocks intruded by Permian granite bodies produced by continental rift. The veins can be divided into siderite-barite-polymetallic and quartz-stibnite type. Cinnabar can be found in the later sulphide stage of the quartz-stibnite-sulphides paragenesis, which concentrates in specific veins (Artur-Terezia, Sadlovsky, Štefan, Kliment, Augusta and Siedmažila), according to Rybár *et al.* (2010). It occurs with native mercury, probably in the Upper Cretaceous, after ankerite paragenesis with chalcopyrite, tetrahedrite and bournonite, as summarized in Table 5.

Table 5 - Paragenesis of the quartz-sulphides hydrothermal mineralization of the Rosenau deposit (modified from Hurai *et al*., 2008). Abundance is reported as high (thick line), medium (thin line) or low (dotted line).

Phase	Quartz-sulphide veins (later stage)
Sericite	
Ankerite	
Pyrite	
Chalcopyrite	
Cinnabar	

The genesis of these veins is probably both concomitant of the opening of the hydrothermal system and of the reduction of the overburden due to uplifting and unroofing. Hurai and co-workers (2008) suggested that this system was probably open when sulphides crystallization happened. They fixed the mineralization in the Late Cretaceous, due to transpressive shearing and extension in a heterogeneous gas-aqueous mixture, in opposition to the previous deposition of siderite in a closed system with homogeneous brine.

CHINESE DEPOSITS

The Chinese strata-bound mercury deposits occur mainly on Cambrian marine carbonate rocks, bearing fossils and organic matter. When the deposition is syngenetic, the veins are intra-layer, without crossing stratigraphic units. Tectonic plays an important role in determining the presence of preferential sites of deposition or remobilizing Hg (Figure 14).

According to Zhang (1996), the link with magmatic rocks can be excluded. A 3-step genetic mechanism has been proposed:

1. ***Enrichment*** – ore-forming compounds are present as gases or complexes. They can be introduced in the marine sediments through the faults system.
2. ***Sedimentary diagenesis*** – origin of source bed and host strata; they correspond to marine sediments rich

in fossils and organic matter, where the ore-material is still not present in economically significant amounts; mineralization occurs after physico-chemical changes and for adsorption in the marine sediment itself; it appears disseminated in veins limited to specific stratigraphic units.

3. ***Epigenetic reworking*** – tectonic produces deformations through folding and faulting, with the concomitant action of meteoric water; the final products can derive both from the reworking of beds and/or host-rocks and from the action of deep hydrothermal fluids; these stockwork orebodies have various forms (veins, pods, columns, etc.).

Cinnabar is the main mineral in the mercury ores. It is essentially pure but further elements have been detected in traces: germanium, selenium, cadmium, indium, tellurium and thallium are reported by Zhang (1996). Selenium is the most abundant, its concentration ranging from 9 to 3980 ppm.

Figure 14 - Schematic map of the Chinese deposits of cinnabar (modified from Ping Li *et al.*, 2008).

Gongguan

The mineral district of Gongguan-Huilong is located in the South of the Shaanxi province. It includes two different deposits: Gongguan Hg-Sb-Au deposit and the Qintonggou Hg-Sb deposit. The orebodies of these mines are dispersed in irregular masses and veins within the Late Devonian argillaceous dolostones (Zhang *et al*., 2014). Mineralization is located in the northern and southern wings of the Gongguan Anticline, forming two belts. The northern one is called "Hg-only", Sb mining being absent; in the southern belt antimony predominates. The mineralization can be disseminated, aggregated, brecciated or drusy. Cinnabar occurs with stibnite and pyrite; sphalerite, orpiment, realgar, galena, stibiconite, kermesite, valentinite, metacinnabar, native Sb, chalcostibnite, tetrahedrite, digenite, malachite and native Hg are present in small amounts. Gangue minerals are milky quartz, dolomite and calcite with minor gypsum, barite, fluorite and clay minerals. Zhang and co-workers (2014) identified 3 stages of mineralization summarized in Table 6. The earliest coincides with dolomitisation and recrystallization of pre-existing carbonate rocks with the association quartz-dolomite-pyrite-stibnite in veins or replacements. Cinnabar belongs to a medium stage, with quartz, stibnite and carbonates. In a later stage, calcite ± quartz veinlets cross-cut the pre-existing ones. According to Zhang (1996), two different hydrothermal fluids are involved in the genetic

process: meteoric water at shallow levels, responsible for the extraction of sulphur, but also fluids from deeper levels, carrying Hg, Sb, radiogenic Sr and HREE. These led to the formation of orebodies younger than the surrounding rocks (Jurassic-Cretaceous/Yenshanian into Devonian).

Table 6 - Paragenetic sequence of the hydrothermal minerals in the province of Shaanxi (modified from Zhang *et al*., 2014).

Mineral	Early	Medium	Late
Dolomite			
Quartz			
Calcite			
Barite			
Stibnite			
Cinnabar			
Sphalerite			
Pyrite			
Metacinnabar			
Galena			

Wanshan

The Wanshan deposit is located in the eastern part of the Guizhou province, in the South-West. It is considered the largest Hg-producing area in China. According to Qiu *et al.* (2005), mining at Wanshan started in the Qin Dynasty (221 BC) and ceased in 2001. This sedimentary reworked mercury deposit is made of thin-layered and laminated fine-grained

dolomite and limestone beds from the Cambrian. The mines belong to an open anticline in the so-called Hunan-Guizhou mercury zone. Silicification and carbonization are common while bituminization, pyritization and baritization have minor occurrence. Epigenetic reworking processes are testified by the diversified appearance of the mineralization: it can be disseminated, brecciated, in veins, banded, massive or drusy. Hydrothermal low-temperature activity is testified by the abundant presence of organic matter and a recurrent association of bitumen with cinnabar. Cinnabar can be also associated to stibnite, sphalerite, native Hg, Zn-metacinnabar and pyrite. Gangue minerals are mostly quartz, calcite, dolomite and barite. Rhythmic sequences of cinnabar-quartz-calcite in thick layers (0.005-0.15m) are common.

SUMMARY

A schematic representation of the main cinnabar mineralization that will be the object of this research is represented in Figure 15 (International Chronostratigraphic Chart 2016 modified with data from Brogi *et al*., 2011; Zhang 1996; Lavrič & Spangenberg 2003; Higueras *et al*., 2000).

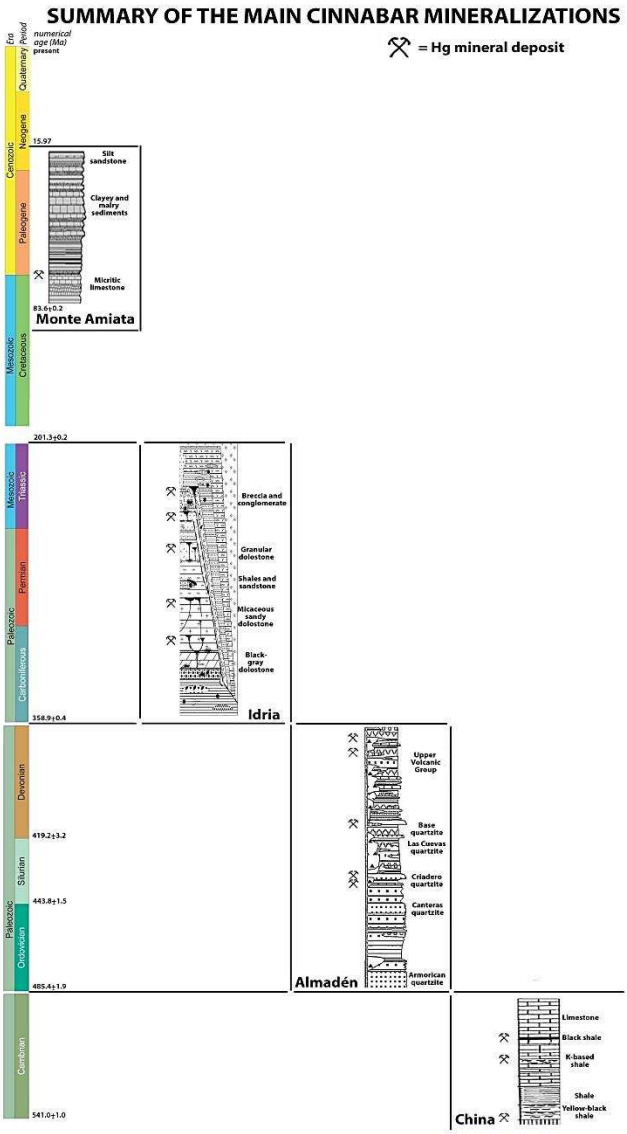

Figure 15 - Schematic representation of the main cinnabar mineralization object of the present study.

1.5 MATERIALS AND METHODS

Thanks to the collaboration with the Mineralogical Museum of the Universities of Rome, Florence and Pavia and the Natural History Museum of Venice, 44 samples of cinnabar have been collected. They come from the main mining localities, as reported in Table 7.

Table 7- List of the samples of cinnabar collected from different museums (MMUR = mineralogical museum of the university of Rome "Sapienza", MMUFI = Mineralogical Museum of the University of Florence, MMUPV = Mineralogical Museum of the University of Pavia, MSNVE = Natural Sciences Museum of Venice); n.c. stands for "not classified" and it corresponds to a private sample.

Sample	Mine	Museum Code
AS1974	Almadén, SPAIN	MMUFI - 1974 G
AS1981	Almadén, SPAIN	MMUFI - 1981 G
AS1991	Almadén, SPAIN	MMUFI - 1991 G
AS2026	Almadén, SPAIN	MMUFI - 2026 G
AS2029	Almadén, SPAIN	MMUFI - 2029 G
AS20854	Almadén, SPAIN	MSNVE - 20854
AS2815	Almadén, SPAIN	MMUPV - 2815
AS54	Almadén, SPAIN	MMUR 1182 - 54
AS60	Almadén, SPAIN	MMUR 1188 - 60
AS61	Almadén, SPAIN	MMUR 1189 - 61
AS64	Almadén, SPAIN	MMUR 1192 - 64
AS76	Almadén, SPAIN	MMUR 1204 - 76
B44	Loc. Hořowitz or Horowice, Bohemia, CZECH REPUBLIC	MMUR 1172 - 44
C15	Carnia (UD), ITALY	MMUR 1143 - 15
C2838	Carnia (UD), ITALY	MMUPV 2838
C34	Loibel Valley, Carnia (UD), ITALY	MMUR 1162 - 34
CH124	Tsa Tien Mine or modern Chatian Mine, Hunan, CHINA	MMUR 22367 - 124

Sample	Mine	Museum Code
CH125	War Shan-Chang Nmer, Guizhou (Kweichow), CHINA	MMUR 22369 - 125
CH126	War Shan-Chang Nmer, Guizhou (Kweichow), CHINA	MMUR 22368 - 126
CH2015_F	Hunan, CHINA	n.c.
CH2015_P	Hunan, CHINA	n.c.
GE46	Moschellandsberg, GERMANY	MMUR 1174 - 46
GR13	Grosseto, ITALY	n.c.
GR141	Cerreto Piano, Scansano (GR), ITALY	MMUR 24048 - 141
GR2814	Grosseto, ITALY	MMUPV - 2814
I13	Idria, SLOVENIA	n.c.
I2042	Idria, SLOVENIA	MMUFI - 2042 G
I2098	Idria, SLOVENIA	MMUFI - 2098 G
I23101	Idria, SLOVENIA	MSNVE - 23101
I24	Idria, SLOVENIA	MMUR 1152 - 24
I2841	Idria, SLOVENIA	MMUPV - 2841
LU10	Serravezza (LU), ITALY	MMUR 1137 - 9
LU9	Val di Castello, Pietrasanta (LU), ITALY	MMUR 1138 - 10
MA2	Miniera del Siele, Castell'Azzara, Monte Amiata (SI), Italia	MMUR 25278 - 2
MA2129	Miniera San Filippo, Monte Amiata (SI), ITALY	MMUFI - 2129 G
MA2136	Abbadia San Salvatore, Monte Amiata (SI), ITALY	MMUFI - 2136 G
MA2169	Monte Amiata (SI), ITALY	MMUFI - 2169 G
MA23100	Monte Amiata (SI), ITALY	MMUFI - 2169 G
MA2831	Monte Amiata (SI), ITALY	MMURPV - 2831
R110	Saizewka, Nikitovka, Charkov train station, Asow, UKRAINE	MMUR 18878 - 110
R2822	Nikitovka Donetz, UKRAINE	MMUPV - 2822
S113	Monte Avala, SERBIA	MMUR 19289 - 113
SYN	Synthetic from SIGMA ALDRICH	243566-50G
U37	Rosenau, SLOVAKIA	MMUR 1165 - 37

All the samples were analysed by X-ray powder diffraction (XRPD) and μ-Raman spectroscopy. Some samples were also chosen for preliminary tests by inductively coupled plasma-mass spectrometry (ICP-MS). The former, when combined to the Rietveld refinement, gives information about crystal structure, cell volume, texture and stress of the sample, all parameters depending on the genesis of the mineral. The latter two give the chemical information on the sample, nominally at molecular and trace elemental scale, respectively. The basic idea is that the statistical merging of both kinds of data could give a distinctive fingerprint of provenance, being all these parameters related to the environment where the mineral grew and underwent modifications.

XRPD AND RIETVELD REFINEMENT

Recent studies (Maras *et al.*, 2013) have demonstrated that conventional XRPD coupled to Rietveld refinements can individuate differences in unit cell parameters and volume among cinnabar samples of different provenance. Those differences are possibly related to variations of the Hg/S ratio. This section can be therefore conceived as a deeper investigation on the topic: the systematic coupling of XRPD with Rietveld refinement allows evaluating significant modifications of the unit cell. In general, unit cell variations can be substantially attributed to two factors: compositional variability or different thermobaric conditions occurring during

crystallization. The first factor refers to cation/anion substitution processes or/and defects occurring within the cinnabar structure. In fact, it has been shown that a deviation of the Hg/S ratio from the ideal value of 1.00 is responsible for detectable variation of cell parameters (Potter & Barnes 1978; Sharma & Chang 1993). The second factor includes the thermodynamic parameters - *i.e.* temperature, pressure, etc. - influencing crystallization and affecting microstructural parameters as micro-strain (Ballirano & Sadun 2009) as well.

To obtain structural data, a preliminary step was necessary: cinnabar samples were mechanically purified from accessory mineralogical phases under a stereo-microscope. The selected material, even with some residual impurities, was ground under ethanol in an agate mortar. A minimum amount of powder (< 5 mg) was then loaded and packed in a non-hermetically sealed borosilicate glass capillary (0.3 mm diameter). The capillary was aligned onto a standard goniometer head and diffraction data were collected on a focussing-beam *Bruker AXS D8 Advance* at the Department of Earth Sciences of the University of Rome "Sapienza". It operates in transmission, θ-θ geometry, using Cu K_α radiation and it is fitted with a *PSD VÅNTEC-1* detector set to a 6° 2θ aperture. Data were collected in the 20-145° 2θ angular range, step-size of 0.022° 2θ, with 3 s of counting time (Ballirano *et al.,* 2013). The goal of the Rietveld analysis is to fit a structural model - i.e. the crystal structure of cinnabar in the present study - to the collected powder diffraction data (Young, 1993).

Diffraction data were evaluated by the Rietveld method using TOPAS v.4.2 (Bruker AXS 2009). Starting structural data of cinnabar were taken from Schleid *et al*. (1999). Peak shape was modelled through the fundamental parameters approach (FPA). Absorption was modelled following the Sabine model for cylindrical samples (Sabine *et al.,* 1998). The background was fitted with a 36-term Chebyshev polynomial of the first kind. Such a large number of terms was required for a proper fit of the amorphous contribution of the glass-capillary. Preferred orientation was modelled by means of spherical harmonics (six refinable parameters up to the 6th order), following the procedure of Ballirano (2003).

The goodness of the fit is expressed by the χ^2 and by the residual functions $R_p = \frac{\sum|I_O - I_C|}{\sum|I_O|}$ and $R_{wp} = \sqrt{\frac{M}{\sum|I_O|}}$, where I_o and I_c are respectively the observed and calculated (gross) intensities and $M = \sum_i w_i(I_o - I_c)^2$. The D_{dw} parameter can be also taken into account, being it a statistical measure of the serial correlation in the powder pattern differences ($\Delta = I_o - I_c$) as given by Durbin and Watson (Hill & Flack 1987). It is calculated as $\mathrm{D_{wd}} = \frac{\sum_{i=2}^{N}\left(\frac{\Delta_{Io}}{\sigma_{Io}} - \frac{\Delta_{Io-1}}{\sigma_{Io-1}}\right)^2}{\sum_{i=1}^{N}\left(\frac{\Delta_{Io}}{\sigma_{Io}}\right)^2}$.

Its value tends to 2, if the refinement is not affected by serial correlation of the residuals. Finally, the R-Bragg value is also calculated to determine the goodness of each fit, intended as the R value derived from the I_K intensity, *i.e.* the intensity

assigned to the K_{th} Bragg reflection at the end of the last TOPAS run, $R_B = \frac{\sum|I_{kO} - I_{kC}|}{\sum|I_{kO}|}$ (Young, 1993).

The refined parameters are: the unit cell parameters ***a (Å)*** and ***c (Å)***, the volume ***V (Å^3)***, the crystallite size ***Cry size***, the fractional coordinate of mercury and sulphur, x_{Hg} and x_S respectively, the displacement parameters for both atoms, B_{Hg} and B_S and the micro-strain ε_0.

According to Potter and Barnes (1978), a correlation exists between the cell parameters of cinnabar and its Hg:S ratio. In particular, a regression equation was derived from the cited reference, for the volume: V (Å^3) = 153.8(5)-12.3(5)·[Hg/S].

This equation was used to extrapolate the Hg:S ratio for the samples under investigation.

μ-Raman

The cinnabar sample-set was also analysed by Raman micro-spectrometry, using a HORIBA Xplora Raman microscope, with capacity increased to 100×, and charge coupled device (CCD) detector. Laser wave-length of 632.8 nm (red He–Ne laser line) was used for excitation.

Wavenumber calibration was performed with the Raman peak of a silicon crystal at 520 cm^{-1}. The laser beam was focused on the grains of the mineral, in fragments or in powder, with 10× objective lens. The laser power at the surface of the sample was held to ≤ 1.0 mW, to avoid any possible alteration of the sample. Raman spectra were obtained in scanning mode, after

five scans in the 100-1250 cm^{-1} range, with acquisition time of 10 s and spectral resolution of 2.7 cm^{-1}. Three or more close spots on the sample surface were analysed. The following instrumental conditions were applied for the analysis of each spot (Table 8):

Table 8 - Instrumental conditions in the μ-Raman analysis. The following abbreviations are chosen: obj. = microscope objective; exp.t. = exposure time; acc.nr = accumulation number.

Laser (nm)	Filter (%)	Hole	Slit	Grating	Obj.	Exp. T.	Acc.nr.
638	25	100	100	1200 T	10 x	10	5

These operative conditions were applied to preventively remove at best the possible sources of background from luminescence processes, non-laser-induced emissive processes or Raman scattering from sources different from the analyte (Maes, 2003). They also allowed revealing the typical doublets of the E degenerate modes of cinnabar. The samples B44 and R110 were measured both in powder and as fragments. For the samples CH2015_P, SYN, and U37, only the powder was available. The samples *AS54*, *AS60, AS61, AS64, AS76* and *AS20854* could only be recorded with a 600T grating: at this lower resolution some of the typical Raman lines of cinnabar could not be identified. Thus, these samples were excluded from data treatments.

Two strategies can be recorded when multivariate statistics is applied to Raman data:

a) each wavenumber is considered as a variable of the PCA matrix;

b) spectral parameters, such as the width/position of the characteristic deconvoluted bands, are used as PCA variables.

In the present work, it was established to assess the efficiency of ***type b)*** strategy with the Origin 9 software package (OriginLab, Northampton, MA).

First of all, some spectral manipulations, such as baseline correction and smoothing were required. To minimize problems of comparison within spectra having different intensities, each spectrum was preventively normalized, so that the smallest absorbance was set to 0 and the highest to +1. Band component analysis was then necessary to perform ***type b)*** investigation. For this purpose, the *Fit Peaks* function was used, after background subtraction (8 anchor points interpolation, spline function) and 2nd derivative positive peak finding on a Savitsky-Golay smoothed curve (10-12 order, 20-22 points window). The 2nd derivative method was chosen in order to reveal hidden doublets (Frost *et al*., 2002; Gotoshia & Gotoshia 2008). In this way, deconvolution was operated assuming the peaks to follow a Gaussian function with the minimum number of component bands used for the fitting process. When the fitting converged, the following parameters were obtained as output for each Raman band:

- ***Peak Area by Integrating Data***, defined as the area between the peak data and the baseline, which will not be considered in the statistical treatment of the data;
- ***Full Width at Half Maximum (FWHM)***, which is the peak width at half the peak maximum value;
- ***Peak Maximum Height***, *i.e.* The Y value for the peak maximum, being Y the normalized Raman Intensity;
- ***Peak Gravity Centre***, which corresponds to the X value of the peak maximum;
- ***Peak Area by Integrating Data (%)***, which is the result of the integration to find the area between the peak data and the baseline, the result being expressed as a percent of the total area.

In the picture below, an example of the entire spectral manipulation is reported (Figure 16):

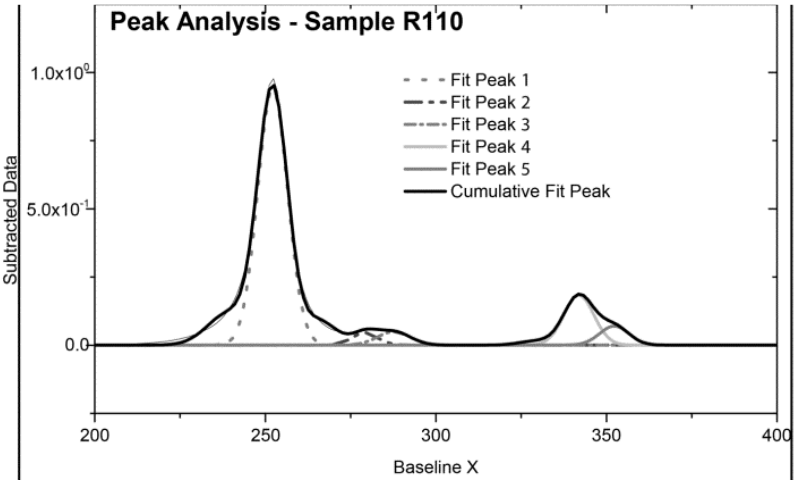

Figure 16 – Example of the peak deconvolution for the average spectrum of sample R110.

Of those parameters, *Peak Maximum Height* was not considered in the multivariate statistical treatment. In fact, intensity is sensibly affected by instrumental parameters. At least, intensity ratios were calculated to minimize the errors due to measuring conditions.

Finally, it was establish to treat each spot as a single specimen. Since vibrational modes act on the position of the Raman bands, we do not expect to see variation of this parameter (Peak Gravity Center) within spots from the same sample. Descriptive statistics were then calculated for the position of the most intense peak at ~252 cm^{-1} so that only the spots belonging to the same sample and showing a standard deviation lower than 0.1, were retained for statistical treatment. This led to the exclusion of the following spots: *AS1981 1fr1, AS2029* (all spots), *B33 fr3, B44 p3, C16 fr1, C16 2fr2, CH124 1fr1, CH125 3fr1, CH126* (all spots), *CH2015_F 3fr1, CH2015_P p2, GE46 p3, I24 3fr1, LU9 1fr1, MA2129 1fr2, MA2136 and MA2169* (all spots), *R110 1fr2, R110 p1, R2822 1fr2, SYN p2, U37 1p/fr2.*

ICP-MS

Inductively coupled plasma mass spectrometry was performed at the Laboratory for Advanced Analytical Technologies (Abteilung 502) of EMPA (Swiss Federal Laboratories for Materials Science and Technology) in Dübendorf, Switzerland.

Since no publication deals with ICP-MS analysis of cinnabar for archaeometric investigations, a first, ***fast semi-quantitative investigation*** (FAST-QUANT) was carried out on a selection of samples to have a quick overview of the elements that must be evaluated. It was necessary to establish which elements were in traces (less than 0.1% in the definition by Rollinson, 1993) in the sample-set and could be discriminant for cinnabar provenance studies. After the list of elements was assessed, their concentration was measured on the entire sample-set at higher resolution, using a ***sector field detector*** (SF-ICP-MS).

FAST-QUANT

One sample for each main mining locality (Almadén, Monte Amiata, Idria, Nikitowska, Avala and Hunan) was selected. The provenance from all the Museums was a further selective criterion. The chosen samples were: AS1991, MA2136, R2822, I23101, S113, CH2015. These samples were digested following the procedure suggested by Mazzocchin *et al.* (2008). An amount of cinnabar ranging from 31 to 40 mg was added to a solution with 2 mL of nitric acid (65% w/w) and 3 mL of hydrochloric acid (30% w/w). Both reagents were of Suprapur® quality, from Merck (Merck GmbH). Blank digestion samples were prepared following the same procedure. Acid digestion (30' program at 453 K) in a Milestone MLS 1200 Mega high performance microwave digestion unit was followed by cooling and filling up to 10 mL with deionized water.

The calibrating standard solution was prepared as follow: 50 µL of the multi-element standards Merck IV (Merck, Germany) and 50 µL of Spexchemical Claritas PPT multi-element solution 1 (CLMS-1) were added to a 15 mL HCl and 10 mL HNO_3 solution. The solution was then diluted up to 50 mL with 18 MΩ/cm deionized water, prepared with a high purity water device "MilliQ Gradient A" (Millipore AG, Switzerland). Elements were quantified with the ELAN 6000 ICP-MS from Perkin Elmer (SCIEX, Canada).

The elements which gave relevant signal intensities were: ***Te, Cu, As, Se, Rb, Sr, Mo, Cd, Sb, Ce, La, Pr, Nd, Sm, Eu, Gd, W, Tl, Pb, Bi, Th*** and ***U***. Any other element was excluded from further investigations.

SF-ICP-MS

Since the digestion in 2 mL of HNO_3 and 3 mL of HCl was not complete, its efficiency was improved adding 0.5 mL of hydrofluoric acid. Standard solutions for all elements were prepared through the following steps:

1. 500µL of each single-element standard solution were put into the same tube and the final solution was brought to 50mL volume with HNO_3 of Suprapur® quality, from Merck (STANDARD 1 = 10mg/L);
2. 500µL of STANDARD 1 were put in a second tube and brought to 50mL volume with HNO_3 (STANDARD 2 = 100µg/L);

3. From STANDARD 1 and 2, standard solutions at lower concentrations were obtained[9].

The concentrations of the chosen elements were calculated from the high resolution magnetic sector field ICP-MS Thermofinnigam Element II measurements, using rhodium as internal standard. Signal intensities were background-subtracted and converted into concentrations from the following equation:

$$C_C\ (\mu g/g) = \frac{C_M \cdot \mathrm{DF} \cdot 0.01}{\mathrm{Wt}_S \cdot 10^{-3}(\mathrm{g})}$$

where C_C is the corrected concentration, C_M is the measured signal, DF is the dilution factor assumed to be 1, and Wt_S is the original weighted amount of sample (converted from mg to g).

[9] STANDARD 2 gave 0.5µg/L, 1µg/L, 2µg/L and 5µg/L concentrations by adding 250µL, 500µL, 1000µL, 2500µL respectively to a solution of 15mL HNO_3 + 10mL HCl then brought up to 50mL volume with distilled water. From STANDARD 1 the concentration of the final standard solutions were 10µg/L, 20µg/L and 50µg/L by taking 50µL, 100µL, 250µL respectively and adding 15mL HNO_3 + 10mL HCl then up to 50mL volume with distilled water.

STATISTICAL DATA TREATMENT

When dealing with statistical treatment of archaeometric data, one must take into account that Arts Objects are heterogeneous, individually distinct in composition, form and history. For this reason, the statistical procedure must be properly assessed in advance, as a function both of the scientific questions to be answered and the structure of the data collected, as evidenced by Reedy & Reedy (1988). The final target of this section is to define a methodology which clearly identifies statistical relationships among samples from the same locality. To do that, trace element data were statistically analysed as follow:

A. Histograms, to detect correlations between different elements in samples from the same locality;
B. Spider diagrams, as defined in Rollinson (1993), to determine the elements showing higher variability and thus characteristic of a single sample or quarry;
C. Binary plots, to underline possible correlations among elements;
D. Principal component analysis to evidence clusters of provenance;

All the steps of the statistical analysis have been carried out using the Origin 9 Software package (OriginLab, Northampton, MA).

Spider diagrams are plots where the measured concentrations are visualised for all the chosen elements in a

scatter + line graph. This kind of data processing is used to detect inter-element associations, as Green & Watling (2007) and Iriarte *et al.* (2009) have done for the provenance of ochres. The comparison of all samples gives an overview on the elements with similar variability among those from the same locality. Spider diagrams and ***bar graphs*** were used to choose elements that could be further compared though bivariate or multivariate statistic.

Binary plots were used to represent the measured concentration (ppm) of one element (y axis) as a function of another (x axis). Their comparison underlines possible correlations and, if these are determined by the same genetic environment, clusters of provenance. Eventually, log10 scale was used.

The same tools were used to compare the parameters calculated from the Rietveld refinement of XRPD data, but also considering as variables the parameters describing the bands identified in the Raman spectra. In particular, the attention was focused on the relative area and position of minor bands resulting from the deconvoluted spectra, following the provenance investigation on Mediterranean obsidians by Bellot-Gurlet *et al.* (2004).

Principal Component Analysis (PCA) was used as a final tool to define clusters of provenance on a larger set of variables. Multivariate analysis has been widely used since the 1980s in archaeometric researches based on elementary data. Applications have been extended to marbles (Moens *et al.*,

1988), pottery (Méry & Schneider, 1996; Marengo *et al*., 2005; Aldrabee & Wriekat, 2011) and glass (Janssens *et al.,* 2000) with the target of detecting clusters of provenance for the raw materials.

In the present study, principal component analysis was firstly applied on the data from a single instrumental technique. In a second step, it was also used to merge variables from different methodologies. Structural data from XRPD and chemical results, both from ICP-MS and Raman analysis, were thus compered.

1.7 FINAL REMARKS: PROVENANCE ASSESSMENT CRITERIA

The combination of structural and compositional data has demonstrated to be an effective tool to gain important information on the provenance of cinnabar.
The possibility to recognize samples from China is given by the individual analysis of data from each technique.
A fast, visual recognition of the samples from the same locality is given by the inspection of the Raman spectra. All the samples from China have shown to be characterized by the presence of selenium, proved by the additional band at ~200 cm^{-1}, with the only exception of the sample *CH2015_P*. The higher ionic radius of selenium is consistent with the increased volume found by X-ray diffraction. Moreover, the coupling of Raman analysis with multivariate statistics suggests that the position of the most intense band at ~252 cm^{-1} has also influence in the discrimination of the Chinese samples.
Raman analysis gives a further insight once the influence of the optical phonon mode at ~350 cm^{-1} is assessed by principal component analysis. This analysis demonstrated that the high purity of a synthetic product may be revealed by the Raman investigation, leading to the discrimination from the natural sources.

X-ray diffraction demonstrated that the Chinese samples have an enlarged unit cell, the distension being more

pronounced along the *c* axis. The recognition is also confirmed once the strain is compared to the volume: a correlation is verified for the samples from European localities, apart from China.

The preliminary chemical inspection carried out by SF-ICP-MS, coupled with principal component analysis, indicates that specific elements are linked to different localities. The Chinese samples could be, once again, easily discriminated from the concentrations of *Se, Cd* and *Sb.* This finding confirms the information previously obtained for selenium. Interestingly, a cluster from Almadén is also partially revealed from the PCA. The influence on its distribution is mainly due to cobalt while *As* was found to be representative for the Russian sample. However it must be remarked that all the European localities are distributed in the same quadrant, making the recognition more difficult. The only exception is the sample from Avala, Serbia. It is clearly recognized, since it is located alone in the lower right quadrant. This finding may have particular importance in the recognition of a local source, being the Prehistoric use of cinnabar recently documented in the nearby site of Vinča. Future studies may verify whether these impurities may be retained during the preparation of the pigment, thus being a marker of provenance even if they do not come directly from cinnabar.

The statistical merging of the structural and chemical data gave further insights: it suggested that their coupling strengthens the discrimination of China, but also of Almadén,

Idria and Russia. In particular, the analysis confirmed that the major influence on the distribution of the samples from China is due to the unit cell volume and to the concentration of *Se, Cd* and *Sb*. As previously explained, the presence of selenium as isomorphic impurity is responsible for the increased volume of the Chinese cinnabar and it leads to its recognition. One of the most significant findings to emerge from this procedure is the possibility to discriminate the samples from Idria to those from Almadén, never achieved in previous works. However, it was not possible to demonstrate that this procedure has the same efficiency for samples from Tuscany.

The most important limitation of the present research lies in the lack of chemical data. The difficulty in the digestion of the samples for ICP-MS and the scarce literature on the same topic led to limit the sample size. This corresponds, of course, to a source of weakness in multi-statistical treatment that usually deals with large sets of data. Further research is needed to implement the chemical data and verify the present findings. However, a preliminary protocol has been produced and summarized in the chart below (Figure 30):

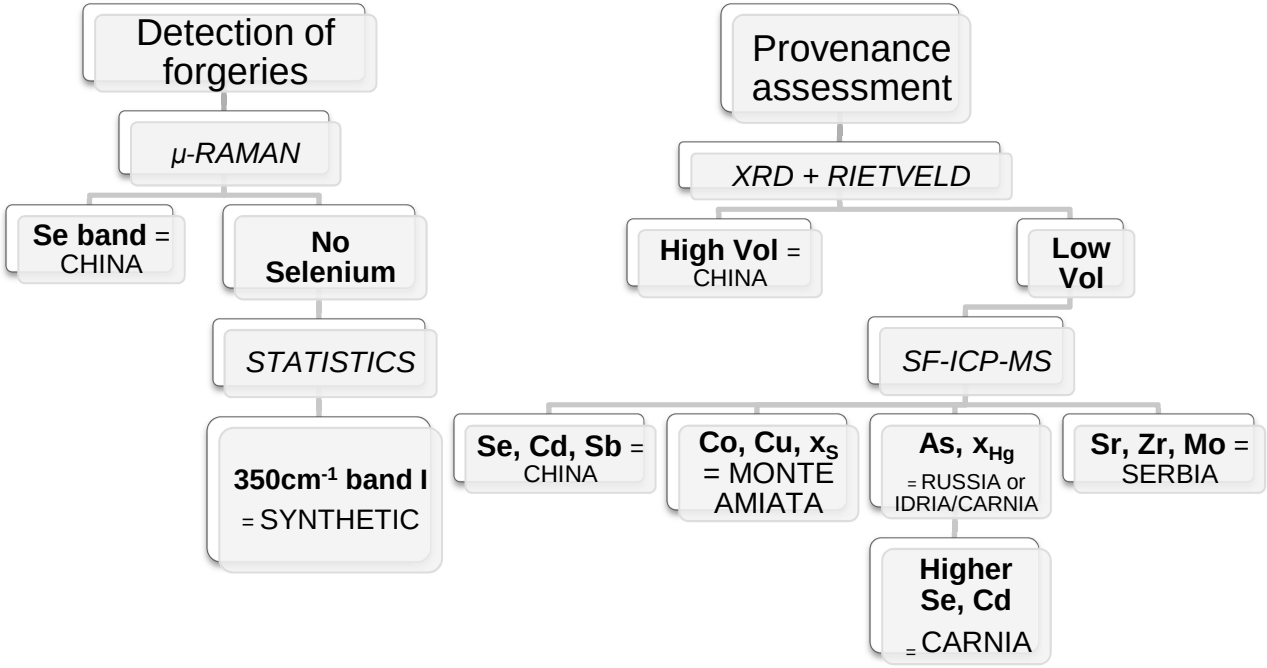

Figure 30 - Flow chart summarizing a preliminary standard protocol for the assessment of cinnabar provenance and for the detection of forgeries.

Despite its exploratory nature, this study has to be considered as a successful test to get information of provenance from a single technique, such as Raman spectroscopy or X-ray diffraction coupled with Rietveld refinement. The recognition of the Chinese samples is fast and has strong implications in the field of Cultural Heritage. These findings provide a framework for the study of ancient commercial routes, especially the use of Oriental sources in the Western area. The attribution of a sample to the Oriental mines can be easily carried out by a technique which is fast and non-destructive, both criteria that are of primary importance in the study of unique artworks. The assignment of a sample of unknown origin to the same cluster could also play a role in the detection of forgeries or retouching. Furthermore, the discrimination of synthetic cinnabar by Raman analysis, when coupled with PCA, has primary importance in a systematic validation of historical references. In fact, the use of synthetic cinnabar is documented from the 8th century AD, despite there is no information about the local spread of these recipes. In this sense, future research is required to determine whether ancient recipes can be discriminated by Raman analysis as well as the modern synthetic cinnabar of the present investigation.

SECTION 2: RED OCHRE

"Sandro sembrava fatto di ferro,
ed era legato al ferro da una parentela antica:
i padri dei suoi padri, mi raccontò,
erano stati calderai ("magnìn") e fabbri ("fré")
delle valli canavesane,
fabbricavano chiodi sulla sforgia a carbone,
cerchiavano le ruote dei carri col cerchione rovente,
battevano la lastra fino a che diventavano sordi:
e lui stesso, quando ravvisava nella roccia
la vena rossa del ferro,
gli pareva di ritrovare un amico."

(P.L. – Il sistema periodico)

Red and yellow ochre are in artists' palette from Prehistory. This is due to aesthetic preference for these hues, as testified by the first examples of paintings in Art History. Another reason is their easy availability. Conservation science has also adduced a third evidence for the red: man has soon learnt to synthesize red ochre by simple heating of the yellow one. The process was certainly known by Romans, as Pliny the Elder states in his *Naturalis Historia* (trans. Rackham *et al*., 1963). Quite recent studies date it back to Prehistory, as Pomiès reported in 1999 for the Paleolithic site of Troubat, France (1998).

The present section is a systematic study to define the best, less invasive methodology in the discrimination of synthetic and natural red ochres. After the laboratory synthesis of both precursory goethite and hematite, the latter derived both from natural and synthetic yellow ochre, all samples have been characterized by means of different analytical techniques. This is to understand which instrument – or a combination of more than one – has higher efficiency in the distinction of synthetic and natural red ochres. In fact, no standard procedure is already available to distinguish synthetic and natural red ochre, Pomiés work (1997, 1998, 1999) being the only one in Cultural Heritage.

The sample-set includes: a sample of synthesized goethite produced in laboratory, some natural and commercialized samples of yellow ochre, some natural and commercialized samples of red ochres and the synthesized red ochre obtained by heating the yellow ones. Red and yellow ochre have been analysed by different diagnostic techniques: scanning electron microscopy coupled with energy dispersive spectroscopy (SEM-EDS), X-ray powder diffraction (XRPD), Fourier transform infrared spectroscopy (μ-FTIR) and thermal analysis. The synthetic pathway was also reproduced and followed through differential thermal analysis (DTA and TG). In this way information about the elemental and molecular composition of natural samples, together with morphological differences between these and the synthesized ones have been obtained. XRPD has a double function: on one hand, it is

necessary to characterize the mineralogical accessory phases in the natural samples and to verify the purity of synthesized goethite and the heated derivatives, after grinding. On the other hand, it has been used in transmission mode to quantitatively evaluate the structural variations produced by the synthesis. For this purpose, diffraction data have been also evaluated by the Rietveld method.

2.1 THE MINERALS

The colour of ochres is mainly due to iron oxides. These compounds are present in all the compartments of the global system, beginning from terrestrial and marine environment: Fe^{III} oxides formation is a consequence of surface weathering in magmatic rocks. The products are then redistributed by mechanical transport or reductive dissolution. Their concentration increases while Fe decreases in the precursory rocks, as pointed out by Cornell & Schwertmann in 2003 (see Figure 31).

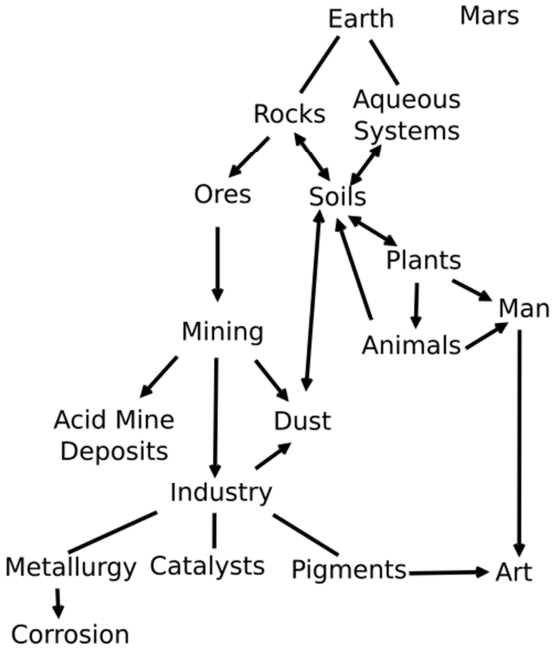

Figure 31 - Iron oxides in the global system, after Cornell & Schwertmann (2003).

In 2010, Triat proposed five mechanisms (eventually overlapping) to describe the origin of ochres:

- ***Metallogenetic***: mainly hematite, in big lamellar crystals (micro or nano-metric) as a mineralization in ancient massifs, which gives extremely pure red ochre if ground. It is usually related to other metallic elements, such as copper. This is a common origin for iron ores;
- ***Volcanic:*** Fe-rich minerals from magmas, after deposition undergo ageing and hydrothermal or surface weathering with subsequent hydrolysis. Fe is released in phreatic water and originates oxides and hydroxides with colour ranging from yellow to red and violet, similar to the metallogenetic ones;
- ***Tropical lateritic***: Close to the equator, the climatic conditions lead to the alteration of all pre-existing rocks into laterite. In this case, hematite and goethite are associated with kaolinite. This kind of alteration can also appear with less extreme weather conditions, leading to the formation of a *gossan*;
- ***Microbiologic***: bio-mineralization involves mainly bacteria and their ability to extract ions from Fe-bearing solutions causing crystallization. The mechanism starts with kaolinite, halloysite and smectite and leads to the deposition of ochres.

- ***Chemical***: secondary product of Cu-based minerals, when treated with sulfuric acid on iron plates giving a strongly hydrated iron sulfate ($FeSO_4 \cdot 7H_2O$).

The most important minerals composing ochre are goethite and hematite. The former is the main colouring agent in yellow ochre and the latter in the red ones. From the heating of goethite or yellow ochres in general, *i.e.* from goethite ***dehydroxylation***, synthetic hematite can be obtained. In the present section, the conversion process will be examined to define a standard protocol for the detection of synthetic hematite in paintings. For this reason, both goethite and hematite features will be described in the following subsections.

CHEMICAL AND STRUCTURAL PROPERTIES

As summarized by Schwertmann and Cornell (2000), the general structure of iron oxides is based on octahedrons, where iron atoms are surrounded by six oxygen and/or hydroxyl units. These units are organized in hexagonally close-packed layers both for goethite and hematite, which are called α-phases. A different arrangement of the $Fe(O, OH)_6$ octahedrons corresponds to a different iron oxide or hydroxide.

Goethite

Goethite, *α-FeOOH*, is the *α* monohydrate of iron oxide, or oxyhydroxide. It is formed by double-bands of edge-

sharing $FeO_3(OH)_3$ octahedron, then linked by corner-sharing. In this way tunnels (dimension equal to 2x1 octahedrons) are created and crossed by hydrogen bridges, as clearly shown in Figure 32.

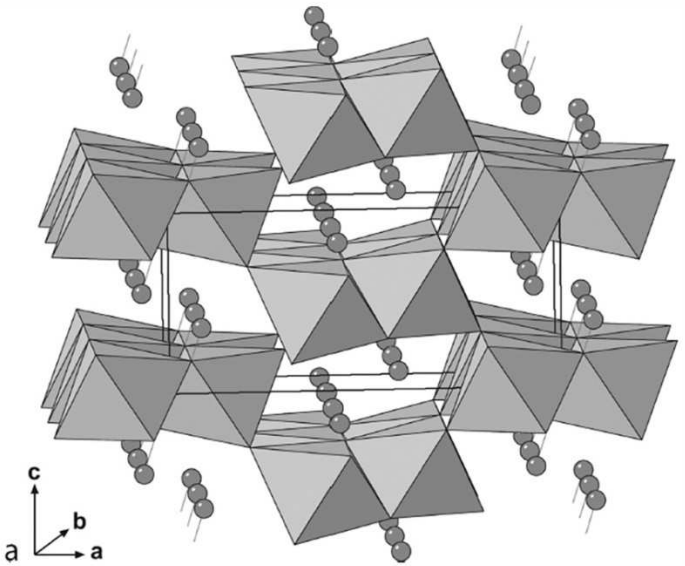

Figure 32 – Idealised structural model of goethite (modified after Schwertmann, 2008). The small balls represent hydrogens in the 2x1-octahedra tunnels.

Goethite crystallizes in the orthorhombic system and can be described either by the space group *Pbnm* (a = 4.587 Å, b = 9.937 Å, c = 3.015 Å according to Lima-de-Faria (1963) or *Pnma* (a = 9.913 Å, b = 3.013 Å, c = 4.580 Å), as proposed by Gualtieri & Venturelli (1999) for an easier comparison with the unit cell of hematite. In the latter case, indeed, the c axis of goethite corresponds to 1/3 of the same axis in hematite (Figure 33b).

Hematite

Hematite belongs to the rhombohedral system, the space group being $R\bar{3}c$ (a = b = 5.0145 Å, c = 13.692 Å, Gualtieri and Venturelli, 1999). The unit cell may also be considered hexagonal.

In the structure of hematite the octahedrons are made of FeO_6 units, which share either edges or faces. They stack perpendicular to the *c* direction. The structure is more compact than in goethite. This is both due to a distortion of the face-sharing octahedrons, with displacement of Fe atoms, and to the absence of H-bonds (Figure 33a).

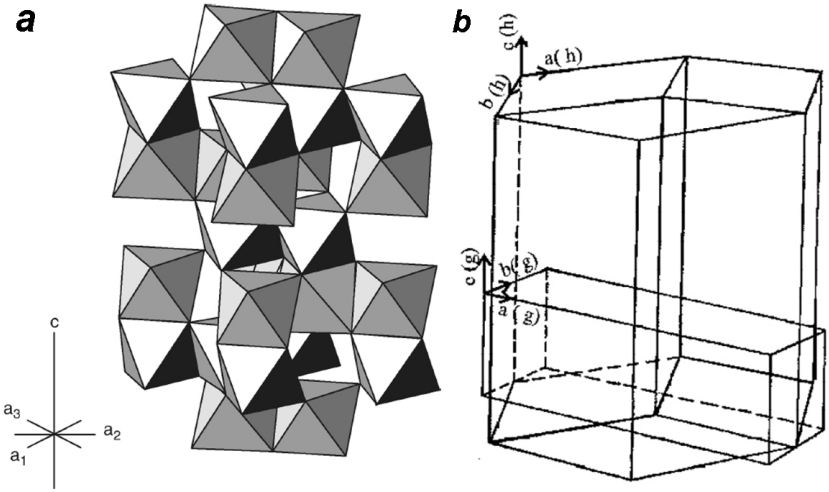

Figure 33 – **a**. Hematite unit cell (modified from Schwertmann, 2008); **b**. Unit cell relationship between goethite and hematite, as pointed out by Gualtieri and Venturelli (1999).

When goethite is heated, it undergoes dehydroxylation and it is converted into hematite without any major breakdown of the atomic patterns (Francombe and Rooksby, 1958). This irreversible pseudomorphic transformation is topotattic. Structural relationships are preserved between the two involved phases: the [001], [110] and $[1\bar{1}0]$ of the newly formed hematite are respectively parallel to [100], [010] and [001] of the precursory goethite (Figure 33b). The process can be described by the crystal-chemical equation (Lima-De-Faria, 1994):

$$2Fe^{o}[O(OH)]^{h} \rightarrow Fe_2^{o}[O_3]^{h} + H_2O \ .$$

The first term is hcp ("h") goethite, with Fe in octahedral coordination ("o"). The second term is hematite, the direct product of goethite dehydroxylation.

OPTICAL PROPERTIES

In plane-polarized light hematite is usually observed in fine-grained particles of translucent to almost opaque red to orange colour. A rounded or bacteroid shape is common, while the platy to tabular appearance is typical of micaceous hematite. The principal habit consists of hexagonal plates or rhombohedra. Also rods, ellipsoids (single or double), cubes, discs or spheres may occur (Eastaugh *et al*., 2008). The mineral has strong dispersion so that the refractive index varies with the light source. The relief is high when the refractive index is

greater than that of the medium. It shows high birefringence under crossed polars, even if masked by the body colour. Hematite has no cleavage, but a weak conchoidal fracture can be observed.

2.2 THE PIGMENT: RED OCHRE

"E reliquis rubricae generibus
fabris utilissima Aegyptia et Africana,
quoniam maxime sorbentur tectoriis.
rubrica autem nascitur et in ferrariis metallis.
ea et fit ochra exusta in ollis novis
luto circumlitis. quo magis arsit in caminis,
hoc melior. omnis autem rubrica siccat
ideoque ex emplastris conveniet igni etiam sacro."

*(*Pliny the Elder, *Naturalis Historia*, *XVI*, *Vol.XXXV)*

Earthy pigments can be divided on the basis of colour into: yellow ochres, red earths and boles, green earths, dark yellow or brown siennas and umbers. They are also classified according to their colouring agent: a specific mineral or a chromogenic element in the clay structure. Chromogens can be found, for example, in green earths, where the colour depends on the specific ratio of divalent and trivalent iron in the structure of minerals glauconite, celadonite, smectite and chlorite (Hradil *et al.*, 2003). On the contrary, the colour depends on the mineral in yellow and red ochres, where the colouring agents are goethite and hematite respectively. Hematite and the associated pigment are the subject of this section. Red ochre is the first ubiquitous colour used in Arts History. In parallel, it is probably the first pigment to be synthesized. Pliny the Elder's *Natural History* (trans. Rackham *et al*., 1963) is the most ancient witness of Roman knowledge

of its synthesis. Even Theophrastus gives a detailed report on ochre, its origin and synthesis (Mottana & Napolitano, 1997): these are the authors that must be cited dealing with the history of red ochre.

ORIGIN OF THE WORD "OCHRE"

The world ochre comes from the latin "*ō*chra", in turn deriving from the greek term "*ṓchra"*, probably close to "*ō*chrós", which means "yellowish". Thus, ochre was initially limited to yellow pigments (Helwig, 2007). It is not a coincidence that Pliny the Elder, in his *Naturalis Historia* (trans. Rackham *et al*., 1963), refers to the red hue, whether natural or not, only with other names, namely *rubrica* or *sinopis*. The former, in particular, was assigned both from Pliny and Vitruvius (rev. Piccolo E., 2009) to a high-quality high-purity hematite, marked with a seal and, for that reason, called *Sphyragidis* (Bevilacqua *et al.*, 2010), coming from Lemnos island, Greece, and from the Turkish region of Cappadocia. Red ochre of lower quality is reported in Pliny's Naturalis Historia as *Sinopis*. Sinope is the name of the town on the Black Sea where it was mined. The same name was also attributed to the preparatory drawing made with this pigment on wall paintings. Cennini is the first author to etymologically compare cinnabar and red ochre: a mixture of *Sinopis* and lime white is called from him "Cinabrese" because of a similar hue. Cennini is also the first to link the mineral hematite and the corresponding pigment with the common word "Amatisto":

before him, the word hematite was only attributed to the mineral. This pigment is even different from *sinopis*, being less pure and with larger particles (rev. Thompson, 1993).

Further terms have been linked to red ochre in the following centuries. *Indian Red*, designated a pigment from East Indies or an artificial red from calcined iron sulphate, also called *English Red*. *Venetian Red* is the name equally attributed to a red from Venice (or transported through it) and to a colour preferred by Venetian painters in the 18th century. *Ocre de Rue*, from iron rust, indicates a yellow-brown variety taken out from the stream of iron mines. *Morellone* or *Caput Mortum*, is the red iron-based pigment mixed with a dark one. Finally, *Mars red* is the synthetic product of the oxidation of iron or steel, a process introduced in the 17th century.

Only from the 16th century the expression "ochre" was extended from yellow to red iron oxide pigments to describe both natural and synthetic materials showing the presence of iron oxides and/or hydroxides. This term is nowadays appropriate when the pigment has a natural origin. It corresponds to "earth" when the pigment as a clayey component. The former is assigned to a huge range of earthy pigments. In the present work, the definition pointed out by Triat (2010) is assumed: *ochre is a ferruginous mineral of micrometric size. It can be easily recognized by an organoleptic feature: it spots the hands. Thus, ferruginous rocks are considered ochres only when ground. The colouring agent, responsible for the high stability of the hue, is always*

associated with clay minerals. However, it must be remarked that more than one ferruginous mineral may be present in the same ochre and that clay minerals are not always present. For example, ochres from mining drainage could contain almost 100% iron (hydro)oxides.

HISTORICAL BACKGROUND

Yellow and red ochres are among the most ancient pigments. In Europe, their first use has been dated back to 300'000 years ago in the archaeological site of Terra Amata, near Nice, France (Triat, 2010). Some examples can be found in the mural paintings of Altamira or Lascaux. The maximum spread is assessed in the range 40'000-10'000 years ago, when ochres have been also used for funerary or social rituals and daily uses, in the Western as in the Eastern hemisphere. Raw materials were often found *in situ*, thanks to the great availability of ochre all over the world. Alternatively, they could be mixed with pigments from further sites, as supposed for Terra Amata. The use of ochres in Art History is widespread as much as their availability. Testimonies can be found in the Assyrian cuneiform tablets and cosmetics, in the Egyptian hieroglyphics or in manuscripts from ancient India, China and Japan (Helwig, 2007). Lucas & Harris (2012) reported that Egyptian craftsmen used ochres as a primary source for yellow and red and that they knew the way to produce synthetic red ochre from the calcination of yellow ochre. Probably Egyptians had no need to synthesize it, being the availability of red ochre

so high in all Egypt, especially near Aswan and in the Western Desert. This explains the intense export of high-quality supply to Rome, as documented by *Dioscorides* (trans. Osbaldeston & Wood, 1933).

Greeks used to import ochres of good quality from Cappadocia, Turkey, and the best one from the island of Keos, as Rapp (2009) summarized quoting Theophrastus' De Lapidibus.

In the Roman period, cinnabar and red ochre were both available. Latin authors recommended the use of cinnabar with parsimony, because of its high price and tendency to darker. In fact, Pompeian paintings are mostly made with red ochre, often adulterating or serving as an undercoating for cinnabar (Augusti, 1967). It was particularly common in wall paintings because of the incompatibility of other pigments with the fresco technique. The pigment was once again imported from Egypt. Spain was a new supply, as reported by Vitruvius (rev. Piccolo, 2009), probably because of the exhaustion of the Attic one. Theophrastus (Mottana & Napolitano, 1997) is the first to inform us about the routine burning of yellow iron oxide pigments to obtain red. The already cited medieval treatise *Mappae Claviculae* reports about the use of *sinopis* with red lead to obtain a pigment similar to cinnabar.

The use of red earth in water gilding must also be mentioned, from the Middle Age, to have its maximum spread in the 14th and 15th century paintings. Earth pigments were also

commonly used in Europe as grounds of paintings in the 16th century, replacing the white grounds made by gesso or chalk. These red-orange preparations were predominant in the 17th and 18th centuries, in the Baroque production of all European countries. These grounds were most probably clayey ochres with white kaolinite as extender (Hradil *et al*., 2003). Later on, the synthetic burned goethite became so frequently used to be cited in numerous treatises from the 16th century to the 19th century. In parallel, calcothar – the artificial red ochre from the calcination of iron sulphate – was also used, its recipe being described in medieval manuscripts. This product was later known as burnt vitriol, and then replaced by the industrial production of the Mars red from the late 18th century. Treatises recommend washing and grinding red ochre after its collection, even in the 18th and 19th century. The washing was carried out to free the pigment from mineral impurities. Normally, it was realized by a system of troughs and basins: this ensured the removal of coarse quartz particles. Then, earthy basins were used to let the remnant part stand and form a mud. This mud was finally cut and allowed to dry before grinding it.

According to Helwig (2007), the expression "***Mars yellow***" has been introduced by de Massoul since the 18th century (1797), from *croccus martis* that, at that time, indicated a red or yellow powder given by the oxidation of iron. In this period and later on Mars yellow was assigned to the yellow pigment obtained by precipitation from an aqueous

solution, eventually mentioned with its French name “Jaune de Mars”. The recipe has been kept secret up to the 19th century, when treatise started describing the reaction. An iron salt and an alkali were involved as reagents. The former was preferentially iron sulphate, eventually replaced by iron chloride, nitrate or acetate; the latter could be chosen among a long list of alkali. Their reaction led to the precipitation of a yellow-brown compound, after oxidation. Light yellow could be obtained by the addiction of alum, while a soft calcination let the colour turn into orange. The whole process was long-lasting: one of the major producers in the 19th century, Jacques Blockx, stated that 6 days were needed for 5 kg of raw pigment, including decantation, washing, pressing and drying (Mérimée, 1830). The monopoly of this production was soon gained by Germany, which was responsible for the 50% of its production in 1989. More recent producers are United States, Italy, United Kingdom, Brazil, China and Japan. From the calcination of the Mars yellow at different temperatures, ***Mars red*** is obtained.

CHROMATIC FEATURES

Three mechanisms are responsible for the colour of ochres, as evidenced in Pomiès thesis (1997) and later summarized in Helwig (2007): charge transfer transitions, particle size and cation substitutions. Photon absorption by Fe^{2+}/Fe^{3+} ions, charge transfer between them or between Fe^{3+} and O^{2-} are the first factors responsible for the perception of

colour in ochres. The redder hues of hematite are then caused by strongly enhanced electron transitions. This is due to adjacent Fe centers (0.29 nm) in face-shared octahedra, which increase the magnetic coupling, thus intensifying the transitions. Particle size also plays an important role in colour perception. Hematite from soil is normally nano-metric with a vivid red colour, despite bigger crystals (micrometric) can be found – the so-called oligist – with a violet colour accompanied by metallic reflections. Schwertmann and Cornell (2000) have analysed a wide range of ochres concluding that hematite is always redder than 4.1 YR. However, they also state that the hue is sensitive to crystallinity and to particle size, shape and aggregation. For example, particles ranging from 0.1 to 0.2 μm appear bright-red while they tend to purple when their size increases (1-5 μm). Heating up to sintering temperatures increases particle size and leads to a change in colour from red to purple. Scheinost *et al.* (1999) also pointed out the variability in colour caused by Al substitutions. The increase in Al in synthetic hematite corresponds to an increased lightness, accompanied by a shift to redder hues with decreasing particle size.

COMPATIBILITY AND DETERIORATION

All kinds of ochres show a high stability in moisture and light, but also when mixed with other pigments and binders, especially in wall paintings. They are also highly resistant to alkali and weak/moderate acids (Rapp, 2009).

However, if the content of clay minerals is high and smectite group minerals are prevailing, this component can expand or swell in increased humidity.

2.3 SYNTHESIS: STATE OF THE ART

It is well known that the main colouring agent of the pigment yellow ochre is goethite, α-FeOOH, even in small quantities. Lepidocrocite or ferrihydrite may also be responsible for the same hue. Natural or synthetic yellow ochre then alters to red as a consequence of a dehydration process. It has been suggested in previous researches that probably this process had been already applied by Prehistoric craftsmen when hematite deposits were not reachable.

This transformation has been widely investigated for its mineralogical aspects: in 1959 Bernal included it in topotaxy. A year later Francombe and Rooksby (1959) underlined a non-uniform peak broadening in the diffraction pattern of heated goethite and identified unit-cell relationships between goethite and hematite. They showed that some reflections of goethite are related to specific reflections of hematite. The corresponding X-ray peaks are sharp, while the others are broad until re-ordering in the hematite structure is completed above 873 K. Pomiés and co-workers (1998, 1999) have shown that during dehydration of goethite, the newly formed hematite retains non-structural water inside elongated nano-pores. Water persists inside the pores even at 973-1073 K, while the shape of the pores turns into spheroidal. The authors observed the pores by transmission electron microscope, underlining the variation in shape through an *in-situ* experiment up to 1273 K. They also noted that, after 873-923 K, grain boundaries form and their coalescence leads to

isomeric recrystallization. X-ray diffraction showed selective broadening for synthetic hematite: (110), (113) and (300) hematite reflections are narrow whatever the temperature is, while the others remain broad up to 673 K. Through Rietveld refinement, they excluded anisotropy and cationic deficiency as a cause of this selective broadening, being the cationic occupation rate close to 100%. For Pomiés, this is a proof of the absence of substituted hydroxyl ions at high temperature: the hypothesis of hydrohematite can thus be neglected. On the contrary, the selective broadening is justified by cationic-plane stacking defects, perpendicular to hematite c-axis. To sum up, Pomiés and co-workers (1998, 1999) have shown that synthesized hematite can be recognized from:

- ***Selective broadening*** and typical intensity ratios of specific lines in the XRPD pattern;
- ***Nano-porosity*** (lamellar and spheroidal), as observed in TEM micrographs;
- Persistence of ***acicular crystals*** typical of goethite (even when the transition is complete);
- ***Recrystallizations***, if the heating temperature is above 873 K.

The analysis of archaeological samples also adduced more evidence. They found that the already cited distinctive features were sometimes coupled to the presence of ***maghemite*** (γ-Fe_2O_3). Maghemite can be a product of the heating when organic matter is also present.

More recent works on the same topic used infrared spectroscopy. Wolska (1981) reported the retention of residual hydroxyl units in hematite formed by dihydroxylation of goethite, clearly shown in the hydroxyl stretching region.

The first application on works of art was carried out by Béarat in 1996. The author analysed fragments from Roman wall painting dating from the 1st to the 3rd century AD from Dietikon, Switzerland, by XRPD. He considered the ***intensity ratio of lines*** $\frac{(104)}{(110)} < 1$, $\frac{(110)}{(024)} \neq 1.25$ and $\frac{(113)}{(024)} \neq 0.75$ as indicative of disordered hematite and hence of heated goethite. However, Béarat also questioned whether this heating was genetic or anthropic.

Frost *et al.* (2003) has recently applied the same conclusions on samples from an ancient aboriginal source in South Australia. No more investigations have been carried out for Cultural Heritage.

The need of a fixed procedure in the identification of synthetic or natural ochre pigments is thus evident.

2.4 MATERIALS AND METHODS

This study was carried on with the aim of detecting morphological and chemical distinctive features between natural and synthetic red ochres. The sample-set was made collecting natural samples, both from the MMUR and from the Hercules Laboratory of Évora, Portugal. Further samples were bought from the Kremer Company[10]. Some other samples were synthesized from goethite. The latter comes both from commercialized yellow ochre (same Company) and from the laboratory synthesis. Below is the complete list of samples under investigation (Table 20). The following terminology will be applied: synthetic or artificial red ochre stands for a pigment derived from the heating of natural yellow ochre, *i.e*. goethite with accessory minerals or limonite; Mars red is the pigment obtained from the calcination of the synthetic goethite, namely Mars yellow.

[10] GmbH & Co. KG - Hauptstr. 41 – 47, DE 88317 Aichstetten

Table 20 - Complete list of the samples of yellow and red ochre under investigation.

	Colour	*Sample*	*Origin*	*Description*
Natural	Yellow	*0263*	HERCULES Lab.	Sienna ground
		3593	MMUR	Limonite
		0324	HERCULES Lab.	Yellow ochre
		116420	Kremer Company	Yellow ochre from Morocco
		11272	Kremer Company	Yellow ochre from Andalusia
	Red	*0261*	HERCULES Lab.	Toasted umber
		116430	Kremer Company	Red ochre from Morocco
		11274	Kremer Company	Red ochre from Andalusia
		40440	Kremer Company	Burnt sienna or Pompeian Red
		H_NAT	Private Collection	Powdered red ochre

	Colour	*Sample*	*Origin*	*Description*
Synthetic	Yellow	*G_SYN*	HERCULES Lab.	Synthesised goethite or Mars yellow
	Red	*0263_300*	“ ”	Goethite 0263 (at 573 K for 18h)
		0263_700	“ ”	Goethite 0263 (at 973 K for 1h)
		3593_300	MMUR	Goethite 3593 (at 573 K for 18h)
		3593_700	MMUR	Goethite 3593 (at 973 K for 1h)
		0324_300	HERCULES Lab.	Goethite 0324 (at 573 K for 18h)
		0324_700	“ ”	Goethite 0324 (at 973 K for 1h)
		116420_300	“ ”	Goethite 116420 (at 573 K for 18h)
		116420_700	“ ”	Goethite 116420 (at 973 K for 1h)
		G_SYN_300	“ ”	Mars red (at 573 K for 18h)
		G_SYN_700	“ ”	Mars red (at 973 K for 1h)

SYNTHESIS OF MARS YELLOW

Synthesis of goethite was conducted in the Hercules Laboratory of the University of Évora, Portugal. As stated before, Mars yellow indicates a pigment precipitated from an aqueous solution of an iron salt and an alkali. Different recipes for the synthesis of goethite were considered (Table 21).

The procedure proposed by Schwermann and Cornell (2000, pp. 73-74) was finally chosen to reproduce Mars yellow. This choice is due to the similarities with the ancient procedure described in Section 2.2 (pp. 148-149) and to the short production time.

Table 21 - List of the methods for the synthesis of goethite taken into account in the present research. The method chosen for the reproduction of Mars yellow is highlighted.

Reagents	*Time*	*T/pH*	*Products*	*Ref.*
$Fe(N0_3)_3$ 1M **Distilled Water** **KOH 5M**	60h	343 K	9g compact acicular goethite	(Schwertmann & Cornell 2000, pp. 73-74)
10g$Fe(N0_3)_3 \cdot 9H_20$ Distilled water KOH 70 mL 1M $NaHCO_3$ 0.045M L-cysteine 3.5g	60h 6h 1h	343 K pH=8.5 Air40L/h	2.25g uniform subrounded crystals	(Schwertmann & Cornell 2000, pp. 76-77)
$FeCl_2 \cdot 4H_20/FeSO_4 \cdot 7 H_20$ Distilled water N_2 bubble $NaHCO_3$ 1M	30' 48h	pH=7 by $NaHCO_3$ bubbling	5-6g goethite+carbonate adsorbed, difficolt to remove (>crystal size	(Schwertmann & Cornell 2000, pp. 78-82)

Reagents	Time	T/pH	Products	Ref.
			with $FeSO_4$)	
· $Fe(N0_3)_3$ 1M · Deionized water · NaOH 2.5M	60h	343 K 323 K dry	9g compact yellow goethite	(Cornell & Schwertmann 2003a)
· High purity water · $NaOH/Ca(OH)_2$ 1M · Fe^{II} source 0.2mol: $(FeCl_2)\cdot 6H_20/Fe(N0_3)_3\cdot 9H_20$	7h 24h+10 Cooling 30'centrifugation 48h	303 K 343 K cooling 333 K dry	-	(Montes-Hernandez *et al.,* 2011)
· $FeSO_4\cdot 7H_20$ Na_2CO_3 · N_2 bubbl. (0.5bar)	15' bubbl. 180'	273-333 K 323 K dry	Greenish/ White precipitate	(Pozas *et al*., 2002)
· $Fe(NO_3)_3$ 0.125M · NaOH 0.25 M · $NaNO_3$ 0.5 M	2days Dyalisis of 1,3,5 days 1 month ageing	pH=2.12	Stable sols of brown nano-goethite, aged to be yellow	(van der Woude & de Bruyn 1984)

First, ***ferrihydrite*** was precipitated adding, while stirring, 200mL 5 M KOH (65.12 g) to 100 mL of 1M $Fe(NO_3)_3$ (40.4 g). The suspension was immediately diluted up to 2L with bi-distilled water and hold in a close polypropylene flask at 343 K for 60h. During that time the red-brown ferrihydrite transformed into a compact yellow precipitate of goethite. The precipitate was three times washed in distilled water, then dried at 333 K for 24 hours (Figure 34).

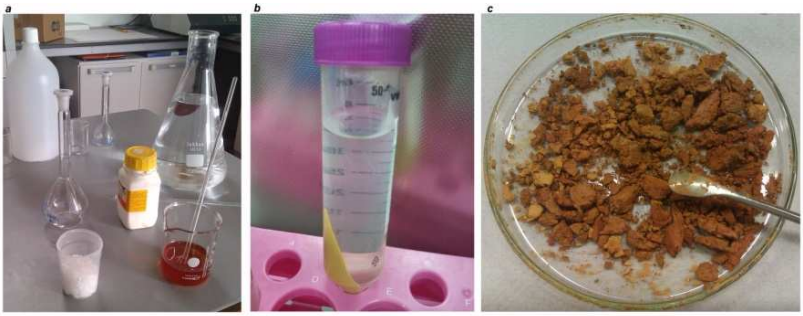

Figure 34 - **a**. Exothermic reaction between $Fe(NO_3)_3$ and KOH, with the production of ferrhydrite. **b**. Washing of the precipitated goethite. **c**. Final product: Mars yellow.

The absence of NO_3^- and OH^- species was also verified by μ-FTIR (negligible residue in the peak at 1348 cm^{-1}, Figure 35) and litmus paper, respectively. Around 10 g of goethite were obtained.

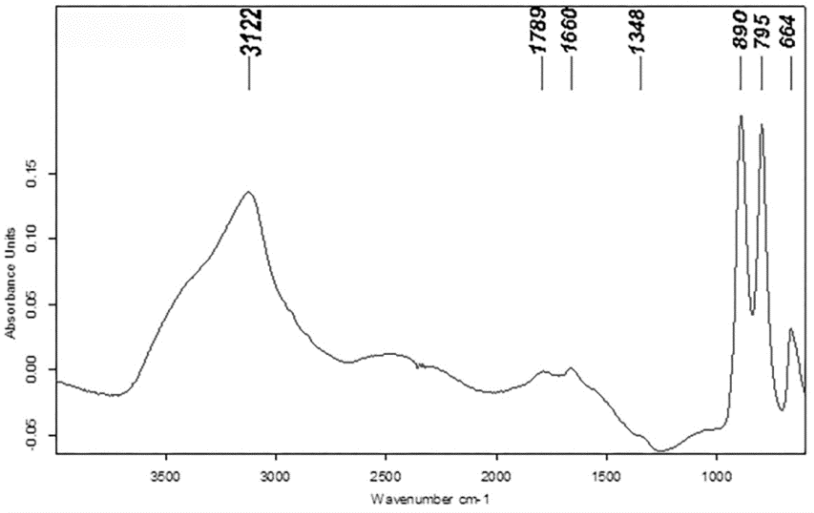

Figure 35 - μ-FTIR spectrum of synthesized goethite, from Hercules Laboratory (Bruker Hyperion 3000), to check for nitrate ions: negligible residues shown by the shoulder at 1348 cm^{-1}.

SYNTHESIS OF MARS RED

Powdered yellow ochres (natural/synthetic) were put in a non-sealed ceramic crucible and heated in a muffle furnace. Two different heating pathways were carried out, both followed by a slow cooling to ambient temperature:

a) At 573 K for 18 hours;
b) At 973 K for 1 hour.

The choice of the heating pathways is motivated by the examination of previous works on the same topic. It is generally assessed that goethite conversion into hematite is completed at 543K and no trace of the former is detected by XRPD (Francombe & Rooksby, 1959; Pomiés *et al.,* 1998). For this reason, the first method was fixed at 573K: this ensured that goethite was no more present in the synthetic product. The second method was set-up at 973K for dual reasons: if a synthetic process was applied in Prehistoric Art, it couldn't reach higher temperature because of the low technological level achieved at that time; sintering effects, as observed by different authors (Walter *et al.,* 2001; Gialanella *et al*., 2003) above 1073K, wanted to be avoided.

Optical Microscopy

Optical microscopy was used to document the powdered samples and have a first idea on the accessory mineralogical phases. The instrument is a Greenough stereo microscope, Leica S8 APO with apochromatic 8:1 zoom, 75mm working

distance and magnification up to 80x, at the Department of Earth Sciences of "Sapienza" University of Rome.

XRPD and Rietveld refinement

X-ray powder diffraction was used first to characterize the natural yellow and red ochres. Powder samples were put in a silicon low background sample holder (diameter 20 mm x 0.5 mm sample cavity). They were then analysed by a BRUKER AXS D8 Discovery diffractometer from the Hercules Laboratory. The instrument operates in reflection, θ-2θ geometry, using Cu K_α radiation at 40 kV accelerating voltage and 30 mA current. Data were collected in the 3-75° 2θ angular range, step scan of 0.05° 2θ/2s. Mineralogical phases were identified using the "EVA Bruker-AXS" software and the "PDF-2 ICDD" database.

A second step was also planned to check on structural variations induced by the synthesis. For example, Norrish & Taylor (1961) have proved that the unit cell of goethite from soils is sensibly higher than pure goethite, because it undergoes Al-substitutions. Thus, the evaluation of the unit cell volume could be determinant in the detection of Mars yellow. The target was achieved using the *Bruker AXS D8 Advance* diffractometer, coupled with the Rietveld method for data analysis, as previously described in the subsection 1.5. The *GSAS Software* package with the EXPGUI interface (Larson & Von Dreele 2004; Toby, 2001) was used. Starting structural

data of goethite and hematite were taken from Gualtieri & Venturelli (1999) and Maslen *et al.* (1994), respectively.

First, the starting structural data of hematite were taken from Maslen *et al*. (1994) because it was supposed that the heated samples corresponded to natural hematite. Then, the Refinement was repeated as dealing with a *proto-hematite*, using structural data from Gualtieri & Venturelli (1999). The term *proto-hematite* was introduced by Wolska (1981) and Wolska & Szajda (1985), to define an intermediate phase in the transformation *α-FeOOH* → *α-*Fe_2O_3, corresponding to the chemical formula *α-*$Fe_{2-x/3}(OH)_xO_{3-x}$ and showing the presence of residual hydroxyls (x) in the structure.

In the present work, the samples heated at 573 K were refined from the cif file given for a sample at T = 586 K (database code: amcsd 0002228), while those heated at 973 K were refined with starting structural data from a sample of at T = 790 K (database code: amcsd 0002229) and at T = 1052 K (database code: amcsd 0002230). The fractional coordinate and displacement parameters of hydrogen were not refined because XRPD cannot locate hydrogen atoms accurately. Finally, since it has been showed by TEM analysis that synthetic hematite preferentially assumes needle-like shape, particle size anisotropy was also evaluated from the profile function parameters, as follows:

a) Perpendicular component $p_{\perp} = \frac{18000K\lambda}{\pi \cdot X}$,

b) Parallel component $p_{\parallel} = \frac{18000K\lambda}{\pi \cdot (X+X_e)}$.

K=1 is the Scherrer costant, λ is the wavelength, X and X_e are respectively the Lorentzian profile term LX and the anisotropic contribution ptec for the Lorentzian broadening, as refined in GSAS.

SEM-EDS

Scanning electron microscopy coupled with energy dispersive spectroscopy was used first to confirm the accessory mineralogical phases determined by XRPD through their elemental composition. It was also used to record the morphology of the synthetic samples and compare it to the features of natural red ochres. The instrument is a FEI-Quanta 400 Scanning Electron Microscope coupled with an Energy Dispersive X-ray Spectroscope EDAX Genesis working at 20 kV. It belongs to the CNR – IGAG, at the Department of Earth Sciences of Sapienza-University of Rome.

A minimum amount of powder was fixed on an adhesive surface over the stub and then metalized with graphite, before being placed over a multi-sample holder.

The energy-dispersive spectrometry was used for a qualitative detection of the elements composing the samples, in order to confirm the accessory mineralogical phases identified by XRPD. Secondary-electron (SE) images were acquired to check and compare the morphology of natural and synthesized hematite. Images were collected up to 30000x of magnification, measuring the length of the particles, when possible. This procedure can be applied especially when

hematite is synthesized from artificial goethite. In fact, this is known to show elongated particles, as evidenced by SEM (de Faria & Lopes, 2007) and TEM images of previous works (González *et al.*, 2000; Walter *et al*., 2001; Kosmulski *et al*., 2004; Löffler & Mader, 2006; Gialanella *et al*., 2010).

Thermal analysis

Thermogravimetry (TGA) and differential thermal analysis (DTA) were performed on a Netzsch STA 449F3 Jupiter analyser at the Hercules Laboratory. A small amount of the powder samples, as listed in Table 22, was put in a platinum crucible after being weighted.

Table 22 - List of the samples analysed by DTA and TG.

Sample	Weight (mg)
0324	27.9
3593	24.9
Mars yellow	26.5

After a careful examination of the previous works on goethite dehydration (Derie *et al*., 1976; Goss 1987; Walter *et al.*, 2001; Frost *et al*., 2003; Gialanella *et al*., 2010) the operating conditions described in Table 23 were chosen.

Analysis was carried out with a heating rate of 10 K/min, from 308 K up to 1263 K (with a starting time of 5 minutes to stabilize the instrument at the initial temperature). The choice of the thermal range is justified by the possibility to observe the overall set of transformation interesting main and

accessory phases. The weight loss of the decomposed phases was determined by Proteus© software for the selected temperature ranges, after background correction and smoothing (8 points).

Table 23 - Comparison of operating conditions for DTA and TG analysis of this work and reported in the previous ones.

Op. conditions	*This work*	*Derie 1976*	*Goss 1987*	*Walter 2001*	*Frost 2003*	*Gialanella 2010*
Initial T	**308K**	273K	273K	273K	323K	293K
Final T	**1263K**	673K	1263K	1073K	1273K	1273K
Heating rate	**10K/m**	2K	1K	5K	2K	10K
More	**N_2 70mL/m**	DryN_2 stream 200mg	N_2 20mL/m 1 atm		N_2 80mL/m	Dry air flux

µ-FTIR

Micro-IR-spectroscopy with Fourier Transform was performed at Hercules Laboratory. It is a fast and micro-destructive technique which requires a minimum amount of powder (1-2 mg). It was used to detect compositional differences between synthetic and natural red ochre. µ-FTIR was preferred because it allows preserving the sample as it is. This is a factor of high importance, if the methodology will be applied in the future to unique artworks.

The instrument used in this study is a Bruker Hyperion 3000, equipped with a nitrogen-cooled MCT-A detector. It operates with a Thermo Scientific™ Nicolet™ Continuµm ™ Infrared

microscope (15x objective). The sample was stored in a diamond anvil compression cell from S.T. Japan.

Spectra were acquired in transmission mode, with a resolution of 4 cm^{-1}, 32 scans, in the spectral range 4000-650 cm^{-1}. For all the acquired spectra, the CO_2 absorption at ~2400-2300 cm^{-1} was removed. To test reproducibility and increase the robustness of the method, 3 spectra were collected from the same spot and the average spectrum was then calculated by the Thermo Scientific™ OMNIC™ Specta Software. Origin® software was used to correct the baseline and smooth the data for bands assignment, after the normalization, following a procedure already proposed by De Benedetto *et al.* (2005) for FTIR data on ancient ceramics. The normalized absorbance I_N, was calculated as $I_N = \frac{I_M - I_{MIN}}{I_{MAX} - I_{MIN}}$, being I_M the measured absorbance and I_{MIN} and I_{MAX} the lowest and highest absorbance value in the same sample, respectively. For the smoothing, the Savizky-Golay method was used, with a third order, 21 points polynomial filter. Band maximum was then calculated with a 1st derivative method on the normalized, background-subtracted data. Previous works, as reported in the subsection 2.5, were compared and taken into account for the attribution of peaks. The RUFF online database (www.rruff.info) was also used.

The intensity and amplitude of characteristic IR bands is often studied by mathematical processing in archaeometric studies on ancient materials such as paper (Fengel, 1992; Calvini & Gorassini, 2002), leather (Puică et al., 2006) varnish on

furniture (Derrik, 1989) and binder on paintings (Centeno *et al.*, 2004).

Thus, it was decided to perform peak deconvolution in specific ranges of the acquired IR spectra. In particular, the ranges ~1300-600 cm^{-1} and 4000-3000 cm^{-1} were taken into account. The deconvolution procedure is analogous to that of the Raman spectra of the previous section, as described in detail in 1.5.

2.7 FINAL REMARKS: DISCRIMINATION OF MARS AND SYNTHETIC PRODUCTS FROM NATURAL OCHRES

The multidisciplinary study carried out on the ochres has shown to be effective in their characterization. First of all, the preliminary diffractometric investigation on the natural samples, coupled with the SEM elemental and morphological analysis, gave information on the genesis of the ochre. This procedure is commonly assessed and successfully applied in the study of pigments. This systematic methodology proved that natural yellow and red ochres mostly come from a lateritic environment where iron oxides and hydroxides are due to weathering processes. They mostly belong to the gesso-based pigments, where the presence of gypsum can be natural or artificial. In the latter case, its addition is justified by the aim of enlighten the final hue of the pigment.

The main goal of discriminating the yellow natural ochres from the Mars product was primarily reached through the observation and comparison of their morphology by scanning electron microscopy. In particular, Mars yellow showed to be characterized by well-developed acicular crystals of goethite. It could be easily distinguished from the other yellow samples, which showed to be all due to the aggregation of rounded particles. Even the dimension of these grains was a distinct feature: the length of the major axis in Mars yellow ranges from 2.5 to 6.5 μm; on the contrary, it was not possible to

assess the diameter of the rounded crystals in natural goethite because they were too small for the achievable level of magnification.

Future investigation is recommended on an enlarged set of samples, to systematically assess the variation of the structural parameters from synthetic to natural ochres. In fact, these conclusions refer to only one sample of Mars yellow recently prepared. It cannot be generalized to all possible Mars yellows prepared at various conditions. Thus, this study is intended as a starting point for further investigations.

More interesting findings were given by the spectroscopic investigation. The evaluation, after deconvolution, of the typical IR bands of iron hydroxides led to discriminate Mars yellow. The intensity of the hydroxyl bands in the fingerprint region was fundamental to this target. Mars yellow showed to have the highest values for both intensities. The correlation between these parameters could be verified for all the yellow samples under investigation, apart from those with high content of quartz. Further investigation is needed to establish the influence of this mineral, eventually present on the same painted area, in the discrimination of Mars yellow. A systematic and quite fast investigation on data-base SE images and FTIR spectra - or directly on the field - can be a key-point to define the spread of Mars yellow in artists' palette through the Ages. Moreover, it should be verified if different recipes can be responsible for a different morphology.

The same procedure is a valid tool even in the discrimination of Mars red from the natural red ochres. In fact, the typical morphology revealed for Mars yellow is retained in the red derivative. Thus, the needle-shaped particles are clearly distinguished starting from 6000x of magnification. They have only rounded shapes in the natural and calcined samples. Indeed, SE images did not allow the morphological differentiation of the samples due to the heating of goethite from the natural reds. This result was conversely achieved from the mathematical processing of the μ-FTIR spectra. The estimation of the vibrational modes of hydroxyl units coupled with those directly due to iron was first performed. It proved that hydroxyl units play a dominant role in the separation of the samples due to a 573 K-calcination. This is in agreement with the formation of *proto-hematite*, *i.e.* with the retention of structural water as a cause of soft heating of goethite.

The relative areas of the bands due to hydroxyl units in different region of the IR spectrum were then compared. This led to distinguish temperatures of preparation (with the same starting materials). The samples derived from the calcination of goethite at 573 K (for 18 hours) typically show the highest values for the ~800 cm^{-1} band. Intermediate values characterize the natural samples. The samples due to the calcination at 973 K (for 1 hour) are recognized by the lowest values of both hydroxyl bands. This indicates that the retention of water from the precursory goethite is almost completely avoided after this synthetic treatment. This is in

agreement with a higher reordering of Fe-deficient layers with residual protons when the temperature of synthesis is higher. However, it must be remarked that a statistically significant set of data must be implemented to make general conclusions. Finally, the Rietveld refinement from XRD data showed that the domain size has the highest variability within the red samples. The lowest values are associated with the natural sample and with the Mars red at 973 K. Further studies may prove if this parameter can give additional information in the detection of synthesized ochres.

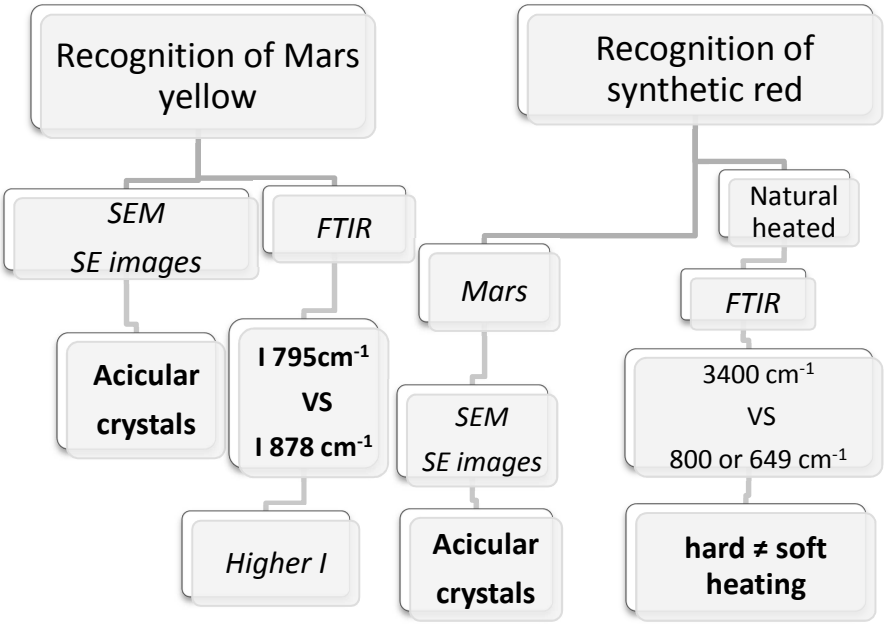

Figure 62 - Flow chart summarizing a preliminary standard protocol for the recognition of Mars yellow and for the discrimination of synthetic pathways in the production of red ochres.

This combined methodology, as summarized in Figure 62 has proved to provide a framework for the exploration of Mars products, for the first time under investigation for archaeometric purposes. In fact, it must be assessed if different synthetic pathways may affect the recognition of Mars red. This study may be intended as a first step, which has to be followed by a deeper, systematic investigation on artefacts and in the laboratory synthesis, in order to highlight morphological differences for different recipes. The introduction and spread of the calcination of goethite in Prehistory is still under debate. The mathematical processing and the data treatment of IR data hereby proposed may be applied to define when and where this praxis has been introduced. It can be assumed that the firing temperatures that could be reached were quite low during Prehistory. The possibility to discriminate low-temperature-calcined samples may be crucial in the recognition of products due to the technological level reached in Prehistoric arts.

REFERENCES

Aldrabee, A. & Wriekat, A.H., 2011. Archaeometric characterization of ancient glazed pottery sherds from Khirbet Faris, Jordan by inductively coupled plasma mass spectrometry (ICP-MS). *Microchemical Journal*, 99(2), pp.289–295.

Allen, E.T.. & Crenshaw, J.L., 1912. The sulphides of zinc, cadmium and mercury; their crystalline forms and genetic conditions. *American Journal of Science*, p.341.

Allocca, C., 2013. *Numerical model of the Amiata Volcano geothermal fields, Italy*. University of Rome 'Sapienza'.

Andersen, F.A. & Brečević, L., 1991. Infrared spectra of amorphous and crystalline calcium carbonate. *Acta Chemica Scandinavica*, 45, pp.1018–1024.

Augusti, S., 1967. *I colori pompeiani* De Luca, ed., Rome.

Balan, E., Saitta, A.M., Mauri, F. & Calas, G., 2001. First-principles modeling of the infrared spectrum of kaolinite. *American Mineralogist*, 86(Giese 1982), pp.1321–1330.

Ball, P., 2004. *Colore. Una biografia. Tra arte storia e chimica, la bellezza e i misteri del mondo del colore*, BUR Biblioteca Univ. Rizzoli.

Ballirano, P., Botticelli, M. & Maras, A., 2013. Thermal behaviour of cinnabar , α-HgS, and the kinetics of the β-HgS (metacinnabar)→ α-HgS conversion at room temperature. *European Journal of Mineralogy*, 25, pp.957–965.

Ballirano, P. & Melis, E., 2009. Thermal behaviour and kinetics of dehydration of gypsum in air from in situ real-time laboratory parallel-beam X-ray powder diffraction. *Physics and Chemistry of Minerals*, 36(7), pp.391–402.

Ballirano, P. & Sadun, C., 2009. Thermal behavior of trehalose dihydrate (T h) and β-anhydrous trehalose (T β) by in-situ laboratory parallel-beam X-ray powder diffraction. *Structural Chemistry*, 20(5), pp.815–823.

Bate, J., 1654. *Mysteries of Nature and Art*, London.

Batini, F., Brogi, A., Lazzarotto, A., Liotta, D. & Pandeli, E., 2003. Geological features of Larderello-Travale and Mt. Amiata geothermal areas (southern Tuscany, Italy). *Episodes*, 26(3), pp.239–244.

Béarat, H., 1996. Chemical and mineralogical analyses of gallo-Roman wall painting from Dietikon, Switzerland. *Archaeometry*, 38(July 1994), pp.81–95.

Bellot-Gurlet, L., Le Bourdonnec, F.-X., Poupeau, G. & Dubernet, S., 2004. Raman micro-spectroscopy of western Mediterranean obsidian glass: One step towards provenance studies? *Journal of Raman Spectroscopy*, 35(8/9), pp.671–677.

De Benedetto, G.E., Fabbri, B., Gualtieri, S., Sabbatini, L. & Zambonin, P.G., 2005. FTIR-chemometric tools as aids for data reduction and classification of pre-Roman ceramics. *Journal of Cultural Heritage*, 6(3), pp.205–211.

Bernal, J.D., 1959. The Oxides and Hydroxides of Iron and Their Structural Inter-Relationships. *Clay Minerals*, 4, pp.15–30.

Beukes, N.J., Gutzmer, J. & Mukhopadhyay, J., 2003. The geology and genesis of high-grade hematite iron ore deposits. *Applied Earth Science: IMM Transactions section B*, 112(1), pp.18–25.

Bevilacqua, N., Borgioli, L. & Gracia, I.A., 2010. *I pigmenti nell'arte: dalla preistoria alla rivoluzione industriale*, Il Prato.

Biagioni, C. & Orlandi, P., 2009. Tiemannite e metacinabro della miniera Buca della Vena (Alpi Apuane). , 114, pp.13–17.

Bianchi Bandinelli, R., 1980. *La pittura antica*, Rome: Editori Riuniti.

Bishop, J.L., Lane, M.D., Dyar, M.D. & Brown, A.J., 2008. Reflectance and emission spectroscopy study of four groups of phyllosilicates: smectites, kaolinite-serpentines, chlorites and micas. *Clay Minerals*, 43(1), pp.35–54.

Boni, M., Benvenuti, M. & Meinert, L., 2004. *Skarn deposits in Southern Tuscany and Elba Island (Central Italy)*, FLORENCE IGC.

Bonizzoni, L., Bruni, S., Guglielmi, V., Milazzo, M. & Neri, O., 2011.

Field and laboratory multi-technique analysis of pigments and organic painting media from an egyptian coffin (26th dinasty). *Archaeometry*, 53(6), pp.1212–1230.

de Boorder, H., Van Beek, A.J.J., Dijkstra, A.H., et al., 1996. Crustal architecture of the Donets Basin: tectonic implications for diamond and mercury-antimony mineralization. *Tectonophysics*, 268(1-4), pp.293–309.

Brigo, L., Camana, G., Rodeghiero, F. & Potenza, R., 2001. Carbonate-hosted siliceous crust type mineralization of Carnic Alps (Italy-Austria). *Ore Geology Reviews*, 17, pp.199–214.

Brogi, A., Fabbrini, L. & Liotta, D., 2011. Sb-Hg ore deposit distribution controlled by brittle structures: The case of the Selvena mining district (Monte Amiata, Tuscany, Italy). *Ore Geology Reviews*, 41(1), pp.35–48.

Bukka, K., Miller, J.D. & Shabtai, J., 1992. FTIR study of deuterated montmorillonites: Structural features relevant to pillared clay stability. *Clays and Clay Minerals*, 40(1), pp.92–102.

Burns, R.G. & Strens, R.G.J., 1966. Infrared study of the hydroxyl bands in clinoamphiboles. *Science*, 153(3738), pp.890–892.

Calvini, P. & Gorassini, A., 2002. FTIR – Deconvolution Spectra of Paper Documents. *Restaurator*, 23(1), pp.48–66.

Cambier, P., 1986. Infrared Study of Goethites of Varying Crystallinity and Particle Size: I. Interpretation of OH and Lattice Vibration Frequencies. *Clay Minerals*, 21, pp.191–200.

Cataldi, R., 1967. Remarks on the geothermal research in the region of Monte Amiata (Tuscany — Italy). *Bulletin Volcanologique*, 30(1), pp.243–269.

Cavallo, G. & Zorzin, R., 2012. Geology, Petrography, Mineralogy, Geochemistry of Natural Fe-based Pigments from Verona Province (Italy). In *39th International Symposium for Archaeometry*. Leuven, pp. 9–15.

Centeno, S.A., Guzman, M.I., Yamazaki-Kleps, A. & Della Védova, C.O., 2004. Characterization by FTIR of the Effect of Lead White on Some Properties of Proteinaceous Binding Media. *Journal of the American Institute for Conservation*, 43(2),

pp.139–150.

Chapman, J., 1981. *The Vinča culture of South-East Europe: studies in chronology, economy and society, Vol. 1*, Oxford: BAR International Series.

Choudhury, A., 2014. *Principles of Colour and Appearance Measurement: Object Appearance, Colour Perception and Instrumental Measurement* 1st ed., Cambridge: Woodhead publishing Ltd.

Cioni, R., 2004. Temperatures of the A.D. 79 pyroclastic density current deposits (Vesuvius, Italy). *Journal of Geophysical Research*, 109(B2), p.18.

Colombo, L., 2003. *I colori degli antichi* Nardini, ed., Firenze.

Cornell, R.M. & Schwertmann, U., 2003a. *The Iron Oxides: Structure, Properties, Reactions, Occurences and Uses, Second Edition*, Wiley-VCH Verlag GmbH & Co. KGaA.

Cornell, R.M. & Schwertmann, U., 2003b. The iron oxydes: structure, Properties, Reactions, Occurences and Uses. In *Wiley-Vch*. p. 571.

Damiani, D., Gliozzo, E., Turbanti, I.M. & Spangenberg, J.E., 2003. Pigments and plasters discovered in the House of Diana (Cosa, Grosseto, Italy): An integrated study between art history, archaeology and scientific analyses. *Archaeometry*, 45(2), pp.341–354.

Daniels, V., 1987. The blackening of vermilion by light. In *Recent advances in the conservation and analysis of artifacts: jubilee conservation conference papers, London 6-10 July 1987*. pp. 280–282.

Danišík, M., Sachsenhofer, R.F., Frisch, W., et al., 2010. Thermotectonic evolution of the Ukrainian Donbas Foldbelt revisited: New constraints from zircon and apatite fission track data. *Basin Research*, 22(5), pp.681–698.

Davidson, R.S. & Willsher, C.J., 1980. Photoelectrochemistry of mercury (II) sulphide. *Faraday Discussions of the Chemical Society*, 70, p.177.

Deer, W.A., Howie, R.A. & Zussman, J., 1992. *An Introduction to the*

Rock-Forming Minerals, London: Longmans.

Derie, R., Ghodsi, M. & Calvo-Roche, C., 1976. DTA study of the dehydration of synthetic goethite αFeOOH. *Journal of thermal analysis*, 9(3), pp.435–440.

Derrik, M., 1989. Fourier transform infrared spectral analysis of natural resins used in furniture finishes. *Journal of the American Institute for Conservation*, 28(1), pp.43–56.

Dickson, F. & Tunell, G., 1959. The stability relations of cinnabar and metacinnabar. *American Mineralogist*, 44(101), pp.471–487.

Dini, A., Benvenuti, M., Costagliola, P. & Lattanzi, P., 2001. Mercury deposits in metamorphic settings: The example of Levigliani and Ripa mines, Apuane Alps (Tuscany, Italy). *Ore Geology Reviews*, 18, pp.149–167.

Dini, A., Benvenuti, M., Lattanzi, P. & Tanelli, G., 1995. Mineral assemblages in the Hg-Zn-(Fe)-S system at Levigliani, Tuscany, Italy. *European Journal of Mineralogy*, 7(2), pp.417–428.

Domínguez-Bella, S. & Morata-Céspedes, D., 1995. Application of the mineralogical and petrological techniques to archaeometry. Study of the dolmen de Alberite (Villamartín, Cádiz, Spain) materials. *Zephyrus*, XLVIII, pp.129–142.

Dubrawski, J. V., Channon, A.-L. & Warne, S.S.J., 1989. Examination of the siderite-magnesite mineral series by Fourier transform infrared spectroscopy. *American Mineralogist*, 74, pp.187–190.

Eastaugh, N., Walsh, V., Chaplin, T. & Siddall, R., 2008. *Pigment Compendium*, Elsevier.

de Faria, D.L.A. & Lopes, F.N., 2007. Heated goethite and natural hematite: Can Raman spectroscopy be used to differentiate them? *Vibrational Spectroscopy*, 45, pp.117–121.

Feller, R.L., 1967. Studies on the Darkening of Vermilion by Light. *Report and Studies in the History of Art*, 1, pp.99–111.

Fengel, D., 1992. Characterization of Cellulose by Deconvoluting the OH Valency Range in FTIR Spectra. *Holzforschung*, 46, pp.283–288.

Fernández-Martínez, R. & Rucandio, M.A., 2003. Study of extraction conditions for the quantitative determination of Hgbound to sulfide in soils from Almadén (Spain). *Analytical and Bioanalytical Chemistry*, 375, pp.1089–1096.

Francombe, M.H. & Rooksby, H.P., 1959. Structure transformations effected by the dehydration of diaspore, goethite and delta ferric oxide. *Clay Minerals Bulletin*, 4(21), pp.1–14.

Frost, R.L., Ding, Z. & Ruan, H.D., 2003. Thermal analysis of goethite - Relevance to Australian indigenous art. *Journal of Thermal Analysis and Calorimetry*, 71, pp.783–797.

Frost, R.L., Edwards, H.G.M., Duong, L., Kloprogge, J.T. & Martens, W.N., 2002. Raman spectroscopic and SEM study of cinnabar from Herod's palace and its likely origin. *The Analyst*, 127(2), pp.293–296.

Le Fur, D., 1990. Les pigments dans la peinture égyptienne. In *Pigments et colorants de l'Antiquité et du moyen Age Teinture, peinture, enluminure, études historiques et physico-chimiques*. Paris: CNRS, France.

Gajić-Kvaščev, M., Stojanović, M.M., Šmit, Ž., et al., 2012. New evidence for the use of cinnabar as a colouring pigment in the Vinča culture. *Journal of Archaeological Science*, 39(4), pp.1025–1033.

Gettens, R.J., Feller, R.L. & Chase, W.T., 1972. Vermilion and Cinnabar. *Studies in Conservation*, 17(2), pp.45–69.

Gettens, R.J. & Sterner, F.W., 1941. The compatibility of pigments in artists' oil paints. *Technical Studies in the Field of the Fine Arts*, 10, pp.18–28.

Gialanella, S., Girardi, F., Ischia, G., et al., 2010. On the goethite to hematite phase transformation. *Journal of Thermal Analysis and Calorimetry*, 102, pp.867–873.

Gil, M., Carvalho, M.L., Seruya, A., et al., 2008. Limewashing paintings in Alentejo urban heritage: Pigment characterization and differentiation by WDXRF and XRD. *Applied Physics A: Materials Science and Processing*, 90, pp.49–54.

Gilbert, R.O., 1987. *Statistical Methods for Environmental Pollution*

Monitoring, John Wiley & Sons.

González, G., Sagarzazu, A. & Villalba, R., 2000. Study of the mechano-chemical transformation of goethite to hematite by TEM and XRD. *Materials Research Bulletin*, 35, pp.2295–2308.

Goss, C.J., 1987. The Kinetics and Reaction Mechanism of the Goethite to Hematite Transformation. *Mineralogical Magazine*, 51, pp.437–451.

Gotoshia, S. V & Gotoshia, L. V, 2008. Laser Raman and resonance Raman spectroscopies of natural semiconductor mineral cinnabar, α-HgS, from various mines. *Journal of Physics D: Applied Physics*, 41, pp.1–6.

Gray, S.F. & Porter, A.L., 1830. *The Chemistry of the Arts: Being a Practical Display of the Arts and Manufactures which Depend on Chemical Principles, Volume 1*, Philadelphia: Carey & Lea.

Green, R.L. & Watling, R.J., 2007. Trace element fingerprinting of Australian ocher using laser ablation inductively coupled plasma-mass spectrometry (LAICP-MS) for the provenance establishment and authentication of indigenous art. *Journal of Forensic Sciences*, 52(4), pp.851–859.

Grygar, T., Hradilová, J., Hradil, D., Bezdička, P. & Bakardjieva, S., 2003. Analysis of earthy pigments in grounds of Baroque paintings. *Analytical and Bioanalytical Chemistry*, 375(8), pp.1154–1160.

Gualtieri, A.F. & Venturelli, P., 1999. In situ study of the goethite-hematite phase transformation by real time synchrotron powder diffraction. *American Mineralogist*, 84(5-6), pp.895–904.

Gunasekaran, S., Anbalagan, G. & Pandi, S., 2006. Raman and infrared spectra of carbonates of calcite structure. *Journal of Raman Spectroscopy*, 37(9), pp.892–899.

Hanaor, D. a H. & Sorrell, C.C., 2011. Review of the anatase to rutile phase transformation. *Journal of Materials Science*, 46(4), pp.855–874.

Harley, R.D., 2001. *Artists' Pigments c.1600-1835: A Study in English Documentary Sources*, Archetype.

Hazen, R.M., Golden, J., Downs, R.T., et al., 2012. Mercury (Hg)

mineral evolution: A mineralogical record of supercontinent assembly, changing ocean geochemistry, and the emerging terrestrial biosphere. *American Mineralogist*, 97, pp.1013–1042.

Healy, J.F., 1993. *Miniere e metallurgia nel mondo greco e romano* Collana Il. L. di Bretschneider, ed., Rome: Lucia Pirzio Biroli Stefanelli.

Helwig, K., 2007. Iron oxide pigments: natural and synthetic. In *Artists' pigments: a handbook of their history and characteristics, Volume 4*. National Galleryof Art and Archetype Publications.

Hendrie, R., 1847. *An essay upon various arts by Theophilus*, London: Woodfall G. and son.

Higueras, P., Munhá, J., Oyarzun, R., Tassinari, C.C.G. & Ruiz, I.R., 2005. First lead isotopic data for cinnabar in the Almadén district (Spain): Implications for the genesis of the mercury deposits. *Mineralium Deposita*, 40, pp.115–122.

Higueras, P., Oyarzun, R., Munha, J. & Morata, D., 2000. The Almaden mercury metallogenic cluster (Ciudad Real, Spain): alkaline magmatism leading to mineralization process ar an intraplate tectonic setting. *Revista de la Sociedad Geológica de España*, 13(1), pp.105–119.

Hill, R.J. & Flack, H.D., 1987. The use of Durbin-Watson d statistic in Rietveld analysis. *Journal of Applied Crystallography*, 20(5), pp.356–361.

Hintelmann, H. & Lu, S., 2003. High precision isotope ratio measurements of mercury isotopes in cinnabar ores using multi-collector inductively coupled plasma mass spectrometry. *The Analyst*, 128, pp.635–639.

Hojdová, M., Navrátil, T., Rohovec, J., Penížek, V. & Grygar, T., 2009. Mercury distribution and speciation in soils affected by historic mercury mining. *Water, Air, and Soil Pollution*, 200(1-4), pp.89–99.

Hradil, D., Grygar, T., Hradilová, J. & Bezdička, P., 2003. Clay and iron oxide pigments in the history of painting. *Applied Clay Science*, 22(5), pp.223–236.

Hunt-Ortiz, M., Consuegra-Rodríguez, S., Río-Español, P.D., Hurtado-Pérez, V.M. & Montero-Ruiz, I., 2011. Neolithic and Chalcolithic – VI to III millennia BC – use of cinnabar (HgS) in the Iberian Peninsula: analytical identification and lead isotope data for an early mineral exploitation of the Almadén (Ciudad Real , Spain) mining district. In J. E. Ortiz, O. Puche, I. Rábano, & L. F. Mazadiego, eds. *History of Research in Mineral Resources*. Madrid: Instituto Geológico y Minero de España, pp. 3–13.

Hurai, V., Chovan, M., Huraiová, M., et al., 2010. Slovak Ore Mountains: Origin of hydrothermal mineralization and environmental impacts of mining. *Acta Mineralogica-Petrographica*, 28, pp.1–36.

Hurai, V., Lexa, O., Schulmann, K., et al., 2008. Mobilization of ore fluids during Alpine metamorphism: Evidence from hydrothermal veins in the Variscan basement of Western Carpathians, Slovakia. *Geofluids*, 8(3), pp.181–207.

Hurst, G.H., 1982. *Painters' Colours, Oils, and Varnishes: A Practical Manual*, London: Griffin, C. & Co. Limited.

Iriarte, E., Foyo, a., Sánchez, M. a., Tomillo, C. & Setién, J., 2009. The origin and geochemical characterization of red ochres from the Tito Bustillo and Monte Castillo Caves (Northern Spain). *Archaeometry*, 51(October 2007), pp.231–251.

Janssens, K., Vittiglio, G., Deraedt, I., et al., 2000. Use of Microscopic XRF for Non-destructive Analysis in Art and Archaeometry. *X-Ray Spectrometry*, 29(1), pp.73–91.

Jébrak, M., Higueras, P.L., Marcoux, É. & Lorenzo, S., 2002. Geology and geochemistry of high-grade, volcanic rock-hosted, mercury mineralisation in the Nuevo Entredicho deposit, Almadén district, Spain. *Mineralium Deposita*, 37, pp.421–432.

Jovanović, B., 1984. *Vinča in Prehistory and Medieval century* Monography., Belgrade: Gallery of Serbian Academy of Sciences and Arts.

Keune, K. & Boon, J.J., 2005. Analytical imaging studies clarifying the process of the darkening of vermilion in paintings. *Analytical Chemistry*, 77(15), pp.4742–4750.

Kieffer, S.W., 1979. Thermodynamics and lattice vibrations of minerals: 2. Vibrational characteristics of silicates. *Reviews of Geophysics*, 17(1), pp.20–34.

King, R.J., 2002. Minerals Explained 37: Cinnabar. *Geology Today*, 18(5), pp.195–199.

Kligfield, R., Hunziker, J., Dallmeyer, R.. & Schamel, S., 1986. Dating of deformation phases using K-Ar and 40Ar/39Ar techniques: results from the northern apennines. *Journal of Structural Geology*, 8(7), pp.781–798.

Kloprogge, J.T., Mahmutagic, E. & Frost, R.L., 2006. Mid-infrared and infrared emission spectroscopy of Cu-exchanged montmorillonite. *Journal of colloid and interface science*, 296(2), pp.640–6.

Kosmulski, M., Durand-Vidal, S., Maczka, E. & Rosenholm, J.B., 2004. Morphology of synthetic goethite particles. *Journal of Colloid and Interface Science*, 271, pp.261–269.

Krupp, R.E., 1989. Paragenesis and conditions of formation of the Moschellandsberg mercury deposit, SW Germany. *Mineralium Deposita*, 24, pp.69–76.

Larson, a C. & Von Dreele, R.B., 2004. General Structure Analysis System (GSAS). *Structure*, 748(LAUR 86-748), pp.86–748.

Lavrič, J. V. & Spangenberg, J.E., 2003. Stable isotope (C, O, S) systematics of the mercury mineralization at Idrija, Slovenia: Constraints on fluid source and alteration processes. *Mineralium Deposita*, 38(7), pp.886–899.

Lazzarini, L., 1987. The use of color by Venetian painters, 1480-1580: materials and technique. In M. B. Hall, ed. *Colour and Technique in Renaissance Painting - Italy and North*. Locust Valley, New York, pp. 115–136.

Lemos, V.P., Da Costa, M.L., Lemos, R.L. & De Faria, M.S.G., 2007. Vivianite and siderite in lateritic iron crust: An example of bioreduction. *Quimica Nova*, 30(1), pp.36–40.

Lewis, I.R. & Edwards, H., 2001. *Handbook of Raman Spectroscopy: From the Research Laboratory to the Process Line*, CRC Press.

Lima-de-Faria, J., 1963. Dehydration of goethite and diaspore. *Zeitschrift für Kristallographie*, 119(3-4), pp.176–203.

Lima-De-Faria, J., 1994. *Structural Mineralogy - An Introduction*, Dordrecht: Springer Science + Business Media, B.V.

Ling, R., 1991. *Roman Painting*, Cambridge University Press.

Löffler, L. & Mader, W., 2006. Anisotropic X-ray peak broadening and twin formation in hematite derived from natural and synthetic goethite. *Journal of the European Ceramic Society*, 26, pp.131–139.

Lucas, A. & Harris, J., 2012. *Ancient Egyptian Materials and Industries* 4th ed. C. Courier, ed., Mineola, New York: Dover Publications, Inc.

Maes, G., 2003. Handbook of Raman Spectroscopy. From the Research Laboratory to the Process Line. *Spectrochimica Acta Part A: Molecular and Biomolecular Spectroscopy*, 59, p.211.

Maras, A., Botticelli, M. & Ballirano, P., 2013. Archaeometric investigations on cinnabar provenance and origin by X-ray powder diffraction: preliminary data. *International Journal of Conservation Science*, 4(Special), pp.685–692.

Marengo, E., Aceto, M., Robotti, E., et al., 2005. Archaeometric characterisation of ancient pottery belonging to the archaeological site of Novalesa Abbey (Piedmont, Italy) by ICP-MS and spectroscopic techniques coupled to multivariate statistical tools. *Analytica Chimica Acta*, 537(1-2), pp.359–375.

Martín-Gil, J., Martín-Gil, F.J., Delibes-de-Castro, G., Zapatero-Magdaleno, P. & Sarabia-Herrero, F.J., 1995. The first known use of vermillion. *Experientia*, 51(8), pp.759–61.

Maslen, E.N., Streltsov, V.A., Streltsova, N.R. & Ishizawa, N., 1994. Synchrotron X-ray Study of the Electron Density in alpha-Fe2O3. *Acta Crystallographica*, B50(1903), pp.435–441.

de Massoul, C., 1797. *A Treatise on the Art of Painting*, London: Baylis, T.

Mazzocchin, G. a., Baraldi, P. & Barbante, C., 2008. Isotopic analysis of lead present in the cinnabar of Roman wall paintings from the Xth Regio '(Venetia et Histria)' by ICP-MS.

Talanta, 74, pp.690–693.

McCormack, J.K., 2000. The darkening of cinnabar in sunlight. *Mineralium Deposita*, 35(8), pp.796–798.

Mérimée, J.-F.-L., 1830. *De la peinture à l'huile*, Paris: M.me Huzard Libraire.

Méry, S. & Schneider, G., 1996. Mesopotamian pottery wares in Eastern Arabia from the 5th to the 2nd Millennium BC: a contribution of archaeometry to the economic history. In *Proceedings of the Seminar for Arabian Studies - Papers from the twenty-ninth meeting of the Seminar for Arabian*. Cambridge: Archaeopress Publishing Ltd., pp. 79–96.

Mioč, U.B., Colomban, P., Sagon, G., Stojanović, M. & Rosić, A., 2004. Ochre decor and cinnabar residues in Neolithic pottery from Vinča, Serbia. *Journal of Raman Spectroscopy*, 35(10), pp.843–846.

Mochi, A., 1915. Indizi di miniere preistoriche di cinabro nella regione dell'Amiata. *Bullettino di paletnologia italiana*, 41, pp.5–12.

Moens, L., Roos, P., de Rudder, J., et al., 1988. White marble from Italy and Turkey: an archaeometric study based on minor- and trace-element analysis and petrography. *Journal of Radioanalytical and Nuclear Chemistry*, 123(1), pp.333–348.

Montes-Hernandez, G., Beck, P., Renard, F., et al., 2011. Fast precipitation of acicular goethite from ferric hydroxide gel under moderate temperature (30 and 70 ℃). *Crystal Growth and Design*, 11, pp.2264–2272.

Monthel, J., Vadala, P., Leistel, J.M., et al., 2002. *Mineral deposits and mining districts of Serbia Compilation map and GIS databases*, BRGM/RC-51448-FR.

Morteani, G., Ruggieri, G., Möller, P. & Preinfalk, C., 2011. Geothermal mineralized scales in the pipe system of the geothermal Piancastagnaio power plant (Mt. Amiata geothermal area): A key to understand the stibnite, cinnabarite and gold mineralization of Tuscany (central Italy). *Mineralium Deposita*, 46, pp.197–210.

Mottana, A. & Napolitano, M., 1997. *Il libro «Sulle pietre» di*

Teofrasto Prima traduzione italiana con un vocabolario dei termini mineralogici, Rome: Accademia Nazionale dei Lincei.

Norrish, K. & Taylor, R.M., 1961. The isomorphous replacement of iron by aluminium in soil goethites. *Journal of Soil Science*, 12(2), pp.294–306.

Nusimovici, M.A. & Meskaoui, A., 1973. Raman Scattering by α-HgS (Cinnabar). *Physica Status Solidi (b)*, 58(1), pp.121–125.

Ohmiya, T., 1974. Thermal expansion and the phase transformation in mercury sulphide. *Journal of Applied Crystallography*, 7(3), pp.396–397.

Osbaldeston, T.A. & Wood, R.P.A., 1933. *trans. De Materia Medica. The Greek herbal of Dioscorides* R. Gunther, ed., Oxford: Ibidis Press cc.

Pattelli, G., Rimondi, V., Benvenuti, M., et al., 2014. Effects of the November 2012 Flood Event on the Mobilization of Hg from the Mount Amiata Mining District to the Sediments of the Paglia River Basin. *Minerals*, 4(2), pp.241–256.

Pianigiani, O., 1993. *Vocabolario etimologico della lingua italiana*, Rome: Società editrice Dante Alighieri di Albrighi, Segati e C.

Piccolo, E., 2009. *rev. De architettura di Vitruvio* book VII., Napoli: Classici Latini Loffredo.

Ping Li, Feng, X., Shang, L., et al., 2008. Mercury pollution from artisanal mercury mining in Tongren, Guizhou, China. *Applied Geochemistry*, 23(8), pp.2055–2064.

Pirri, V., 1977. Le paragenesi a Zn, Cu, Pb, Sb, Hg, Ni, As, fluorite, barite nel Devonico della catena Carnica. *Rendiconti della Società Italiana di Mineralogia e Petrografia*, 33(2), pp.821–844.

Pomiés, M.-P., 1997. *Pigments rouges prehistoriques: goethite chauffee ou hematite nanocristalline naturelle?* Université Paris 6 et Labo Rech. Musée de Fr.

Pomiès, M.P., Menu, M. & Vignaud, C., 1999. Tem observations of goethite dehydration: application to archaeological samples. *Journal of the European Ceramic Society*, 19, pp.1605–1614.

Pomiès, M.P., Morin, G. & Vignaud, C., 1998. XRD study of the goethite-hematite transformation: Application to the identification of heated prehistoric pigments. *European Journal of Solid State and Inorganic Chemistry*, 35, pp.9–25.

Potter, R.W. & Barnes, H.L., 1978. Phase relations in the binary Hg-S. *American Mineralogist*, 63, pp.1143–1152.

Pozas, R., Ocaña, M., Morales, M.P. & Serna, C.J., 2002. Uniform nanosized goethite particles obtained by aerial oxidation in the FeSO4-Na2CO3 system. *Journal of colloid and interface science*, 254, pp.87–94.

Prasad, P.S.R., Chaitanya, V.K., Prasad, K.S. & Rao, D.N., 2005. Direct formation of the γ-CaSO4 phase in dehydration process of gypsum: In situ FTIR study. *American Mineralogist*, 90(4), pp.672–678.

Prasad, P.S.R., Prasad, K.S., Chaitanya, V.K., et al., 2006. In situ FTIR study on the dehydration of natural goethite. *Journal of Asian Earth Sciences*, 27(4), pp.503–511.

Prencipe, M., Pascale, F., Zicovich-Wilson, C.M., et al., 2004. The vibrational spectrum of calcite (CaCO3): an ab initio quantum-mechanical calculation. *Physics and Chemistry of Minerals*, 31(8), pp.559–564.

Prieto, M.Z., Ochoa, C.F., Esteban, G. & Hevia, P., 2012. El área de Almadén (Ciudad Real) en el territorio de Sisapo. Investigationes arqueo-históricas sobre las etapas más antiguas de explotación del cinabrio hispano. *De Re Metallica*, 19, pp.67–78.

Puică, N.M., Pui, A. & Florescu, M., 2006. FTIR spectroscopy for the analysis of vegetable tanned ancient leather. *European Journal of Science and Theology*, 2(4), pp.49–53.

Qiu, G., Feng, X., Wang, S. & Shang, L., 2005. Mercury and methylmercury in riparian soil, sediments, mine-waste calcines, and moss from abandoned Hg mines in east Guizhou province, southwestern China. *Applied Geochemistry*, 20, pp.627–638.

Quirke, S., 1993. *Owners of Funerary Papyri in the British Museum*, London: British Museum Press, 92.

Rackham, H., Jones, W.H.S. & Eicholz, D.E., 1963. *Pliny Natural history, with an English translation in ten volumes*, Cambridge: Harvard University Press.

Radepont, M., Coquinot, Y., Janssens, K., et al., 2015. Thermodynamic and experimental study of the degradation of the red pigment mercury sulfide. *Journal of Analytical Atomic Spectrometry*, 30(3), pp.599–612.

Radepont, M., de Nolf, W., Janssens, K., et al., 2011. The use of microscopic X-ray diffraction for the study of HgS and its degradation products corderoite (α-Hg3S2Cl2), kenhsuite (γ-Hg3S2Cl2) and calomel (Hg2Cl2) in historical paintings. *Journal of Analytical Atomic Spectrometry*, 26, p.959.

Rapp, G.R., 2009. *Archaeomineralogy*, Springer Netherlands.

Rečnik, A., 2013. *I minerali del giacimento di mercurio di Idrija* Istituto ". V. Bode, ed., Ljubljana: Birografika BORI d.o.o.

Reedy, T.J. & Reedy, C.L., 1988. *Statistical Analysis in Art Conservation Research* J.Paul Getty Trust, ed., United States of America: The Getty Conservation Institute.

Rodriguez-Navarro, C., Ruiz-Agudo, E., Luque, A., Rodriguez-Navarro, A.B. & Ortega-Huertas, M., 2009. Thermal decomposition of calcite: Mechanisms of formation and textural evolution of CaO nanocrystals. *American Mineralogist*, 94(4), pp.578–593.

Rogerio-Candelera, M.Á., Herrera, L.K., Miller, A.Z., et al., 2013. Allochthonous red pigments used in burial practices at the Copper Age site of Valencina de la Concepción (Sevilla, Spain): Characterisation and social dimension. *Journal of Archaeological Science*, 40(1), pp.279–290.

Rollinson, H.R., 1993. *Using Geochemical Data: Evaluation, Presentation, Interpretation* Longman ge. Longman, ed., Harlow.

Romei, M., 1890. *Le miniere del Monte Amiata: notizie storiche e corografiche*, Firenze: Le Monnier.

Ruan, H.D., Frost, R.L. & Kloprogge, J.T., 2001. The behavior of hydroxyl units of synthetic goethite and its dehydroxylated

product hematite. *Spectrochimica Acta Part A: Molecular and Biomolecular Spectroscopy*, 57(13), pp.2575–2586.

Ruan, H.D., Frost, R.L., Kloprogge, J.T. & Duong, L., 2002. Infrared spectroscopy of goethite dehydroxylation: III. FT-IR microscopy of in situ study of the thermal transformation of goethite to hematite. *Spectrochimica Acta - Part A Molecular and Biomolecular Spectroscopy*, 58, pp.967–981.

Rybár, P., Molokáč, M., Hvizdák, L., Štrba, Ľ. & Böhm, J., 2012. Territory of Eastern Slovakia - area of mining heritage of mediaeval mining. *Acta Geoturistica*, 3(2), pp.29–35.

Rybár, P., Sasvári, T., Hvizdák, L., Hvizdáková, J. & Baláž, B., 2010. Geotouristic excursion to selected historical mining sites developed by Slovak and German miners in the Gelnica-Smolník region, Slovakia. *Geoturystyka*, 1(20), pp.23–30.

Rytuba, J.J., 2003. Mercury from mineral deposits and potential environmental impact. *Environmental Geology*, 43(3), pp.326–338.

Sabine, T.M., Hunter, B.A., Sabine, W.R. & Ball, C.J., 1998. Analytical Expressions for the Transmission Factor and Peak Shift in Absorbing Cylindrical Specimens. *Journal of Applied Crystallography*, 31(1), pp.47–51. Available at: http://scripts.iucr.org/cgi-bin/paper?hw0059 [Accessed March 30, 2016].

Saikia, B.J. & Parthasarathy, G., 2010. Fourier Transform Infrared Spectroscopic Characterization of Kaolinite from Assam and Meghalaya, Northeastern India. *Journal of Modern Physics*, 01(04), pp.206–210.

Saupé, F. & Arnold, M., 1992. Sulphur isotope geochemistry of the ores and country rocks at the Almadén mercury deposit, Ciudad Real, Spain. *Geochimica et Cosmochimica Acta*, 56(10), pp.3765–3780.

Schafer, E.H., 1956. The Early History of Lead Pigments and Cosmetics in China. *T'oung Pao*, 44, pp.413–438.

Scheinost, A.C., Schulze, D.G. & Schwertmann, U., 1999. Diffuse Reflectance Spectra of Al Substituted Goethite: A Ligand Field

Approach. *Clays and Clay Minerals*, 47(2), pp.156–164.

Schleid, T., Lauxmann, P. & Schneck, C., 1999. Röntgenographische Einkristallstruktur-untersuchungen an α-HgS (Zinnober). *Zeitschrift für Kristallographie*, 95(Suppl. 16).

Schwertmann, U., 2008. Iron oxides. In W. Chesworth, ed. *Encyclopedia of Soil Science*. Encyclopedia of Earth Sciences Series. Dordrecht: Springer Netherlands, pp. 363–369.

Schwertmann, U., 1984. The double dehydroxylation peak of goethite. *Thermochimica Acta*, 78(1-3), pp.39–46.

Schwertmann, U. & Cornell, R.M., 2000. *Iron Oxides in the Laboratory* 2nd ed. U. Schwertmann & R. M. Cornell, eds., Weinheim, Germany: Wiley-VCH Verlag GmbH.

Sharma, R.C. & Chang, Y.A., 1993. The Hg-S (Mercury-Sulfur) System. *Journal of Phase Equilibria*, 14(1), pp.100–109.

Singh, B., 1999. Mineralogy and Chemistry of Ochre Sediments from an Acid Mine Drainage Near a Disused Mine in Cornwall, UK. *Clay Minerals*, 34(2), pp.301–317.

Smith, D., 1971. Stability of the assemblage iron-rich orthopyroxene-olivine-quartz. *American Journal of Science*, 271(4), pp.370–382.

Sodo, A., Artioli, D., Botti, A., et al., 2008. The colours of Etruscan painting: A study on the Tomba dell'Orco in the necropolis of Tarquinia. *Journal of Raman Spectroscopy*, 39(8 SPEC. ISS.), pp.1035–1041.

Spangenberg, J.E., Lavrič, J. V., Meisser, N. & Serneels, V., 2010. Sulfur isotope analysis of cinnabar from Roman wall paintings by elemental analysis/isotope ratio mass spectrometry - tracking the origin of archaeological red pigments and their authenticity. *Rapid Communications in Mass Spectrometry*, 24, pp.2812–2816.

Spring, M.. & Grout, R., 2002. The Blackening of Vermilion: An Analytical Study of the Process in Paintings. *National Gallery Technical Bulletin*, 23, pp.50–61.

Su, C. & Suarez, D.L., 1997. In situ Infrared seciation of adsorbed carbonate on aluminium and iron oxides. *Clays and Clay*

Minerals, 45(6), pp.814–825.

Thompson, D.V., 1993. *The Craftsman's Handbook (Il Libro dell' Arte) by Cennino Cennini trans.*, New York: Dover Publications - Yale University Press.

Toby, B., 2001. EXPGUI, a graphical user interface for GSAS. *Journal of Applied Crystallography*, 34(2), pp.210–213.

Triat, J.-M., 2010. Les Ocres. *CNRS Editions*, p.198.

Urban, M., Thomas, R., Hurai, V., Konečný, P. & Chovan, M., 2006. Superdense CO2 inclusions in Cretaceous quartz-stibnite veins hosted in low-grade Variscan basement of the Western Carpathians, Slovakia. *Mineralium Deposita*, 40(8), pp.867–873.

Vaculíková, L., Plevová, E., Vallová, S. & Koutník, I., 2011. Characterization and differentiation of kaolinites from selected Czech deposits using infrared spectroscopy and differential thermal analysis. *Acta Geodynamica et Geomaterialia*, 8(1), pp.59–67.

Velebil, D. & Zachariáš, J., 2013. Fluid inclusion study of the Horní Luby cinnabar deposit, Saxothuringian Zone, Bohemian Massif: Clues for the metamorphic remobilization of mercury. *Journal of Geosciences (Czech Republic)*, 58, pp.287–302.

Villieras, F., Yvon, J., Cases, J.M., et al., 1994. Development of microporosity in clinochlore upon heating. *Clays and Clay Minerals*, 42(6), pp.679–688. Available at: papers2://publication/uuid/BB29B2E6-77BD-4B80-B694-697DE0E4C689.

Vuk, A.Š., Ješe, R., Orel, B. & Dražič, G., 2005. The effect of surface hydroxyl groups on the adsorption properties of nanocrystalline TiO2 films. *International Journal of Photoenergy*, 7(4), pp.163–168. Available at: http://www.scopus.com/inward/record.url?eid=2-s2.0-26044479676&partnerID=tZOtx3y1.

Walter, D., Buxbaum, G. & Laqua, W., 2001. The Mechanism of the Thermal Transformation From Goethite to Hematite. *Journal of Thermal Analysis and Calorimetry*, 63(3), pp.733–748.

Williams, Q., Hemley, R.J., Kruger, M.B. & Jeanloz, R., 1993. High-Pressure Infrared Sepctra of alpha-Quartz, Coesite, Stishovite and Silica Glass pressures. *Journal of Geophisical Research*, 98(B12), pp.22,157–22,170.

Williams, W., 1787. *An Essay of the Mechanic of Oil Colours*, Bath: Hazard S.

Wolska, E., 1981. The structure of hydrohematite. *Zeitschrift für Kristallographie*, 154, pp.69–75.

Wolska, E. & Szajda, W., 1985. Structural and spectroscopic characteristics of synthetic hydrohaematite. *Journal of Materials Science*, 20, pp.4407–4412.

van der Woude, J.H.A. & de Bruyn, P.L., 1984. Formation of colloidal dispersions from supersaturated iron(III) nitrate solutions V. Synthesis of monodisperse goethite sols. *Colloids and Surfaces*, 12(1-2), pp.179–188.

Yang, H., Lu, R., Downs, R.T. & Costin, G., 2006. Goethite, α-FeO(OH), from single-crystal data. *Acta Crystallographica Section E Structure Reports Online*, 62(12), pp.i250–i252.

Young, R., 1993. *The Rietveld Method* Oxford Uni., Oxford.

Younkin, R.L., 1966. A search for limonite near-infrared spectral features on mars. *Astrophysical Journal*, 144, pp.809–818.

Zallen, R., Lucovsky, G., Taylor, W., Pinczuk, A. & Burstein, E., 1970. Lattice Vibrations in Trigonal HgS. *Physical Review B*, 1(10), pp.4058–4070.

Zema, M., Ghigna, P., Domeneghetti, M.C. & Tazzoli, V., 2002. Oxygen diffusion in orthopyroxene TG study. *Journal of Thermal Analysis and Calorimetry*, 67(3), pp.713–720.

Zhang, 1996. Geochemistry of Strata-bound Hg, Sb and As Deposits. In *Geochemistry of Strata-bound Deposits in China*. Beijing: VSP, pp. 396–430.

Zhang, Y., Tang, H.-S., Chen, Y.-J., Leng, C.-B. & Zhao, C.-H., 2014. Ore geology, fluid inclusion and isotope geochemistry of the Xunyang Hg-Sb orefield, Qinling Orogen, Central China. *Geological Journal*, 49(4-5), pp.463–481.

Zucchini, R., 1998. *Miniere e mineralizzazioni nella provincia di Udine: aspetti storici e mineralogici*, Udine: Museo Friulano di Storia Naturale.

INDEX OF FIGURES

INDEX OF TABLES